Topological study of the brain functional organization at the early stages of Alzheimer's disease using electroencephalography

Majd Abazid

INSTITUT POLYTECHNIQUE DE PARIS

NNT : 2022IPPAS026

Thèse de doctorat

Topological study of the brain functional organization at the early stages of Alzheimer's disease using electroencephalography

Thèse de doctorat de l'Institut Polytechnique de Paris
préparée à Télécom SudParis

École doctorale n°626 École doctorale de l'Institut Polytechnique de Paris (EDIPP)
Spécialité de doctorat: Mathématiques et Informatique

Thèse présentée et soutenue à Palaiseau, le 13/12/2022, par

MAJD ABAZID

Composition du Jury :

Gérard Dray Professeur, IMT Mines Alès	President
Sylvain Chevallier Professeur des universités, Université Paris-Saclay	Reviewer
Jordi Solé-Casals Professor, Université de Vic, Universitat Central de Catalunya	Reviewer
Kiyoka Kinugawa Bourron Professeur des universités, Praticien hospitalier, Sorbonne Université/CNRS, UMR 8256 - Biological Adaptation and Aging	Examiner
Jérôme Boudy Professeur, Télécom SudParis	Thesis supervisor
Nesma Houmani Maître de conférences, Télécom SudParis	Supervisor
Bernadette Dorizzi Professeur émérite, Télécom SudParis	Guest supervisor
Jean Mariani Professeur émérite, UMR 8256 - Biological Adaptation and Ageing	Guest

Abstract

Electroencephalography (EEG) is still considered nowadays as a convenient neuroimaging technique in clinical applications, suitable for cognitively and physically disabled patients, as well as for serial tests. In fact, EEG is a non-invasive, cost-effective, and mobile technology. It is characterized by a high temporal resolution, which is crucial for the analysis of fast brain functional dynamics.

There is a rich literature addressing the use of EEG to investigate brain activity alterations due to neurodegenerative diseases, especially Alzheimer's disease (AD). AD is a chronic neurodegenerative disease that leads to progressive decline of cognitive functions along with behavioral disorders and insidious loss of autonomy in daily living activities. We observe a growing interest in the earlier stages of the disease since curative treatments are still lacking. The preclinical stage of AD is asymptomatic, but the brain lesions due to AD are present. At this phase, the term of subjective cognitive impairment (SCI) has been recently defined. In the prodromal stage, mild cognitive impairment (MCI) patients show measurable memory impairments but their functional capacity is maintained. SCI and MCI patients are at high risk of developing AD. In the Mild AD stage, cognitive deficits are more marked, such as memory and learning impairments. Some psychological symptoms can thus also appear at this stage, such as compulsive behavior and suspiciousness. AD is often diagnosed at this stage.

According to the most recent guidelines, AD can be diagnosed in preclinical and prodromal stages, before the manifestation of any cognitive and behavioural symptoms. This could be possibly based on pathophysiological markers, revealed by CSF and PET biomarkers of Aβ42 and tau in the brain. However, such guidelines also underline the need to extend research to non-invasive and inexpensive instrumental techniques, which can be deployed in clinical environment and used for large-scale assessment. Electroencephalography (EEG) is a neuroimaging technology suitable to fulfil this need.

This thesis investigates the early diagnosis of AD at preclinical and prodromal stages using resting-state EEG, and addresses brain network analysis by studying the functional connectivity over several clinical stages of cognitive decline (SCI, MCI and Mild AD). To this end, we conduct a retrospective study using a clinical database that contains EEG signals recorded in real-life conditions.

We first propose to exploit an entropy measure, termed "Epoch-based Entropy" (EpEn), as a measure of functional connectivity, that relies on a refined statistical modeling of EEG signals based on Hidden Markov Models. This measure characterizes the spatiotemporal changes in EEG signals by quantifying the information content of EEG signals, both at the time and spatial levels. Furthermore, we conduct a topological brain network analysis over the three stages of cognitive decline by employing the Graph Theory. The novelty of our work is twofold. Actually, this is the first work that: (i) addresses EEG brain network analysis over SCI, MCI and Mild AD stages simultaneously, and (ii) combines EpEn to Graph Theory since we have shown its effectiveness in quantifying the complete spatiotemporal alteration due to AD.

In this thesis, we decided to invest the largest amount of EEG information for brain network analysis, by exploiting several frequency ranges (delta, theta, alpha, beta), several electrodes locations (instead of regions), and several network density scales (multiple graph thresholding). Therefore,

another issue tackled in this thesis concerns the identification of relevant EEG markers to discriminate automatically between SCI, MCI and AD patients in the context of graph analysis framework. To this end, we propose an automatic hierarchical method for EEG analysis, which allows the extraction of relevant markers from large amount of information based on a single EEG connectivity measure. Finally, we also assess the correlation between the relevant EEG markers and the clinical markers at our disposal (MMSE, RL/RI-16, BREF).

Résumé

L'électroencéphalographie (EEG) est encore considérée de nos jours comme une technique de neuroimagerie très utile dans les applications cliniques, adaptée aux patients souffrant de troubles cognitifs et physiques, ainsi qu'aux tests à grande échelle. L'EEG est une technologie non invasive, peu coûteuse et facilement accessible. Elle se caractérise par une haute résolution temporelle, ce qui est crucial pour le suivi de la dynamique cérébrale.

Plusieurs travaux dans la littérature ont exploité l'EEG pour étudier les altérations de l'activité cérébrale liées aux maladies neurodégénératives, notamment la maladie d'Alzheimer (MA). La MA est une maladie neurodégénérative chronique qui entraîne un déclin progressif des fonctions cognitives, ainsi que des troubles du comportement et une perte insidieuse d'autonomie au quotidien. En l'absence de traitements curatifs, nous observons un intérêt croissant à la caractérisation de l'activité cérébrale aux stades précoces de la maladie. Le stade préclinique de la MA est asymptomatique, mais les lésions cérébrales dues à la MA sont présentes. A ce stade, on parle de troubles cognitifs subjectifs (subjective cognitive impairments, SCI). Au stade prodromal, les patients atteints de troubles cognitifs légers (mild cognitive impairment, MCI) présentent des troubles de la mémoire mesurables, mais leur capacité fonctionnelle est maintenue. Les patients atteints de troubles subjectifs ou légers présentent un risque élevé de développer la MA. Au stade léger de la MA, les déficits cognitifs sont plus notables, tels que les troubles de la mémoire et des apprentissages. Certains symptômes psychologiques peuvent donc également apparaître à ce stade, comme des comportements compulsifs et la méfiance. La MA est souvent diagnostiquée à ce stade.

Selon les études les plus récentes, la MA peut être diagnostiquée aux stades préclinique et prodromique, avant la manifestation de symptômes cognitifs et comportementaux. Cela est possible en exploitant des marqueurs physiopathologiques, révélés par les biomarqueurs CSF et PET de Aβ42 et tau dans le cerveau. Cependant, ces études soulignent également la nécessité d'étendre la recherche à des techniques instrumentales non invasives et peu coûteuses, qui peuvent être déployées dans un environnement clinique et utilisées pour une évaluation à grande échelle. L'électroencéphalographie (EEG) est une technologie de neuroimagerie adaptée pour répondre à ce besoin.

Cette thèse s'intéresse au diagnostic précoce de la MA aux stades préclinique et prodromal en utilisant l'EEG au repos, et aborde l'analyse des réseaux cérébraux en étudiant la connectivité fonctionnelle à différents stades cliniques du déclin cognitif (SCI, MCI et MA au stade léger). Pour cela, nous avons mené une étude rétrospective en exploitant une base de données clinique qui contient des signaux EEG enregistrés en conditions réelles.

En premier lieu, nous avons proposé d'exploiter une mesure d'entropie, appelée "Epoch-based Entropy" (EpEn), pour quantifier la connectivité fonctionnelle. Cette mesure repose sur une modélisation statistique fine des signaux EEG avec des modèles de Markov cachés. Cette mesure caractérise les changements spatio-temporels des signaux EEG en quantifiant le contenu d'information dans les signaux au niveau temporel et spatial. Par la suite, nous avons effectué une analyse topologique du réseau cérébral cortical de manière différentielle, en exploitant la théorie des graphes. La contribution de notre travail est double. En effet, il s'agit du premier travail qui : (i) aborde l'analyse du réseau cérébral chez les patients ayant des troubles subjectifs, des troubles légers et la MA au stade léger, et (ii) combine la mesure d'entropie à la théorie des graphes puisque nous avons démontré

son efficacité à quantifier les changements spatio-temporels liés à la MA.

Dans cette thèse, nous avons aussi abordé le problème de la grande quantité d'information extraite des signaux EEG, analysés sur plusieurs bandes de fréquences (delta, theta, alpha, beta), plusieurs électrodes, et plusieurs échelles de densité de réseau (seuillages multiples des graphes). Par conséquent, une autre contribution de ce travail de thèse concerne l'extraction de marqueurs EEG les plus pertinents pour discriminer automatiquement les trois groupes de patients. Ainsi, nous avons proposé une méthode hiérarchique pour l'analyse des signaux EEG, permettant d'identifier les descripteurs les plus pertinents à partir d'une grande quantité d'information issue d'une seule mesure de connectivité fonctionnelle. Enfin, nous avons évalué la corrélation entre les marqueurs numériques extraits des signaux EEG et les marqueurs cliniques à notre disposition (MMSE, RL/RI-16, BREF).

Acknowledgements

I would first like to thank my supervisor Dr. Nesma Houmani for teaching me the meaning of scientific research throughout these years. Her enthusiasm, her perfectionism and her skills gave me the will of continuing in scientific research. I will absolutely never forget her human qualities during the most difficult moments that I had throughout this thesis. Be assured of my deepest gratitude.

I would also like to thank the director of my thesis Pr. Jérôme Boudy for his wise advice and his great sympathy. I hope that he will find in this work the expression of my respectful gratitude.

I would like to express my deep gratitude to the co-supervisor of my thesis Pr. Bernadette Dorizzi for the precious help she gave me, for her generosity and her human qualities. May this work represent the testimony of my great appreciation.

I want to thank the entire hospital team at Charles-Foix Hospital, especially MD. Kiyoka Kinugawa Bourron and Pr. Jean Mariani who provided us with valuable assistance in analyzing the results. Their help has been precious and essential to validate this work.
I also have to thank the members of my PhD committee, Pr. Gérard Dray, Pr. Sylvain Chevallier and Pr. Jordi Solé-Casals.

I also thank my friend Maxime Bedoin, the laboratory's scientific research engineer, for his valuable remarks and comments over the years.

I would also like to show gratitude to my family:
My mother, who has always been the main motivator for every effort I made during my study journey. None of this could have happened without you.
To my eternal friend, my father, who showed me the beauty of freedom. I know you have outdone everyone with your dreams, including this place where I am writing to you. But you didn not know how hard the road would have been without you, my friend.
To my sisters Mariam and Ruba, and my little brother Mustafa.
To my friends, the family that I have chosen and often supported me in moments of weakness, stress and distress. They were a source of security and gave me the psychological support I needed to complete the journey: Manaf, Yasar, Khaled, Mekdad, Yara, Ahmed ,Dima, and Rawan.

I am grateful for the Maison des Étudiants Canadiens (MEC), with a special mention to Ms. France Mainville, Director of the MEC who gave me the opportunity to stay at the residence and warmly welcomed me.
Thanks to all my friends at the MEC. Those who directly or indirectly supported me throughout these years of thesis: Laurent, Érik, Jean François, Valentina, Michaela, Sofiane, Su, Florencia, Jad, Thomas, Laura, Kyrian and Sébastien. I want to also thank all the staff of the MEC, especially Ilham, Isabella, Maxime, Rafael, Frédéric, Estelle, Alice and Armanda.

To Galbi, the light soul that came to bloom my life. I love you so much and I know that the road with you to the impossible is beautiful.

Finally, to all the friends of the Syrian revolution, especially those who made freedom a higher goal and did not lose the way and did not become like their enemy. This enemy to whom I do not want to give the honor to be mentioned here, the one who destroyed my great beloved Syria, to keep his throne and crushed the dreams of millions who revolted for freedom.

"Did we have to fall from so high and see our blood on our hands
To realize that we were not angels, as we thought?
And did we also have to reveal our faults in public
So that our truth would no longer remain virgin?
How we lied when we said: we are an exception!" Mahmoud Darwish

Majd Abazid
Paris, December 2022

Contents

List of Figures

List of Tables

Acronyms

EEG : Electroencephalography

AD : Alzheimer's Disease

MCI : Mild Cognitive Impairment

SCI : Subjective Cognitive Impairment

EpEn : Epoch-based Entropy

PS : Phase Synchrony

PLV : Phase-Locking Value

PLI : Phase Lag Index

MI : Mutual Information

COH : Coherence

MSC : Magnitude Square Coherence

K : Degree

CC : Clustering coefficient

L : Shortest path

E_{loc} : Local efficiency

SW : Small-world index

BW : Betweenness

Q : Modularity

SVM : Support-Vector Machine

LDA : Linear Discriminant Analysis

PT : Proportional Threshold

HMM : Hidden Markov Model

Chapter 1

Introduction

1.1 Scientific context

One of the greatest challenges in modern science is to understand how the brain processes information and how its functioning is altered with ageing or due to neurological disorders. The human brain is considered as a highly complex and self-organizing system. Its functioning relies on the collective dynamics of around 100 billion of neurons interconnected through a sophisticated network of synapses, well organized in their structure and connectivity. Synaptic dysfunction has received significant attention, particularly since there has been evidence that the loss of neuronal synapses occurs in the early stage of neurodegenerative diseases (NDD) (Querfurth and LaFerla, 2010). Recent research suggests that synapses are sites of aberrant protein misfolding in NDD (Forner et al., 2017).

Alzheimer's disease (AD) is the most prevalent form of NDD, which accounts for 50% to 70% of cases (Prince et al., 2015). The World Alzheimer Report 2015 estimates there are 46.8 million people living with dementia worldwide (Prince et al., 2015). AD is the most frequent cause of dementia in Western societies. As the world population ages, the number of individuals with AD is expected to double by 2030 and to reach 115 million by 2050 (Gaugler et al., 2022). Accordingly, and because of the unprecedented level of aging in the world, the health care costs associated with AD are exceptionally high, imposing an important burden on modern societies.

AD is a chronic neurodegenerative disorder that leads to progressive decline of cognitive functions along with behavioral disorders and insidious loss of autonomy in daily living activities. The evolution of AD follows five stages. The "*preclinical*" stage is asymptomatic, but the brain lesions of AD are present. At this stage, the concept of *Subjective Cognitive Impairment* (SCI) has been proposed recently, defined by a self-experienced persistent decline in cognitive capacity in comparison with a previously normal status (Forner et al., 2017). These subjective complaints are considered as a risk factor for AD (Prince et al., 2015; Jessen et al., 2014). Then, in the "*prodromal*" stage, *Mild Cognitive Impairment* (MCI) patients exhibit measurable memory impairments, but maintain their functional capacities (Jessen et al., 2014; Mitchell et al., 2014). In the "*Mild AD*" stage, cognitive deficits are more notable, such as memory and learning impairments. These symptoms become more severe in the "Moderate AD" stage. In the final "severe" stage of the disease, almost all cognitive and motor functions are deeply deteriorated and patients lose autonomy becoming completely dependent on caregivers. The average duration of survival of AD patients is 5-8 years after clinical diagnosis (Dubois et al., 2016).

Nowadays, no medication exists for curing this pathology, and many therapeutics trials failed. Current major anti-AD medication trials are focusing on the preclinical stage, in order to treat before symptoms development. Therefore, AD detection at MCI and preclinical stages becomes an important issue for the scientific community. Besides, there are currently no specific markers that can confirm the AD diagnosis with sufficient certainty, especially in the early stages. Thus, there is a crucial need for real advances to identify reliable AD markers for profiling elderly at-risk, diagnosis and monitoring disease progression. By relying on biomedical engineering field, we can identify neuro-imaging and new neuro-dynamic markers correlated with AD, which contribute to a better understanding of the brain dynamics related to AD, and improve the reliability of AD diagnosis.

According to recent guidelines (McKhann et al., 2011; Dubois et al., 2014), AD can be diagnosed in preclinical and prodromal stages, before the manifestation of any cognitive and behavioral symptoms. This is possibly based on pathophysiological markers, revealed by cerebrospinal fluid (CSF) and positron emission tomography (PET) markers of Amyloid-beta (Aβ 42) and tau in the brain. Although these clinical methodologies are relevant for AD assessment, these guidelines underline the need to extend research to non-invasive and inexpensive instrumental techniques that can be deployed in clinical environment and used for the large-scale assessment over time of a great number of individuals.

Recent advances in functional neuroimaging techniques have greatly enhanced clinical research and practice to assess brain neural networks involved in normal brain functions as well as neurological disorders. Functional MRI has considerably developed during past decades and is now commonly used for brain connectivity analysis. In the meantime, numerous studies demonstrated that electroencephalography (EEG) associated with appropriate signal processing methods can also bring valuable information for brain networks analysis (Hampel et al., 2018).

EEG has been considered as a convenient neuroimaging technique in clinical applications, suitable for cognitively and physically disabled patients, as well as for serial tests in the absence of objective cognitive decline (Babiloni et al., 2020). Besides, EEG is a non-invasive, relatively inexpensive, and potentially mobile technology. It is characterized by a high temporal resolution (about milliseconds), which is crucial for the analysis of fast dynamics in the cortex over very short duration and at different frequency ranges. Each frequency band conveys a specific physiological information on brain functional activity.

This thesis investigates the early diagnosis of AD at preclinical and prodromal stages using EEG. One of our work novelties is that we address brain network analysis by studying functional connectivity over different clinical severity stages of cognitive decline (SCI, MCI and Mild AD). To this end, we conduct a retrospective study using a clinical database that contains EEG signals recorded in real-life conditions at Charles-Foix Hospital (Ivry-sur-Seine, France).

In the literature, EEG has been exploited successfully to investigate AD-related alterations in the brain dynamics using spontaneous resting-state EEG (rsEEG) (Giaquinto and Nolfe, 1986; Briel et al., 1999). The rsEEG with eyes-closed represents a simple acquisition procedure and has three main interests : (*i*) it may be carried out rapidly in clinical settings; (*ii*) the recording at rest does not require auditory or visual stimuli that could induce fatigue commonly observed during task performance; (*iii*) EEG signals can be recorded in relatively comparable experimental conditions on

healthy subjects and patients suffering from neuropathological disorders. Nevertheless, diagnosing AD with EEG at the early stage remains a challenge. This is mainly due to the complex nature of EEG signals, which must be modeled as nonstationary, nonlinear and multidimensional time series. Moreover, EEG signal is known to have a low Signal-to-Noise Ratio (SNR), since it is strongly affected by different sources of noise that might be biological or electronic. In addition, it is difficult to extract proper EEG markers since EEG signals convey a large amount of information. Besides, the early symptoms of AD are often dismissed as normal consequences of ageing.

The literature has largely highlighted that EEG coupled with appropriate signal processing and machine learning techniques can provide precious information on normal and impaired brain networks. Some studies on early AD diagnosis have reported that AD leads to a slowing of EEG activity and a reduction of signal's complexity. These changes have been quantified as EEG markers of AD. Besides, there is a rich literature addressing the analysis of abnormalities in functional connectivity across brain regions, since AD is considered as a synaptic disconnection syndrome in its early stages. To this end, various measures have been proposed to quantify functional connectivity changes between electrodes (channels) for AD diagnosis. However, some modeling challenges are still unaddressed in such prior studies. Indeed, such measures were applied without considering the non-stationarity and multidimensionality characteristics of EEG signals.

- By contrast, in a **first study** of this thesis, we propose to use an entropy measure, termed "*Epoch-based Entropy*" (*EpEn*), that relies on a refined characterization of the local statistical properties of the EEG signal using a Hidden Markov Model (HMM), which takes into account the non-stationarity and multi-dimensionality of the EEG time series.
  This work demonstrates the effectiveness of *EpEn* for AD detection, compared to other *functional connectivity* measures largely used in the literature.

More recently, *graph theory* has gained a considerable ground to investigate topological differences between normal and abnormal brain networks. In the context of AD detection, many works have focused on the analysis of functional connectivity based on graph theory to study the brain network topology. In this case, different graph parameters are computed to characerize the graph network, and used as discriminative features for AD detection. In spite of the fact that the majority of studies have reported that the network's topology is altered in AD and MCI patients compared to healthy control subjects (HC), contradictory results are observed in the literature and common patterns of topological parameters cannot be obtained in these studies.

This is mainly due to the use of sparse data sets with different characteristics, as well as methodological differences. Indeed, the majority of works exploit databases with different characteristics, and which are subject to experimental constraints that do not correspond to the reality on the ground. Also, most studies use binary graph networks that necessitate the application of an optimal threshold on functional connectivity matrices. Usually, such a threshold value is chosen empirically which affects the resulting network.

Moreover, different metrics are used to quantify the connectivity links in brain networks. Intuitively, these classical metrics may reflect different processes leading to different brain network topologies. The majority of studies encouraged the use of a specific metric, without comparing it to others on the same database. Additionally, it is important to notice that all graph-based studies in AD express links in graph networks using only the degree of signal synchronization between electrodes,

without taking into account the complete spatiotemporal alterations due to AD, namely in terms of both complexity and inter-channel connectivity.

- Thereby, in a **second study**, we address brain network analysis over SCI, MCI and Mild AD stages using an EEG database acquired in real-life clinical conditions. The novelty of this study is twofold. Actually, this is the first study that : (*i*) addresses EEG brain network analysis over SCI, MCI and Mild AD stages simultaneously, and (*ii*) combines *EpEn* measure to graph theory since we have shown in the first study the effectiveness of this entropy measure in quantifying the complete spatiotemporal alteration due to AD.
  More precisely, we extend the use of *EpEn* to construct graph networks and demonstrate that the statistical modeling of EEG with HMM combined with entropy measure allows a better differentiation between SCI, MCI and Mild AD stages, compared to two widely used metrics, coherence and phase-lag index.
  In this study, we performed the brain network analysis on weighted and fully connected functional connectivity matrices. In other words, the adjacency connectivity matrices, which are real-valued, were not thresholded to preserve all the available information.

In this thesis, we decided to invest the largest amount of EEG information for brain network analysis, by exploiting several frequency ranges (delta, theta, alpha, beta), several electrodes locations (instead of regions), and several spatial scales (multiple graph thresholding). Therefore, another issue we tackled in this thesis is *the extraction of relevant EEG markers* to discriminate automatically between SCI, MCI and AD patients in the context of graph analysis framework.
In addition, the crucial aspect in functional networks studies is how the connectivity threshold is defined in order to obtain a graph from a connectivity matrix.

- Therefore, in a **third study**, we conduct a comparative analysis by investigating the classification performance of *EpEn* and three additional connectivity measures, namely phase lag index, coherence and mutual information, when exploited to quantify the connectivity links in brain networks. Besides, in this study, we propose a method to find the optimal connectivity threshold value that permits to obtain the best performance accuracy based on extracted binary graph parameters.

- Then, in a **fourth study**, we propose an automatic hierarchical method for EEG analysis, which allows the extraction of pertinent markers from large amount of information based on a single EEG marker (functional connectivity measure). The analysis of functional connectivity is carried out for different brain network densities, based on *binary* and *weighted* graph frameworks.
  Our proposal provides a refined analysis of EEG functional network at different density scales. It also proposes an automatic selection of the frequency band, the electrode location, and the density scale of brain network that we have to consider for discriminating between SCI, MCI and AD patients.
  To assess the robustness of our methodology, we applied it to different connectivity measures, and different weighted and binary graph parameters, and different classifiers (SVM and LDA). Finally, we assess the correlation between EEG markers that have been obtained in the last study and clinical markers at our disposal (MMSE, RL/RI-16, BREF).

1.2 Objectives of thesis

This thesis concentrates on extracting, selecting and analyzing pertinent EEG markers of early AD diagnosis, aiming at improving some of the literature lacks. In this way, this thesis:

- First, investigates the progression towards dementia by analyzing the evolution of EEG markers, especially functional connectivity, in a transversal way from SCI, MCI to Mild AD.
  - To this end, we conducted the first study that have published as book chapter in advances in Signal Processing (Houmani et al., 2021).
- Second, addresses EEG brain network analysis over the three stages of cognitive decline (SCI, MCI and Mild AD) by employing the graph theory.
  - To this end, we conducted the second study published in Bioengineering journal (Abazid et al., 2022).
- Third, investigates topological markers in a differential diagnosis context, by confronting them to the task of distinguishing AD patients from SCI and MCI subjects.
  - To this end, we conducted the third study published in Entropy journal (Abazid et al., 2021).
- Fourth, proposes a new methodology to identify relevant features to discriminate between SCI, MCI and Mild AD, considering different frequency bands, electrode locations and network density scales.
  - To this end, we conducted the fourth study published as international Patent.

1.3 Outline of this thesis

- Chapter 1 introduces the scientific context, objectives, outline, and contributions of this thesis.
- Chapter 2 introduces the background statement:
  - The first section introduces Alzheimer's disease (AD), crucial factors in AD, the evolution of AD, and diagnostic tools of AD.
  - The second section introduces electroencephalography (EEG), the electric source of EEG signals, the mechanism of EEG recording, and EEG rhythms.
- Chapter 3 reports the most pertinent findings of studies that addressed the early diagnosis of AD with EEG. Since the thesis focuses on the analysis of abnormalities in brain functional connectivity, we present in details some functional connectivity measures that are exploited in this thesis.
- Chapter 4 introduces graph theory, graph basics and graph parameters. In this chapter we also summarize precedent works that have exploited graph theory in the context of brain network analysis for cognitive decline patients.
- Chapter 5 introduces the first study investigating the use of the statistical entropy-based measure (*EpEn*) for AD detection to demonstrate its effectiveness as a connectivity measure.

- Chapter 6 introduces the second study on weighted brain network analysis that addresses brain network analysis over different clinical severity stages of cognitive dysfunction. In this study, we extend the use of *EpEn* to brain network assessment and demonstrate its effectiveness with different weighted graph parameters.

- Chapter 7 introduces the third study that performs a comparative study of several connectivity measures for AD detection. We investigate the classification performance of *EpEn* as well as three additional connectivity measures, namely phase lag index, coherence and mutual information. In this study, we demonstrate the effectiveness of *EpEn* with different binary graph parameters.

- Chapter 8 introduces the fourth study which consists on a multi-scale density analysis of EEG signals for AD diagnosis context, proposing a new approach of features selection based on an automatic hierarchical method for EEG analysis, which allows the extraction of pertinent markers from big amount of information based on a single functional connectivity measure. The analysis of functional connectivity is carried out for different brain network densities, based on both weighted and binary networks. In addition, we assess the correlation between EEG markers and clinical data (MMSE, RL/RI-16, BREF).

1.4 Research publications

- **M. Abazid**; N. Houmani; B.Dorizzi ; J.Boudy, ; J.Mariani ;K. Kinugawa, Weighted Brain Network Analysis on Different Stages of Clinical Cognitive Decline. Bioengineering 2022, 9, 62. https://doi.org/10.3390/bioengineering9020062

- N. Houmani, **M. Abazid**, K. De Santiago, J. Boudy, B. Dorizzi, J. Mariani, K. Kinugawa-Bourron, EEG signal analysis with a statistical entropy-based measure for Alzheimer's disease detection, open access book, Advances in Signal Processing: Reviews, Book Series, Vol. 2 published by IFSA Publishing, S.L., accepted, publication in 2021.

- **M. Abazid**; N. Houmani; B.Dorizzi ; J.Boudy, ; J.Mariani ;K. Kinugawa, A Comparative Study of Functional Connectivity Measures for Brain Network Analysis in the Context of AD Detection with EEG. Entropy 2021, 23, 1553. https://doi.org/10.3390/e23111553

- N. Houmani, **M. Abazid**, J. Boudy, B. Dorizzi. Epoch-based Entropy: A Statistical EEG Marker for Alzheimer's Disease Detection, in Proceedings of the Entropy 2021: The Scientific Tool of the 21st Century, MDPI: Basel, Switzerland, 5–7 May 2021.

- N. Houmani, **M. Abazid**, Method for selecting features from electroencephalogram signal, Patent N° et date of publication : WO2021254788 - 23/12/2021, EP3925520 - 22/12/2021.

Chapter 2

Background statement

This thesis investigates the early diagnosis of Alzheimer's disease (AD) at preclinical and prodromal stages using electroencephalography (EEG). This research topic involves different basic knowledge that should be presented. Therefore, in this chapter, we first present AD, its evolution stages, and the associated clinical markers, as well as the current clinical tools and neuroimaging techniques used to establish the AD diagnosis. Then, we introduce EEG and motivate its use for pathology detection.

2.1 Alzheimer's disease

Today, with the unprecedented aging of the population in the world, linked to the improvement of living conditions through advances in medicine and hygiene, dementia and neurodegenerative diseases have become a major societal concern, imposing an important burden on modern societies.

Dementia involves several neurodegenerative disorders caused by damage and death of neurons. It induces alterations in cognitive and behavioral functions sufficiently important to affect daily life, and which last for at least 6 months (DSM-IV- TR). The loss of autonomy of the patient is not necessarily severe at the beginning and can last for several years.

Alzheimer's disease (AD) is the most common form of dementia (Reitz et al., 2011); it affects 11% of the world population aged over 65 (Ferri et al., 2005) and is responsible for nearly 70% of all dementia cases. Its incidence increases exponentially with age, and doubles every 5 years after the age of 65 (Qiu et al., 2009; Corrada et al., 2010). According to the French study by PAQUID, it is estimated that beyond the age of 75, there is a 17.8% chance of developing AD (Ramaroson et al., 2003). The number of individuals with AD is expected to reach 115 million by 2050 (Li et al., 2013). Unlike other diseases that have reported decrease incidence in recent years, the number of deaths related to AD has increased by 89% between 2002 and 2014 (Gaugler et al., 2022).

AD is characterized by progressive and irreversible brain damage, associated with cognitive dysfunctions and possibly behavioral or personality disorders. AD begins long before the dementia stage. As the disease evolves, the patient will develop severe memory impairments inducing a complete loss of autonomy. The causes of AD are not identified; however, there is an increase evidence that the aggregation of two proteins, amyloid-beta and tau, are characteristics of AD. Historically, memory impairment is one of the first symptoms that helps in the clinical characterization of AD.

No medication exists for curing this pathology and many therapeutics trials failed. Therefore, the early detection of AD becomes an important issue for the scientific and medical community. Even if the available treatments cannot stop or reverse the disease progression, early therapeutic interventions may delay its evolution and maintain the independence of the patient for a time. Moreover, AD diagnosis at the early stage can help the patient and his caregivers to anticipate the future.

2.1.1 Brief history

It was in 1906 when Alois Alzheimer (1864-1915), a German psychiatrist, described for the first time a disease linked to aging which he called "disease of forgetting", later called Alzheimer's disease, following his experience with a patient named Auguste Deter (see Fig. 2.1). She was admitted to a hospital in Frankfurt, Germany, in November 1901, when she was 51 years old. Dr. Alzheimer has observed in the patient severe memory loss, disorientation, aphasia, unpredictable behavior as well as paranoia, hallucinations and severe social isolation.

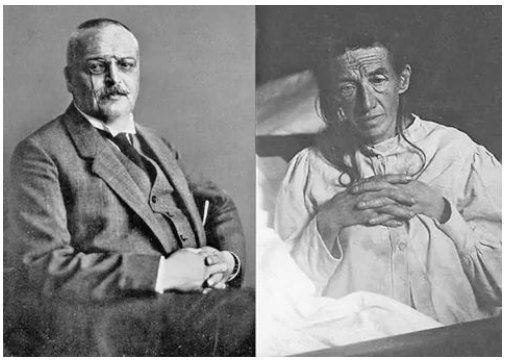

Figure 2.1: Dr. Alois Alzheimer and his first patient Auguste Deter (Maurer et al., 1997).

During the follow-up of the patient, Dr. Alois Alzheimer asked her to perform psychophysical tests including a panel of questions such as if she was still able to perform simple calculations, to answer certain questions correctly. He reported that if we take too long to ask her the question, she answers off-topic. This exchange, published in 1997 (Maurer et al., 1997), perfectly transcribes the influence of the pathology on his patient:
"I show her three fingers; how many fingers? Three.
Are you still anxious? Yes.
How many fingers have I shown you? Well, this is Frankfurt am Main."

She also had great reading difficulties. If she deciphers the letters correctly, she does not seem to understand the meaning of the words, and rereads the same first three sentences repeatedly. Writing skills are also impaired; when she was asked to write her name and surname, the words had been repeated many times because she forgets what she writes quickly. It was during trying to write her name that she repeated this famous sentence: "*I've lost myself*".

When Auguste died in April 1906, Dr. Alzheimer asked her family for permission to carry out an autopsy to undertake an in-depth study of her brain to investigate the causes of the disease that led her to die. He then observed a brain atrophy (see Fig. 2.2), without macroscopic focal degeneration,

and the vascular tissues showed an arteriosclerotic change. The microscopic observation allows him to report the microscopic changes in the cortex of Auguste describing miliary foci of extracellular structures, which later would be known as *neuritic plaques* and intracellular bundles that would be named *neurofibrillary tangles*. This is how Dr. Alzheimer first described the neuropathological features of AD, which were later found in other patients presenting the same symptoms as Auguste Deter.

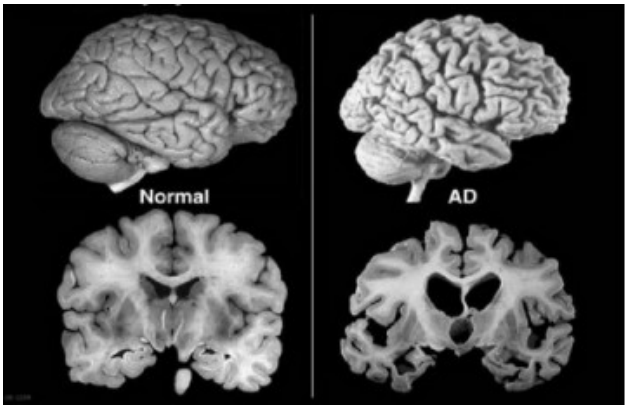

Figure 2.2: Brain atrophy in advanced Alzheimer's Disease (Bagad et al., 2013).

2.1.2 Crucial factors in AD

Growing evidence shows that AD is clinically characterized by the pathological deposition of extracellularly neuritic plaques and intracellularly neurofibrillary tangles, as well as the loss of basal forebrain cholinergic neurons (Sadigh-Eteghad et al., 2015). The *neuritic plaques*, produced outside neurons, are composed of a core of amyloid-beta peptide (Aβ) that alter the synaptic transmission between neurons (Wong et al., 1985; Daulatzai, 2010; Shen, 2004). The *neurofibrillary tangles* (see Fig. 2.3), produced inside neurons, contain hyperphosphorylated tau peptides that obstruct the transport of nutrients to the neuron. The number of neurofibrillary tangles is related to the degree of brain damage exhibited in the patient (Brion, 1998).

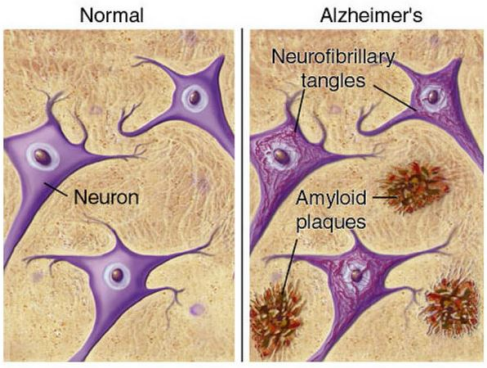

Figure 2.3: Amyloid Plaques and Neurofibrillary Tangles (Famer, 2007).

It has been suggested that many years prior the appearance of clinical symptoms of AD, the aggregation of both (Aβ) and neurofibrillary tangles occurs within the neocortex, hippocampus, and other subcortical structures (Nordberg, 2008) (see Fig. 2.4). At the early stage, AD affects limbic regions related to episodic memory, which leads to a relative inability to retain new information. In addition, a disruption of fronto-hippocampal connections has been observed in the early stage of AD, in parallel with hippocampal atrophy, and it has been reported that it may contribute to the initial memory impairment in AD patients (Rémy et al., 2015). Over time, AD spreads to other brain regions (Braak et al., 1999) and affects other cognitive functions, such as executive functions, attention, visuospatial and language abilities (see Fig. 2.4).

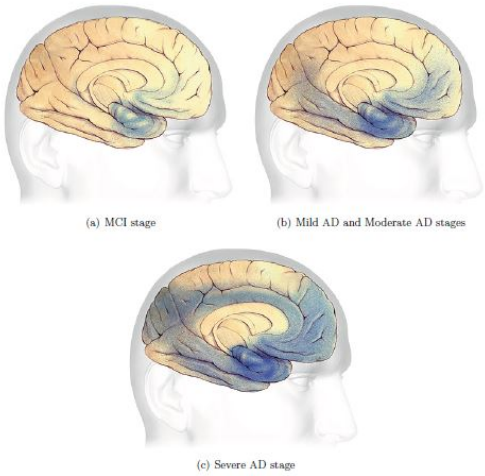

Figure 2.4: Evolution of AD in the brain. Plaques and tangles (shown in the blueshaded areas) tend to spread through the cortex in a predictable pattern as AD progresses (Gaugler et al., 2022).

AD can be caused by multiple factors. Age is one of the most risking factors to develop a cognitive impairment. AD is considered to be early-onset Alzheimer's if it affects a person under 60. People with early-onset AD can be in the early, middle or late stage of the disease. Genetic factors also take part in AD development; they are more obvious for the early-onset AD (Tanzi, 2012). It is reported that 70% of AD cases were related to genetic factors (Silva et al., 2019). Other risk factors such as vascular disease, head injury, infection and environmental factors can also be involved in the disease. All the above-mentioned risk factors may act collectively to cause AD pathology.

2.1.3 Progression of the disease

AD is a chronic neurodegenerative disorder, characterized by progressive brain damages, including memory impairments and a wide range of cognitive dysfunctions. AD is a continuous process that can progress through five stages: preclinical AD, mild cognitive impairment due to AD, mild, moderate and severe dementia stages. It is worth noticing that these stages are just rough view of the disease continuum and the symptoms might vary between individuals.

The term "*dementia*" is used to describe a group of symptoms that affect intellectual and social abilities severely enough to have an impact on the daily life of the patient. In this case, the patient must be helped or supervised, at least for the most complex activities. Dementia is not

a single condition; it is caused by different diseases of the brain, such as AD, vascular disease, frontotemporal lobar degeneration, Lewy body disease, and Parkinson's disease.

AD dementia is preceded by the asymptomatic "*preclinical*" stage, before the onset of the clinical phenotype. It is characterized by the absence of overt symptoms (Price et al., 2009), but the brain lesions of AD start to occur. At this stage, the concept of *Subjective Cognitive Impairment* (SCI) has been proposed recently, defined by a self-experienced persistent decline in cognitive capacity in comparison with a previously normal status (Jessen et al., 2014). These subjective complaints are considered as elderly at-risk for AD (Mitchell et al., 2014; Dubois et al., 2016). Indeed, this phase may start up to years or decades before the first clinical symptoms of AD become apparent.

Then, in the "*prodromal*" stage, *Mild Cognitive Impairment*(MCI) patients maintain their functional capacities but exhibit measurable memory impairments, some language difficulties and concentration deficits (Dubois et al., 2016; Petersen et al., 2009). These subtle changes are not significant enough to affect work or social relations yet, but they are generally noted by the persons who are closely to the MCI patient. It has been observed that over a 5 to 10 year period after a diagnosis of MCI due to AD, 30% to 50% of people progress to Alzheimer's dementia. Nevertheless, 30% of MCI subjects will not progress to AD in near future (Mattsson et al., 2009; Dubois et al., 2007; Albert et al., 2011). Due to the long prodromal period of AD, early diagnosis of AD at this stage is of high interest.

In the "*Mild AD*" stage, cognitive deficits are more marked, such as memory and learning impairments. At this stage, the patient may experience memory troubles, loss of spontaneity, difficulty with problem-solving and daily tasks execution, trouble handling money and paying bills, getting lost and misplacing belongings. The patient perceives these symptoms, which induces frustration. Some psychological symptoms can thus also appear at this stage, such as compulsive behavior and suspiciousness. AD is often diagnosed at this stage.

The above-mentioned deficits become more severe in the "*moderate*" stage. During this stage, the patient grows more confused and begins to need more help with daily activities and self-care. The patient may show greater memory loss, increasingly poor judgment leading to bad decisions and deepening confusion, as well as significant changes in personality and behavior. Assistance is required to help in daily life activities.

In the final "*severe*" stage of the disease, almost all cognitive functions and motor abilities are significantly deteriorated. The patients lose the ability to communicate coherently and lose autonomy in daily life activities, becoming completely dependent on caregivers. The average duration of survival of AD patients is 5-8 years after clinical diagnosis (Helzner et al., 2008).

2.2 Diagnosis of Alzheimer's disease

The early diagnosis of AD has three main interests. First, the early detection can prepare the patient and his family emotionally and financially to better face the future. Second, it helps the patient and his caregivers to understand the daily consequences of the disease. Finally, even if treatments cannot stop the disease, it is very likely that the effectiveness of therapeutic interventions will be higher in the early stages of the disease, before neurodegeneration spreads too much (Dauwels et al., 2010a).

However, a reliable early diagnosis of AD is still a challenge. Indeed, the pathophysiological development of AD may start up to 20 years before the appearance of clinical symptoms (Dubois et al., 2007; Sperling et al., 2014). Also, the early symptoms of AD are often dismissed as normal consequences of aging, which frequently delays the diagnosis (Alberdi et al., 2016). In addition, AD is a pathology whose evolution presents a large inter-subject variance, as illustrated by the different phases of cognitive decline that can be observed. Consequently, it is easier to diagnose a patient in the severe stages of the disease than in its early stages.

Up to now, definite AD diagnosis is only possible postmortem, when examination after death reveals the presence of structural brain damage related to the disease. Establishing the in vivo diagnosis of AD relies on a battery of various clinical criteria, including neurological tests and medical recordings. The current clinical criteria for AD diagnosis were determined in 2011 by the National Institute on Aging and the Alzheimer's Association (NIAAA) (McKhann et al., 2011; Albert et al., 2011; Jack Jr et al., 2011; Sperling et al., 2011). These criteria are an update of the previous widely used guidelines established in 1984 by the National Institute of Neurological and Communicative Disorders and Stroke (NINDS) and the Alzheimer's Disease and Related Disorders Association (ADRDA) (MCKHANN, 1984).

The Mini Mental State Examination (MMSE) (Folstein et al., 1975; Mitchell, 2009), established in 1975, is the most used test to assess cognitive functions for AD diagnosis. The maximum test score is 30; if the score is lower than 10, cognitive impairment is considered severe; if the score is lower than 18, cognitive impairment is moderate; if the score is higher than or equal to 23, the cognitive impairment is mild. In practice, it is considered that there is a probability of developing AD if the MMSE is less than 26 (see Fig. 2.5). No specialized equipment or training is required to perform this test, making longitudinal assessment of AD more feasible.

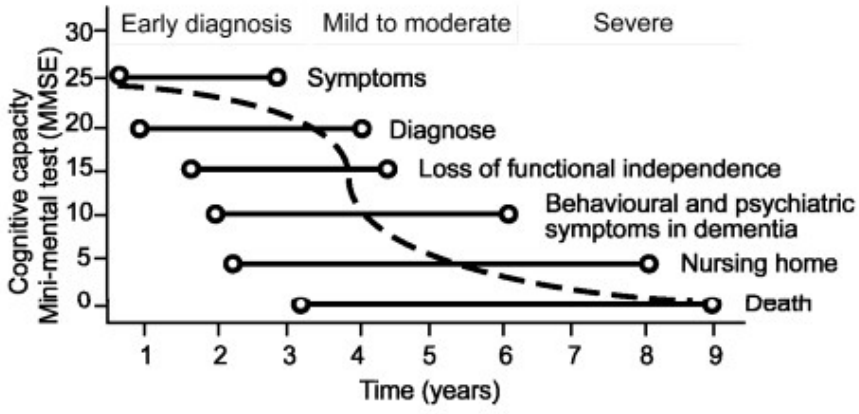

Figure 2.5: Clinical stages in Alzheimer's Disease: cognitive capacity measured with MMSE (Freund-Levi et al., 2006).

However, the MMSE is greatly affected by demographic factors, particularly age and education, in addition to its lack of sensitivity to MCI. Thus, additional tests are also used, such as the Montreal Cognitive Assessment (MoCA) (Nasreddine et al., 2005) and Addenbrooke's Cognitive Examination revised (ACE-R) (Mathuranath et al., 2000). Other neurological tests used in clinical practices are

the Severe Cognitive Impairment Scale, the Alzheimer's Disease Assessment Scale Cognitive, the neuropsychological test battery, and the Severe Impairment Battery (Alberdi et al., 2016). Moreover, the Trail Making Test (Amodio et al., 2002) and the clock-drawing test (Shulman, 2000) are frequently used to assess cognitive abilities, as well as attention and executive functions. The Rey Auditory Verbal Learning Test is also a neuropsychological test designed to evaluate verbal memory in patients (Al-Qazzaz et al., 2014).

Using neuropsychological tests and medical recordings for AD diagnosis is time consuming and requires experienced clinicians. As an alternative, during the last few years, there has been an increase development of markers (Dubois et al., 2016; Al-Qazzaz et al., 2014; Tapiola et al., 2009). Some of them evaluate the brain myloidosis and tauopathy, such as amyloid and tau tracer PET (Positron Emission Tomography) scans, and Cerebrospinal fluid (CSF) concentrations of Aβ42 and P-tau. Other markers evaluate neural injury, such as T-tau in CSF and Fluorodeoxyglucose-PET (FDG-PET) (Tapiola et al., 2009). It has been shown for example that Aβ42, the most common CSF biomarker, present low values in AD patients compared to healthy subjects (Ferreira et al., 2014). Of note, such markers are obtained after a lumbar puncture, which is an invasive process limiting its use in daily clinical practice. Blood markers, such as plasma T-tau, are also exploited since the extraction process is less invasive, but stills expensive (Olsson et al., 2016).

Neuroimaging techniques like Magnetic Resonance Imaging (MRI), Magnetoencephalography (MEG), PET, and Computed Tomography (CT) are also used to analyze the brain damage due to the disease. However, these techniques are costly, time consuming, and require expertise for maintaining and running the systems. Besides, when the brain damage is detected by these technologies, AD is often already well progressed and the brain atrophy is already extended (Alberdi et al., 2016). Also, such technologies present some accessibility issues. Actually, they are not available in all hospitals, particularly in low-income countries or remote regions, causing displacements of patients, which is not comfortable and practical.

According to the most recent guidelines (McKhann et al., 2011; Dubois et al., 2014), AD can be diagnosed in preclinical and prodromal stages, before the manifestation of any cognitive and behavioural symptoms. This could be possibly based on pathophysiological markers, revealed by CSF and PET markers of Aβ42 and tau in the brain. However, such guidelines also underline the need to extend research to non-invasive and inexpensive instrumental techniques, which can be deployed in clinical environment and used for large-scale assessment. Electroencephalography (EEG) is a neuroimaging technology suitable to fulfil this need.

2.3 Electroencephalography

Electroencephalography (EEG) is a very old neuroimaging technique used for recording the brain electrical activity. The first known neurophysiologic recording on animals was conducted by Richard Caton in 1875. Hans Berger, a German psychiatrist, pioneered EEG in humans in 1924 by developing a recording technique connecting the electrodes to the scalp.

Since then, EEG has widely used to evaluate the dynamic cerebral functioning, particularly for medical applications. Actually, EEG is appropriate for cognitively and physically disabled pa-

tients, as well as for serial tests particularly in the absence of objective cognitive decline (Sperling et al., 2014). It has the advantage of being a non-invasive, cost-effective, and mobile neuroimaging technology. Besides, it allows recording the brain dynamics with excellent time resolution in the millisecond range. Figure 2.6 shows the classification of the neuroimaging techniques in terms of time and spatial resolution.

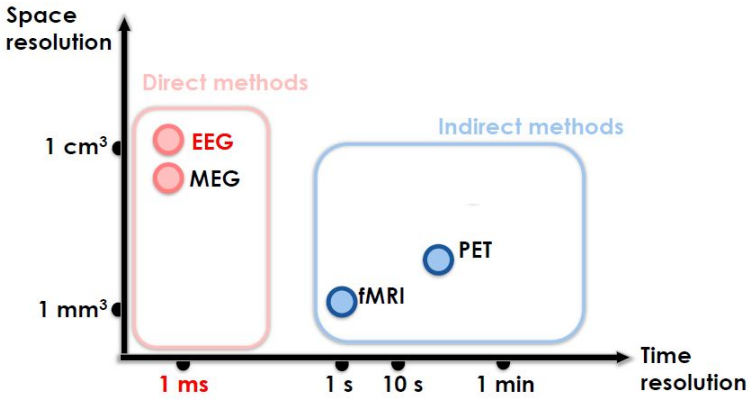

Figure 2.6: Temporal and spatial resolutions of the most commonly used functional brain imaging techniques (Pfister et al., 2014).

Nevertheless, EEG is not yet largely deployed in clinical settings, mainly due to the difficulty of its interpretation that requires specific neurophysiology expertise. Initially, the analysis of EEG signals in hospitals is done manually by electrophysiologists, which perform visual inspection and interpretation of EEG traces. The results were thus unreliable and the analysis process was time consuming. Thanks to progress in biomedical engineering and data processing, it became possible to analyze EEG signals digitally. Recent advances in bioinstrumentation coupled with relevant AI-based techniques have made possible consistent improvements in extracting digital markers for EEG signals and characterizing normal brain activity and impaired activity related to AD (Alberdi et al., 2016).

2.3.1 Electric source of EEG signals

The brain consists of approximately 100 billion of neurons interconnected through synapses (see Fig. 2.7). The synaptic activity generates a subtle electrical impulse, called postsynaptic potential. The electrical activity measured by scalp EEG (in micro-volts) is generated by the ionic currents in the dendritic membrane of similarly oriented groups of cortical pyramidal neurons (see Fig. 2.8). These pyramidal cells of neurons are oriented perpendicularly to the surface of the head. These neurons have cell bodies primarily in layers III and V of the cerebral cortex.

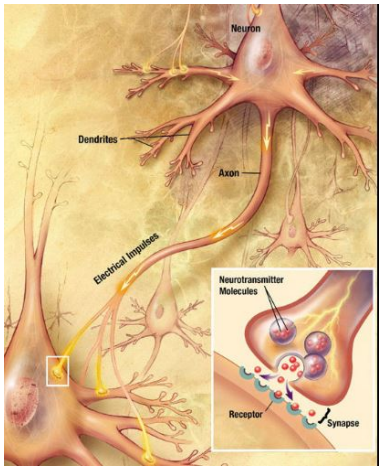

Figure 2.7: Major elements in chemical synaptic transmission and the process of synaptic transmission in neurons. Source: US National Institutes of Health, National Institute on Aging.

The electrical activity recorded on the scalp represents the summation of the postsynaptic potentials from thousands of pyramidal neurons fire in synchrony. This summated activity of extracellular ionic currents is strong enough to flow through the brain tissue, bone, and skull to the recording electrodes on the scalp (Figure 2.8). This biophysical phenomenon is referred as to head volume conduction. Each scalp electrode collects, at a minimum, approximately 10 cm^2 synchronous cortical activity. This limits the spatial resolution of EEG unlike functional MRI. Thus, EEG can be considered as a complex combination of electrical activities generated in different parts of the brain at the same time.

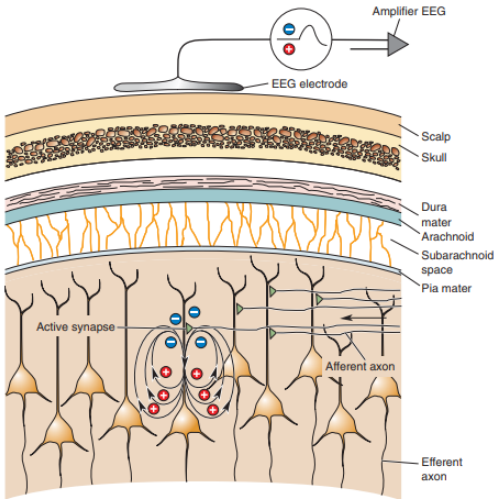

Figure 2.8: Electrical fields generated by aligned pyramidal cells (Nunez, 1981).

Of note, when measuring brain activity with scalp EEG, the recorded signals may be unfortunately contaminated by various biological and instrumental noises. Biological noise is related to non-neuronal ionic currents or potentials, such as ocular, muscular and cardiac activities. While,

instrumental noise is due to recording systems and environmental electromagnetic sources. Such artifacts may interfere with neural information and thus affect the analysis of EEG signals. Thereby, it is essential to effectively pre-process the captured raw EEG signals to detect and extract clean EEG data. Several techniques exist to remove artifacts; nevertheless, the related research is still an open problem.

2.3.2 EEG recording

EEG signal is commonly recorded by placing electrodes (sensors) on the scalp. We distinguish wet electrodes that require an electrolytic substance (electro gel), and dry electrodes that do not need the use of any substance, making contact directly with the scalp.

Gel electrodes are the most frequently used sensors for recording EEG signals in clinical practice. They have long been the gold standard in EEG research. The electrodes are commonly made of silver with a coating of silver chloride (Ag/AgCl). By applying between the skin and this electrode a gel containing chloride ions, the conductivity is improved and the impedance at the interface of the skin and the electrode is reduced. This allows obtaining a signal recording with good quality.

The recording of EEG signals is typically obtained by placing scalp electrodes at standard positions (see Fig. 2.9), according to the *international 10-20 system*. It relies on four stable anatomical points of the skull, referred as skull landmarks: nasion (point between the forehead and nose), inion (bump at the back of the skull) and two pre-auricular points. The "10" and "20" refer to the fact that the actual distances between adjacent electrodes are either 10% or 20% of the total distances measured from nasion to inion, and from left pre-auricular to right pre-auricular.

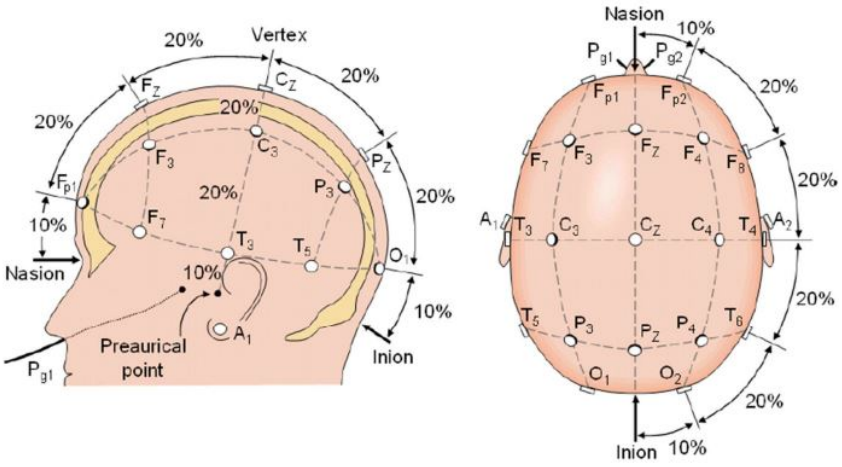

Figure 2.9: Placement of electrodes used for EEG signal recordings according to the 10-20 system (Malmivuo et al., 1995).

Each electrode has a standardized name that consists of a letter abbreviation of the underlying brain region and a number indicating the precise location on the right or the left side of the head. The letters are Fp (frontal-polar), F (frontal), T (temporal), C (central), P (parietal) and O (occipital).

Even numbers (2, 4, 6 and 8) denote electrode positions on the right hemisphere, while odd numbers (1, 3, 5 and 7) correspond to those on the left hemisphere. The electrodes placed on the midline are identified by the letter "z" instead of a number: Fz, Cz, Pz, and Oz. Electrodes closer to the midline have lower numbers and those that are farther away from the midline have higher numbers.

As the electrical activity measured at the scalp electrodes is very small (in the range of microvolts), the collected data is digitized and amplified. Price differences of EEG recording systems are generally due to the number of electrodes, the sampling rate value, the quality of the digitization and the amplifier.

Electrophysiology can be studied in AD patients during a variety of experimental conditions, including sleep, quiet wakefulness, and during sensorimotor activities. The literature has shown that EEG has been exploited successfully to investigate AD-related alterations in the brain dynamics using resting-state EEG (rsEEG) with eyes-closed (Giaquinto and Nolfe, 1986; Briel et al., 1999). EEG recordings performed in a resting state allows capturing spontaneous neural activity, which is pertinent to investigate the fundamental brain state. The recording of rsEEG represents a simple acquisition procedure and has three main interests. First, it may be carried out rapidly in clinical settings. Second, the recording at rest does not require auditory or visual stimuli that could induce fatigue commonly observed during task performance. Third, EEG signals can be recorded in relatively comparable experimental conditions on healthy subjects and patients suffering from neuropathological disorders. A routine EEG recording lasts between 20 and 40 minutes, including some preparation time at the beginning and some time at the end. To faster the recording, electrodes are often mounted in elastic caps, ensuring that EEG signals are captured from identical scalp positions in all patients. To record rsEEG, the patient is usually seated in an armchair in a comfortable position and quiet environment, and will be asked to close his eyes.

2.3.3 EEG frequency rhythms

The analysis of EEG signals for AD diagnosis is performed either in the time domain or in specific standard frequency bands, each of which has different functional characteristics. In adults, typical frequency bands and their approximate spectral boundaries are: delta (1–4 Hz), theta (4–8 Hz), alpha (8–12 Hz), beta (12–30 Hz), and gamma (30–100 Hz). The decomposition of the overall power in the EEG signal into specific frequency bands is commonly achieved through spectral analysis methods. Figure 2.10 shows examples of EEG signals extracted in such frequency ranges.

Delta: 1 - 4 Hz

Delta rhythm is the slowest of the five rhythms with the highest amplitude. It is related to unconscious and deep sleep state. In fact, it occurs during deep sleep with rapid eye movements, and during severe brain pain. It is prominent frontally in adults and posteriorly in children. This is the dominant rhythm for young children under one year old. We are increasing our delta rhythm in order to decrease our awareness of the physical world; at that moment, the cellular divisions take place as well as the production of growth hormone, which explains why sleep is important for children.

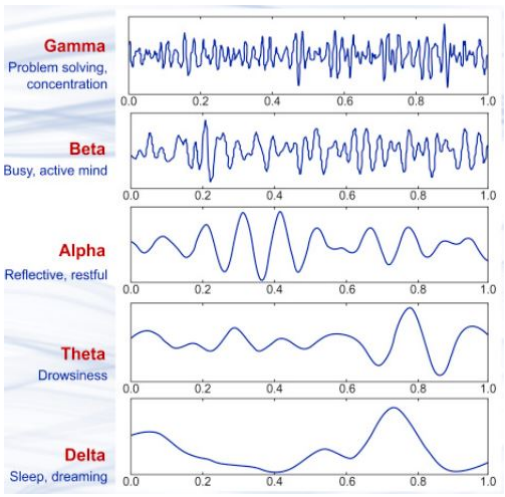

Figure 2.10: EEG dominant rhythms (Abhang et al., 2016).

Theta: 4 - 8 Hz

Theta rhythm is classified as slow activity. It is often associated with drowsiness, childhood and young adulthood. It reflects the state between wholeness and sleep. It appears during meditation and spiritual activities. It is located in the prefrontal part of the cortex. Accentuated theta waves during the waking state may indicate brain performance issues due to neurological impairments.

Alpha: 8 - 12 Hz

Alpha rhythm is the well-known and most investigated human brain rhythm since it is observable in almost all the populations. Alpha brainwaves are dominant in normal relaxed adults. They clearly appear when closing the eyes and relaxing, particularly in the occipital region. This state of relaxation is a transition stage between wakefulness and sleep. The subject is then dozed off but remains very sensitive to external stimuli. Alpha rhythm is present during most of life especially after the thirteenth year. Accentuated alpha waves in the frontal region has shown to indicate for example ADHD and depressive symptoms.

Beta: 12 - 30 Hz

Beta rhythm is classified as fast activity. It shows low amplitude with a large range of frequencies. Beta rhythm is associated with the engaged brain. This rhythm is observable at different locations in the cortex according to the cognitive state (busy thinking, reasoning, active concentration, etc.). This rhythm is dominant in persons during normal state of wakefulness with eyes open and in persons who are alert or anxious. It is accentuated by the effect of sedative hypnotic drugs, particularly the benzodiazepine, and it may be reduced in regions of cortical damage. The theta/beta ratio reveals how much resting brainwave activity (theta) we have and how much active brainwave activity (beta) we have. This ratio was for example used to diagnose Attention Deficit Hyperactivity Disorder (ADHD) using EEG.

Gamma: 30 - 100 Hz

One of the first articles describing this rhythm appeared in 1964. Gamma rhythm reflects how the brain is hard at work. It is associated with conscious awareness, feelings of happiness and higher mental activity, including perception, learning, problem solving, and fear.

Gamma brainwaves are hard to measure accurately with current EEG technology, which explains the limited studies in the literature investigating this rhythm. In this thesis, we do not consider this rhythm. Actually, we decided to focus only on delta, theta, alpha and beta rhythms, which are largely addressed in the literature for AD detection using resting state EEG. This allows us to compare our results to the state-of-the-art findings.

2.4 Conclusion

In this chapter, we presented basic knowledge related to our research topic. We motivated on the one hand the utility to conduct our research work on AD diagnosis; and on the other hand, the crucial need to detect AD at early stages, especially at preclinical and prodromal stages.

We have also highlighted the utility of using EEG as a convenient technique for AD diagnosis. However, it is not easy to extract proper digital markers from EEG signals for AD diagnosis, particularly at the early stage. Indeed, EEG signals are of complex nature; they should be modeled as multidimensional time series and analyzed in frequency domain. Also, EEG signals have low signal-to-noise ratio (SNR) since they are strongly affected by various biological and electrical noises. Besides, the early symptoms of AD are often dismissed as normal consequences of ageing. Furthermore, AD is a multifactorial pathology which makes its diagnosis more difficult.

In this thesis, we aim at proposing novel methods inherited from information theory, pattern recognition and signal processing to process and analyze EEG time series for early diagnosis of AD. We will investigate specifically brain functional connectivity since AD is considered as a disconnection disease whose early stages are due to synaptic failures.

Chapter 3

Early diagnosis of Alzheimer's disease using EEG

Numerous studies in the literature have revealed changes in EEG signals recorded in eyes-closed resting-state condition at the early stage of AD. It is largely admitted that AD induces three impacts on EEG signals: *(i)* slowing of EEG activity; (*ii*) reduction in the complexity of EEG signals; and (*iii*) perturbation in EEG functional connectivity. By using appropriate signal processing methods, several measures have been proposed to quantify these AD-related changes, then considered as EEG markers, referred to as features, for AD diagnosis.

In this chapter, we report the most pertinent findings of the above-mentioned studies addressing the early diagnosis of AD with EEG. Since the thesis focuses on the analysis of abnormalities in brain functional connectivity, we also present in details some functional connectivity measures that are exploited in this thesis.

3.1 Slowing of EEG activity

Signal slowing is one of the main effects of AD on EEG time series. As mentioned in Section 2.3.3, one is often interested in specific frequency bands in the EEG, namely delta, theta, alpha, and beta. AD affects these frequency bands in specific ways. Therefore, in order to assess the slowing effect on EEG, we usually compute the relative power in the above-mentioned standard EEG frequency bands. In case of a larger relative power in low frequency bands (*i.e.* delta or theta) than usual, it is said that EEG slowing occurs.

Previous studies on EEG and evoked potential have highlighted increased background EEG delta and theta slow activity, accompanied by decreased or absent of alpha (Duffy et al., 1984). These findings were obtained based on the comparison of healthy age-matched controls with patients suffering from presenile and senile dementia of the Alzheimer type.

On resting-state EEG (rsEEG), many studies have reported a common finding: MCI and AD lead EEG signals to slow down (Babiloni et al., 2020; Dauwels et al., 2010a; Babiloni et al., 2016; Jelic et al., 2000; Brassen and Adler, 2003; Onofrj et al., 2003; Ponomareva et al., 2003; Jeong, 2004; Dauwels et al., 2011). Indeed, EEG spectral analysis have highlighted an increase of power in low frequencies (delta and/or theta band) and a decrease of power in higher frequencies (alpha and/or beta) in MCI and AD comparatively to healthy controls. Note that the alteration of EEG relative

power is more clear in the literature for AD patients.

Early stages of AD have been associated with an increase of theta activity and/or a decrease of alpha activity (Ihl et al., 1996; Vialatte et al., 2011). In more severe stages of AD, an increase of both theta and delta activities has been noticed together with a decrease of both alpha and beta activities, additionally to a reduction in the amplitude of the peak of alpha frequency band (Ihl et al., 1996; Vialatte et al., 2011). Moreover, alpha rhythms are usually localized in the occipital region for healthy controls; in AD patients, they increasingly move towards anterior brain regions as the disease evolves (Babiloni et al., 2004a; Claus et al., 1998; Kowalski et al., 2001).

Power density of rsEEG rhythms have also been evaluated in many longitudinal studies in order to predict cognitive decline at follow-up. Actually, in (Jelic et al., 2000), the authors investigated the progression towards the MCI stage. It has been reported that MCI leads to power activity increase in the occipital and temporal regions for delta and theta bands, while the power activity for the same regions is reduced in alpha and beta. The same phenomenon has been observed in the occipital brain region of AD patients (Coben et al., 1985). Furthermore, in (Babiloni et al., 2011), high power density of the posterior lobe in alpha band has been exploited to predict the global cognitive stability status in MCI subjects at 1-year follow-up.

Besides, a more recent study reported that microstate transitioning was slower and less complex in AD. More precisely, the microstate associated with the fronto-parietal working-memory/attention network was altered in AD due to parietal inactivation (Tait et al., 2020).

3.2 EEG complexity reduction

Several measures have been used to quantify the complexity of EEG signals. The fractal dimension was exploited to assess the complexity of EEG signals for discriminating between healthy controls and AD patients (Adeli et al., 2008; Ahmadlou et al., 2011; Grassberger, 1983; Grassberger and Procaccia, 2004). The correlation dimension and the first positive Lyapunov exponent were used (Adeli et al., 2005; Jelles et al., 1999; Jeong et al., 1998, 2001a; Takahashi, 2013; Yagyu et al., 1997). The correlation dimension quantifies the number of degrees of freedom that are necessary to characterize a dynamical system. The Lyapunov exponent quantifies the divergence of trajectories starting at nearby initial states. A positive maximal Lyapunov exponent is associated to a chaotic system. It has been largely reported that EEG signals of AD patients show lower values of such measures (lower complexity) than signals of age-matched healthy controls. However, the literature pointed out that these two measures need high consuming calculation because of the reconstruction of a phase space trajectory.

Many studies used alternative methods more adapted for sparse data to quantify signal complexity. Most of these methods are inherited from information theory and exploit the concept of entropy (Thomas and Joy, 2006): sample entropy (Abásolo et al., 2006a), Tsallis entropy (De Bock et al., 2010), approximate entropy (Abásolo et al., 2005; Pincus, 2006), multi-scale entropy (Escudero et al., 2006), and Lempel-Ziv complexity (Abásolo et al., 2006b).

Entropy is one of the most commonly used nonlinear concept to evaluate the characteristics of a dynamic system or a signal. The formulation of entropy was introduced by Shannon in 1948 and is generally referred to as "*Shannon's entropy*". The concept of entropy is central in physics

and information theory, and its interpretation depends on the application. In physics, entropy is a measure of the disorder: the higher the disorder, the larger the entropy of the system. In information theory, entropy is a measure of the uncertainty associated with a random variable: it quantifies the predictability of future realizations of the signal based on the probability distribution of past realizations. In other words, it quantifies the randomness of a given process or a variable (Thomas and Joy, 2006).

Given a discrete random variable X, with n possible realizations $x_1, ..., x_n$, which occur with probabilities $P(x_1), ..., P(x_n)$, the Shannon's entropy of X is formally defined as:

$$H(X) = -\sum_{i=1}^{n} P(x_i).log_2(P(x_i)) \tag{3.1}$$

where $P(x_i)$ is the probability of outcome x_i, with $\sum P(x_i) = 1$. For n outcomes, the Shannon entropy is maximum, equal to $log_2(n)$, if $P(x_i) = 1/n \forall\ i$. Base 2 logarithm is used to obtain an entropy value that represents the average number of *bits* necessary to characterize the random variable.

Accordingly, entropy can also be used to quantify the complexity of a signal. Actually, entropy relates the complexity of the signal to its unpredictability: irregular signals are more complex than regular ones because they are unpredictable.

All the studies that have investigated EEG complexity in the context of AD diagnosis with entropy-based measures (Abásolo et al., 2006a; De Bock et al., 2010; Abásolo et al., 2005; Pincus, 2006; Escudero et al., 2006; Abásolo et al., 2006b) rely on the same principle; they mainly differ in terms of their extraction. Indeed, approximate entropy and sample entropy are computed directly on time series. Multiscale entropy quantifies the complexity of underlying neural systems in a wide-range of temporal scales. Spectral entropies, such as Tsallis entropy, extract information from the amplitude component of the frequency spectrum.

Interestingly, all these studies found that MCI and AD patients tend to exhibit more regular and equivalently less complex EEG signals than age-matched healthy controls. This could be explained in part by the fact that MCI and AD induce loss of neurons that makes the brain dynamics simpler.

3.3 Perturbations in functional connectivity

In parallel to the analysis of EEG complexity, a considerable amount of research has focused on the analysis of the abnormalities in functional connectivity between electrode pairs, to assess the degree of signal synchronization between different brain regions. Note that two locations are functionally connected if they have coherent or synchronized dynamics in their captured EEG signals.

The analysis of functional connectivity is motivated by the fact that AD can be viewed as a disconnection syndrome mainly due to destructive characteristics of AD (Al-Jumeily et al., 2015; Delbeuck et al., 2003). Nevertheless, it is likely that the loss in EEG synchrony is related not only to the loss of cortical neurons, but it is also attributed to a functional disconnection of the neocortex.

A large variety of measures has been proposed to quantify functional connectivity, stemming from

statistics, information theory, physics and signal processing (Dauwels et al., 2010a,b). In the following, we first present the most used measures to assess functional connectivity. Then we make an overview of the results obtained with these measures in the context of AD diagnosis.

3.3.1 Connectivity measures

3.3.1.1 Pearson's correlation coefficient

Pearson's correlation coefficient (PCC) is probably the most basic metric of connectivity. It is based on the covariance of two variables divided by the product of their standard deviations, as presented in the following:

$$PCCxy = \frac{cov(x,y)}{\sigma_x \sigma_y} \tag{3.2}$$

where $cov(x,y)$ is the covariance between signals x and y, σ_x and σ_y are, respectively, the standard deviation of the variables x and y.

3.3.1.2 Magnitude Square Coherence

The magnitude square coherence (MSC) measures the linear component of the functional coupling between two EEG signals x and y as a function of the frequency f (Dauwels et al., 2010b; Escudero et al., 2011; Sankari et al., 2012). The signals x and y are first subdivided in M segments of equal length L, then the coherence is calculated by averaging over such segments. The MSC is computed as:

$$MSC(f) = \frac{|<X(f)Y^*(f)>|^2}{|<X(f)>|.|<Y(f)>|} \tag{3.3}$$

where *X(f)* and *Y(f)* are the Fourier transforms of variables x and y respectively; Y^* is the complex conjugate of Y; $|Y|$ is the magnitude of Y, and $<X(f)>$ stands for the average of *X(f)* computed over the M segments, likewise $<Y(f)>$ and $<X(f)Y^*(f)>$.

3.3.1.3 Phase Synchrony

The general principle of phase synchrony is to detect the existence of phase locking between two oscillatory signals. It was extensively discussed in (Pikovsky et al., 1996). Phase Synchrony (PS) refers to the interdependence between instantaneous phases ϕ_x and ϕ_y of two signals x and y (Dauwels et al., 2007a; Czigler et al., 2008; Park et al., 2008). The instantaneous phase ϕ_x of a signal x is defined as:

$$\phi_x(t) = arg[x(t) + i\acute{x}(t)] \tag{3.4}$$

where $\acute{x}$ is the Hilbert transform of x.

The phase synchrony index for two instantaneous phases ϕ_x and ϕ_y, called Phase-Locking Value (PLV), is computed as:

$$PLV = |<e^{i(\phi_x - \phi_y)}>| \tag{3.5}$$

where $\langle . \rangle$ denotes average over time.

Phase synchrony range is between 0 and 1: for uncorrelated signals, PLV is close to 0, whereas it

tends to 1 for strong phase synchronization.

3.3.1.4 Phase Lag Index

The phase lag index (PLI) measures consistency across time of the instantaneous delay between two signals. It is largely used in the literature because of its robustness to head volume conduction, which is a common problem in EEG data (Babiloni et al., 2020).

Phase lag index is computed from the asymmetry of the distribution of instantaneous signal phase differences. A non-zero phase difference (phase lag) reflects a time lag between two EEG signals (Kasakawa et al., 2016; Stam et al., 2007a). The main approach is to neglect phase differences that are centered around 0 mod ϕ (Stam et al., 2007a). The index of the asymmetry in the phase difference distribution is calculated as:

$$PLI = \ |<sign(sin(\Delta(\phi(t_k)))>| \tag{3.6}$$

where $\Delta(\phi)$ is the phase difference at time t_k between two time series, computed for all sample points per epoch; sign stands for signum function; $\langle . \rangle$ indicates the mean value.

The phase lag index varies between 0 and 1: a zero value indicates no coupling or coupling with a phase difference centered around 0 mod π; a PLI equal to 1 indicates a perfect phase locking at a value of $\Delta(\phi)$. The higher this non-zero phase locking is, the higher the PLI is.

Weighted PLI (wPLI) is an extension of the PLI by weighting phase differences based on the magnitude of their lag (Vinck et al., 2011). Thus, the wPLI is computed as:

$$wPLI = \ |<\frac{|sin(\Delta(\phi(t_k))|}{sin(\Delta(\phi(t_k))}>| \tag{3.7}$$

where $\langle . \rangle$ denotes the average over time.

3.3.1.5 Mutual Information

Mutual information (MI) estimates the information gained from observations of one random variable X on another Y:

$$I(X,Y) = H(X) + H(Y) - H(X,Y) \tag{3.8}$$

where *H(X)* and *H(Y)* is the Shannon entropy of X and Y respectively, and *H(X,Y)* is the joint entropy of X and Y. It is always positive, and it vanishes when X and Y are statistically independent.

Applied to EEG signals, mutual information quantifies the dynamical coupling or information transmission between pairwise electrodes (Brassen and Adler, 2003; Locatelli et al., 1998). As reported in (Dauwels et al., 2007a), computing mutual information by quantizing the signals from the resulting histograms generally leads to unreliable estimation of the measure. Therefore, for a

reliable estimation of mutual information, it is computed in the time–frequency domain using the normalized spectrograms as follows:

$$C_x(k,f) = \frac{|X(k,f)|^2}{\sum_{k,f}|X(k,f)|^2} \tag{3.9}$$

where the summation in the denominator is carried out over the time window k and frequency range f. Then, the MI of the normalized spectrograms is calculated as :

$$I_w(C_x, C_y, C_{xy}) = \sum_{k,f} C_{xy}(k,f) log \frac{C_{xy}(k,f)}{C_x(k,f)C_y(k,f)} \tag{3.10}$$

where the normalized cross time–frequency distribution $C_{xy}(k,f)$ of x and y is computed as follows:

$$C_{xy}(k,f) = \frac{|X(k,f)Y^*(k,f)|}{\sum_{k,f}|X(k,f)Y^*(k,f)|} \tag{3.11}$$

High mutual information indicates high dependence between the two random variables, reflecting a large reduction in uncertainty; while low mutual information value indicates a small reduction of uncertainty. We obtain a zero mutual information when the two random variables are independent.

3.3.1.6 Granger causality

Granger causality is based on the general concept that the prediction of a given time series could be improved by considering the information of past values of another time series. In this setting, the latter time series is said to have a causal influence on the former one (Escudero et al., 2011; Sankari et al., 2012; Dauwels et al., 2007a; Babiloni et al., 2009a). Ganger causality suggests that a variable X causes another variable Y, if the past of X contains information that help predict the future of Y, over and above the information already in the past of Y itself.

This measure requires the estimation of vector autoregressive (VAR) models, in which the value of a variable *X(t)* in time domain is modeled as a linear weighted sum of its own past and of the past of another variable *Y(t)*:

$$Y(t) = \sum_{n=1}^{p} a_n Y_{t-n} + \varepsilon_1(t) \tag{3.12}$$

$$Y(t) = \sum_{n=1}^{p} a_n Y_{t-n} + \sum_{n=1}^{p} b_n X_{t-n} + \varepsilon_2(t) \tag{3.13}$$

where $\varepsilon_1(t)$ and $\varepsilon_2(t)$ are the prediction errors, a_n and b_n are the coefficients (gain factors) of the model, and p is the maximum number of lagged observations included in the autoregressive model ($p \ll T$).

The linear influence from *X(t)* to *Y(t)* can be calculated as the log ratio between the variance of the residual errors:

$$GCI_{X\to Y} = \log \frac{var(\varepsilon_1)}{var(\varepsilon_2)} \tag{3.14}$$

Finally, Granger causality index (GCI) is given by the ratio of the variance of the prediction-error terms for the reduced (when omitting the signal of the potential cause) and full regressions (when including the signal of the potential cause).

3.3.2 Overview of the literature

Several methods and a large variety of measures have been proposed to quantify linear and non-linear relationship between EEG channels, including correlation coefficient (Dauwels et al., 2010b), phase synchrony (Dauwels et al., 2010b; Czigler et al., 2008; Park et al., 2008), phase lag index (Kasakawa et al., 2016; Stam et al., 2007a), coherence (Locatelli et al., 1998; Adler et al., 2003; Besthorn et al., 1994), synchronization likelihood (Czigler et al., 2008; Pijnenburg et al., 2004), space-based synchrony (Dauwels et al., 2010b; Czigler et al., 2008; Kramer et al., 2007), stochastic event synchrony (Dauwels et al., 2010b; Sankari et al., 2012; Park et al., 2008), mutual information (Jeong et al., 2001b), and Granger causality (Dauwels et al., 2010b; Babiloni et al., 2009a). All these studies revealed that alterations of resting-state connectivity are metric-, band- and region-dependent. The majority of these studies reported a loss of functional connectivity in AD and MCI compared to healthy controls in high frequency ranges, especially in alpha. Delta and theta functional connectivity measurement provided less straightforward outcomes.

Most of functional connectivity measures are derived from phase synchrony concept (Pikovsky et al., 1996). In (Stam et al., 2007a), it has been reported a decrease of phase synchrony in AD patients compared to healthy controls, using three different metrics: phase coherence, phase lag index, and imaginary component of coherence. This study has also shown that phase lag index is the most robust metric against the influence of common sources and active reference electrodes. Another work (Tóth et al., 2014) reported an increase of phase lag index between several regions of the two hemispheres in amnestic MCI (aMCI, n=9) patients compared to healthy controls (HC, n=14) at low frequency ranges, particularly in theta band. Besides, a decrease in delta and theta phase synchrony is observed in aMCI patients within frontal and between frontal and temporo-parietal regions, which was more pronounced 1-year later.

Other studies have found a decrease in magnitude and phase coherence in EEG signals of MCI and AD patients comparatively to HC (Stam et al., 2007a; Locatelli et al., 1998; Besthorn et al., 1994; Stevens et al., 2001; Brassen et al., 2004; Wada et al., 1998; Hogan et al., 2003; Anghinah et al., 2000; Hidasi et al., 2007; Jelles et al., 2008; Başar et al., 2010). In other studies, however, no significant effect has been observed when using these measures, neither between HC and AD patients (Dauwels et al., 2010b; Stam and Van Dijk, 2002; Stam et al., 2003), nor between MCI patients and healthy controls (Dauwels et al., 2010b, 2007a).

Some studies reported decreased spectral coherence in posterior alpha and beta in AD patients comparatively to age-matched HC. This phenomenon was also observed in temporo-parieto-occipital brain region (Jelic et al., 2000; Locatelli et al., 1998; Adler et al., 2003; Jelic et al., 1997), and in fronto-central region (Besthorn et al., 1994; Leuchter et al., 1994; Fonseca et al., 2013). Conversely, delta and theta coherence provided less straightforward findings (Locatelli et al., 1998; Adler et al., 2003; Knott et al., 2000; Babiloni et al., 2010), with either an increase of delta and theta coherence in AD patients (Babiloni et al., 2010), or a decrease of the theta coherence, especially at central electrodes (Adler et al., 2003; Knott et al., 2000). Additionally, in (Babiloni et al., 2010; Vecchio

et al., 2013), the authors reported an increased widespread of delta coherence.

In (Adler et al., 2003), left temporal alpha coherence and global theta power have been used as features to distinguish between HC and AD patients. This allows to classify correctly 27 of 31 AD patients (87.1%) and 13 of 17 healthy controls (76.47%). Another study investigating coherence measure to discriminate between 35 AD and 30 HC reported a classification accuracy around of 73% (Knott et al., 2000). Then, by assessing the correlation between coherence values and the MMSE, the obtained results show a significant difference between the two groups.

In (König et al., 2005), Global Field Synchrony (GFS) has been evaluated on controls and patients with varying degrees of cognitive decline (46 HC, 30 SCI, 92 MCI, 89 mild AD, and 39 moderate AD patients). The authors reported a decreased GFS in alpha, beta, and gamma bands, as well as an increased GFS in delta band due to cognitive decline. However, in (Dauwels et al., 2010b, 2009a), no significant effect was observed by such a measure in MCI and AD patients compared to HC. Other studies reported a reduction of the synchronization likelihood across all electrode pairs at beta in AD patients compared with MCI and HC (Pijnenburg et al., 2004; Stam and Van Dijk, 2002; Stam et al., 2003; Babiloni et al., 2004b), and a reduction of alpha synchronization likelihood between frontal and parietal regions in AD and MCI patients compared to HC (Babiloni et al., 2004a, 2006). In (Stam et al., 2003), considering 20 SCI, 17 MCI and 10 AD, the synchronization likelihood was significantly decreased in alpha and lower beta (14-18 HZ) in AD patients compared with both MCI and SCI subjects. Besides, authors reported a positive correlation (p=0.46) between lower beta band synchronization and MMSE scores. According to these findings, authors suggest that a loss of beta band synchronization is a sign of cognitive decline, and the synchrony loss is developed gradually from MCI to AD stage.

A large number of studies have investigated the state space-based synchrony measure for AD diagnosis. These studies have observed a loss of EEG synchrony in MCI (Stam et al., 2003) and AD patients (Jeong, 2004; Pijnenburg et al., 2004; Stam et al., 2003; Babiloni et al., 2006; Stam et al., 2005; Pijnenburg et al., 2008). This synchrony loss is developed gradually from MCI to AD stage (Stam et al., 2003). In (Stam et al., 2003), the authors mentioned that state space-based synchronization seems to be more sensitive than coherence to detect changes in AD patients.

Different Granger measures have been assessed for the analysis of EEG signals in MCI (Dauwels et al., 2010b) and AD patients (Dauwels et al., 2009b). A significant decrease of the full frequency Directed Transfer Function (DTF) was observed in MCI (Dauwels et al., 2010b) and AD patients (Dauwels et al., 2009b). The DTF has been evaluated in (Babiloni et al., 2009b) to quantify the causality relationship between the EEG signals of 69 amnestic MCI subjects and 73 AD patients. Findings reported a weakness of information flux from the parietal to frontal direction was observed in MCI and AD subjects; this weakness was more significant in alpha and beta.

Another study (Gallego-Jutglà et al., 2012) evaluated multiple measures, including correlation, phase synchrony and Granger causality. Using Linear Discriminant Analysis (LDA) with a leave-one-out cross validation protocol, the best classification results were obtained using Granger causality measure (4.88% classification error rate), considering 17 mild AD patients and 24 HC. Interestingly, the corresponding optimized frequency range is 5-6Hz that lies within the standard theta band (4-8 Hz). The authors thus concluded that EEG signals of AD patients are more synchronous than EEG signals of healthy controls, within the optimized range 5-6 Hz.

Another measure belongs to synchrony measures family is the Stochastic Event Synchrony (SES) (Dauwels et al., 2007b). In (Dauwels et al., 2010b), a significant reduction of SES was observed in MCI and AD patients compared to HC. Then, by combining SES and a Granger measure as features in discriminant analysis was helpful to perform a classification between 38 HC and 22 MCI patients, reaching 83% of classification performance following a leave-one-out process.

Finally, a previous study (Jeong et al., 2001b) showed that mutual information is lower for AD than in HC, especially in frontal and antero-temporal regions. Moreover, there was a decrease in information transmission between corresponding inter-hemispheric electrodes and between distant electrodes in the right hemisphere. In (Dauwels et al., 2010b), the authors have also evaluated the mutual information measure, however, results do not show a significant impact in MCI patients in both time and frequency domains.

3.4 State-of-the-art limitations

As mentioned earlier, numerous studies in the literature have highlighted that AD induces a reduction in the complexity of rsEEG signals. This change in EEG signals has been exploited as discriminative feature for AD diagnosis. Various methods have been used to quantify the complexity of EEG signals, such as the correlation dimensions and the first positive Lyapunov exponent (Adeli et al., 2005; Jelles et al., 1999; Jeong et al., 1998, 2001a; Takahashi, 2013; Yagyu et al., 1997). However, these two measures involve the reconstruction of a phase space trajectory, which requires a high computation cost. Other methods relying on the concept of entropy have been also proposed (Abásolo et al., 2006a; De Bock et al., 2010; Abásolo et al., 2005; Pincus, 2006; Escudero et al., 2006). Usually, these measures were applied with two main drawbacks.

First, they were applied on EEG signals without considering the non-stationarity and nonlinearity properties of EEG signals. The assumption of stationarity and linearity are generally not appropriate for physiological data. In (Lo et al., 2009), the authors stated that non-stationarity is an intrinsic property of physiological data, even without external stimulus. In (Klonowski, 2009), the authors claimed that the human brain is a complex system generating nonstationary and nonlinear signals. Non-stationarity means that the statistical properties of the signal varies with time. The authors suggested that the observed non-stationarity in EEG signals reflects a switching of the inherent metastable states of neural assemblies during brain functioning. In (Kaplan et al., 2005), the authors claimed that the EEG signal can be modeled as a sequence of quasi-stationary epochs separated by sudden transitions. In (Vakorin et al., 2013), the authors indicated that EEG signals are characterized in terms of metastability, which refers to the ability of the brain to move from one stable state to another, remaining for an extended time period. In (Bodenstein and Praetorius, 1977), EEG is described as a piecewise stationary process, segmented into stationary epochs with different probabilistic characteristics. Additional studies (Brandeis et al., 1995; Lehmann and Skrandies, 1980; Flexer and Bauer, 1998) identified quasi-stationary states in EEG, referred to as "*microstates*", reflecting coherent neural dynamics. Also, in (Freeman, 2006), the author suggested that perception is based on sequences of stationary patterns demarcated by discontinuities.

Secondly, such measures did not exploit the EEG signal as a multivariate time series. Actually, the predominant approach in the literature consists in extracting information from EEG signals by averaging them over channels. The EEG signal being a multidimensional signal recorded by a multiplicity of electrodes (channels), it is of high interest to take advantage of its spatiotemporal

nature using techniques that can catch the inter-channel relations. In that sense, alternative methods were used for assessing the inter-channel relations, such as mutual information (Jeong et al., 2001b), coherence (Locatelli et al., 1998; Adler et al., 2003; Besthorn et al., 1994), Granger causality (Dauwels et al., 2010b; Babiloni et al., 2009a) and phase lag index (Kasakawa et al., 2016; Stam et al., 2007a). Nevertheless, these measures quantify only the information transmission between different channels, without considering the temporal characteristics of EEG signals.

In order to face these two drawbacks, we propose in this thesis to exploit a specific spatiotemporal connectivity measure, termed "*Epoch-based Entropy*", already introduced and published in (Houmani et al., 2013, 2015, 2018). This entropy measure stems from a refined characterization of the local statistical properties of EEG signal using Hidden Markov Models (Rabiner and Juang, 1986). It has been shown in previous works (Houmani et al., 2013, 2015, 2018; Aljane and Houmani, 2017) that this modeling approach is suitable to the analysis of the underlying neuronal dynamics in the context of AD, since it quantifies on piecewise stationary epochs the information content conveyed by EEG signals locally over time (as done by classical complexity measures) and also spatially by estimating inter-channels relationship.

3.4.1 Epoch-based Entropy measure

Entropy quantifies the information content of a random variable and depends only on its probability density value (refer to Section 3.2). Epoch-based Entropy measure (*EpEn*) relies on the fundamental assumption that the EEG signal can be modeled as a sequence of quasi-stationary epochs separated by abrupt transitions, as reported in Section 3.4.

In that sense, Hidden Markov Model (HMM) can be considered as an appropriate statistical modeling technique to estimate the information content in piecewise stationary signals (Rabiner and Juang, 1986, 1993). The use of HMM is also motivated by the fact that its structure is adapted for modeling hidden neural dynamics underlying the observed EEG signals (the captured time series).

Actually, HMM can segment the signals into quasi-stationary epochs, and at the same time perform a local estimation of the probability density on each epoch. A HMM consists of a doubly stochastic process employed to characterize the evolution of observable realizations (the captured time series), which depend on an internal process that is not directly observable, called "hidden states". Mathematically, HMM is defined by a finite set of states, and transitions from one state to another are governed by "transition probabilities". Continuous probability density function is used to characterize the relationship between states and the observable realizations. Specifically, the "emission probabilities" correspond to the conditional distributions of the observations from a given state (Rabiner and Juang, 1986, 1993).

As in previous works (Houmani et al., 2013, 2015, 2018), to characterize the evolution of EEG signals over time, we naturally used a continuous left-to-right HMM structure (see Fig. 3.1), which allows transitions from each state to itself and to its immediate right-hand neighbor only. The hidden states of the HMM correspond to the stationary segments of the signal, and the transitions correspond to the abrupt changes in the signal (Rabiner and Juang, 1986, 1993). EEG signal of a subject is thus represented by a succession of epochs, segmented automatically with the Viterbi algorithm using the corresponding subject's HMM (Rabiner and Juang, 1986, 1993).

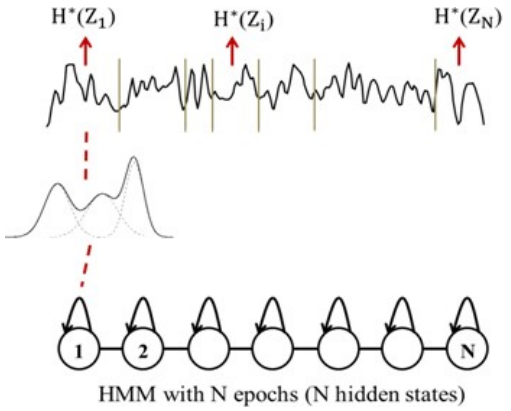

Figure 3.1: Modeling a univariate EEG signal with HMM (Houmani et al., 2015).

Each epoch S_i, corresponding to a hidden state of the HMM, contains a given number of observations (sample points). Each observation z in such epoch is considered as a realization Z_i of a random variable Z, which follows the observation probability distribution $P_i(z)$ modeled by a weighted sum of M Gaussian distributions (see Fig 3.1). Note that we used a diagonal covariance matrix for each multivariate Gaussian.

The entropy $H^*(Z_i)$ of the epoch S_i is computed as follows considering the ensemble of realizations of Z_i:

$$H^*(Z_i) = -\sum_{z \in S_i} P_i(z) log_2 P_i(z) \tag{3.15}$$

Then, the entropy *EpEn(Z)* of the whole signal is obtained by averaging the entropy values computed for the N epochs:

$$EpEn(Z) = \frac{1}{N} \sum_{i=1}^{N} H^*(Z_i) \tag{3.16}$$

The use of HMM is also driven by the multi-channel EEG analysis. Indeed, a HMM can manage multidimensional signals using multivariate probability density functions on such signals. To characterize the inter-relations between two EEG signals captured from two electrodes, we trained a HMM for each subject on such couple of EEG signals. At time t, a hidden state emits a two-dimensional observation vector. By applying the Viterbi algorithm, each signal is segmented into N epochs, and the entropy $H^*(Z_i)$ of an epoch is computed considering the probability density function estimated by the HMM on all the observations (sample points) from the two signals belonging to the associated epoch (see Fig. 3.2). Note that although the N epochs are matched between EEG channels, the model does not constrain these epochs to have the same duration.

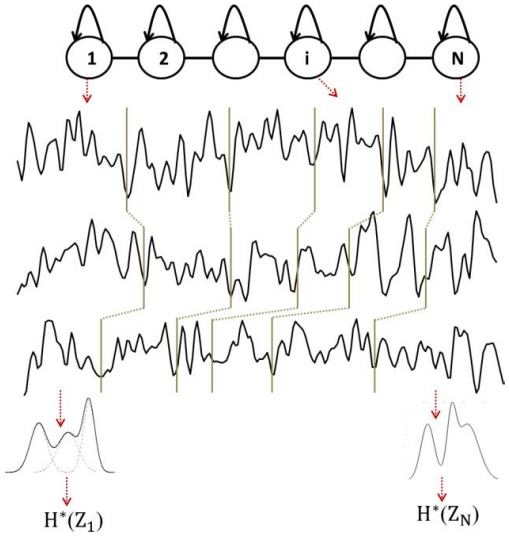

Figure 3.2: Illustration of multi-channel (D=3, N=6) EEG signal modeling with HMM (Houmani et al., 2015).

Finally, by averaging the entropy over all the N epochs, an Epoch-based Entropy value associated to the multivariate EEG of the subject is obtained. A high value of *EpEn* indicates a high information content conveyed by the coupling of two EEG signals.

3.4.2 Illustration of EpEn functioning

In this section, we illustrate the functioning of *EpEn* for measuring the information content of multivariate piecewise stationary EEG signals. To this end, we compute *EpEn* value of four signals displayed in Figure 3.3, considering them first separately in a univariate analysis, then as pairs of signals for a multivariate analysis.

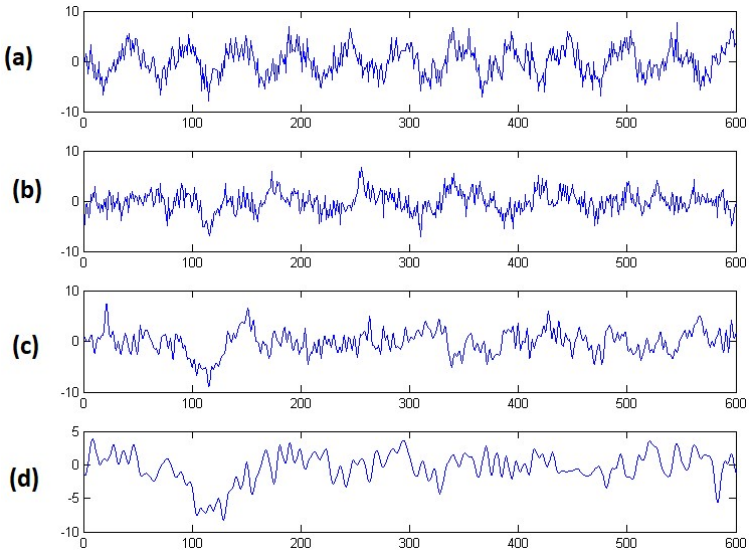

Figure 3.3: Examples of four signals of different complexities (Houmani et al., 2015).

Visually, these signals exhibit different complexities reflected by their *EpEn* values reported in Table 3.1. In fact, higher *EpEn* value is associated with high "irregular" or "complex" signals.

Table 3.1: EpEn values computed on the four signals when considered separately.

Signal	**a**	**b**	**c**	**d**
EpEn	8.79	8.56	7.89	6.38

Then, considering four pairs of signals ([a-a], [a-b], [a-c] and [a-d]), *EpEn* measure detects the inter-channel statistical dependencies, as reported in Table 3.2. The proposed *EpEn* measure reflects both intra-channel complexity (complexity over time) and the inter-channel complexity (spatial complexity, or heterogeneity between all the signals).

Table 3.2: Epoch-based Entropy computed on pairs of signals.

Signal	**a-a**	**a-b**	**a-c**	**a-d**
EpEn	7.51	7.38	7.81	8.70

When computing the *EpEn* value on identical signals [a-a], there is no inter-channel difference and thus the combined distribution becomes more regular. This leads to a reduction of the *EpEn* value to when the signal is considered alone (from 8.79 in Table 3.1 to 7.51 in Table 3.2). Nevertheless, the combined entropy is still nonzero since it considers intra-channel disorder.

When computing entropy on two signals of different complexities, for example on the most complex signal (a) with a signal of lower complexity (c or d), the entropy increases as well as the difference increases between signals (inter-channels) and also over time for each signal (intra-channel).

The statistical estimation of entropy with HMM allows to quantify the information content of multivariate EEG signals at two levels simultaneously: at the time level, *EpEn* quantifies the information content or the disorder on piecewise stationary epochs of EEG signals over time; and at the spatial level, *EpEn* quantifies the functional connectivity in terms of the heterogeneity of piecewise stationary epochs between multi-channel EEG signals.

3.5 Conclusion

In this chapter, we presented the state-of-the-art studies addressing AD diagnosis using EEG. All the mentioned studies pointed out the effectiveness of using EEG to differentiate between AD patients and MCI or healthy control subjects. Nevertheless, several limitations were highlighted and several modeling challenges are still not addressed in such prior studies. In order to face some of these limitations, we proposed to exploit an entropy-based measure, called *Epoch-based Entropy*, that we will extend its use in this thesis for functional connectivity assessment.

Chapter 4

Brain network analysis

Over the past decade, the scientific community has shown a considerable interest in interpreting EEG neurophysiological data using graph theory to characterize normal and abnormal brain networks (Bullmore and Sporns, 2009; Stam, 2014; Yu et al., 2018).

In the context of AD diagnosis, it has been proposed to exploit graph theory to study the topological properties of the network mapping from EEG functional connectivity computed between pairs of electrodes (Tijms et al., 2013). Functional connections may highlight information on network organization underlying specific brain functions.

In this way, by modeling a brain network as a graph involving nodes (electrodes) interconnected by edges that represent the connectivity between cortical nodes, it is possible to conduct a topological analysis of the brain functional organization. Nodes usually represent brain sites, while links represent functional connections. Of note, functional connections in the network correspond to statistical relationships between EEG signals rather than physical linkages, and therefore carry no direct metabolic event.

In this chapter, we first supply a brief description of fundamental notions for constructing the brain network based on EEG data using graph theory. Then, we present some graph parameters that are informative about brain network's topology. We also provide an overview of the literature addressing brain network analysis with graph theory in the context of AD diagnosis.

4.1 Brain network construction

A network is a mathematical representation of a complex system. To investigate the brain system, information about the system's components is needed, but it is also required to know how these components interact with each other. Mathematical principles of graph theory applied on EEG data to construct brain networks allows retrieving valuable information about the organization and interactions of brain areas.

In our framework, the brain network is a mathematical representation of the brain system. It is typically represented by a graph, defined by a set of *nodes* (technically called *vertices*) and *links* (known as *edges*) representing the functional connectivity value between pairs of electrodes. That value is commonly computed with quantitative functional connectivity measures, such as coherence, phase lag index, mutual information among others.

Brain network is represented by its connectivity matrix (*adjacency matrix*). Rows and columns in the matrix correspond to nodes, while matrix entries correspond to links (see Fig. 4.1). The order of nodes in the adjacency matrix has no influence on the computation of network measures, but it is useful for network visualization and interpretation.

Links may be differentiated based on their weight and directionality. *Binary links* denote the presence or absence of connections, while *weighted links* also convey information about connection strengths. The interpretation of the connection strength depends on the exploited functional connectivity measure. A binary network is obtained by applying an absolute or a proportional weight threshold to the adjacency matrix (see Fig. 4.1).

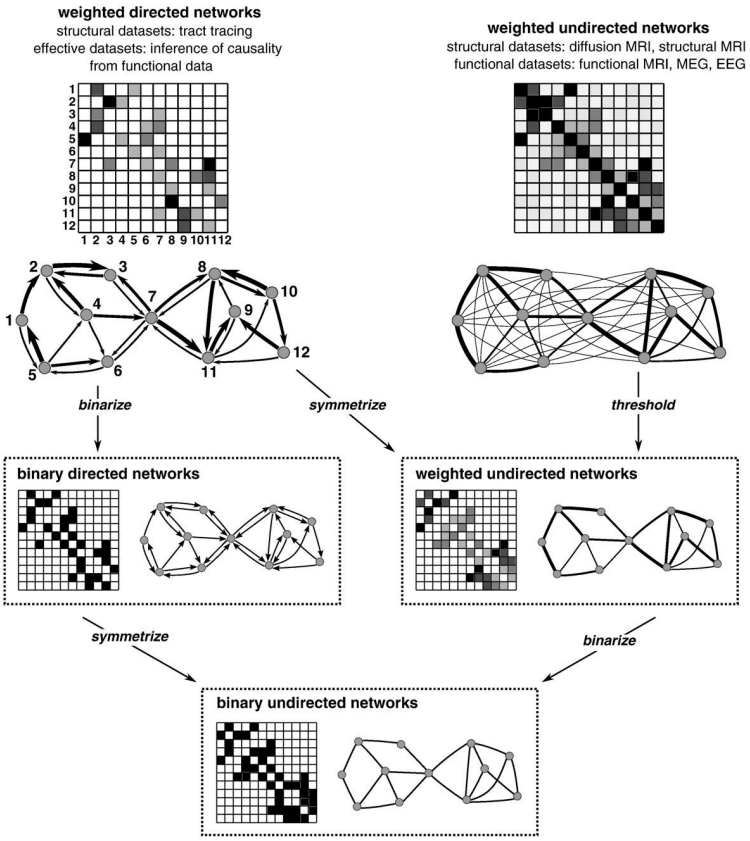

Figure 4.1: Construction of brain networks (different types of graphs) represented by their connectivity matrices (Rubinov and Sporns, 2010).

More precisely, for a given adjacency matrix where w_{ij} denotes the edge (link) between i and j nodes (electrodes):

- We obtain the *binary* graph as follows :

  $a_{ij} = 1$ when $w_{ij} > Threshold$ (link (i, j) exists and i and j are neighbors);
  $a_{ij} = 0$ otherwise ($a_{ii} = 0$ for all i).

- We obtain the *weighted* graph as follows:

  $a_{ij} = w_{ij}$ when $w_{ij} > Threshold$ (link (i, j) is quantified by w_{ij} and i and j are neighbors);
  $a_{ij} = 0$ otherwise ($a_{ii} = 0$ for all i).

Besides, we distinguish undirected and directed networks (see Figure 4.1). In the first case, links indicate symmetric relationships links; while in the second case, links correspond to directed relationships. Unfortunately, current neuroimaging methods are not able to provide a valid causal directionality. Hence, we consider in this thesis only undirected networks.

In the following section, we present the mathematical definition of the most exploited graph parameters in the context of AD diagnosis using EEG signals. Next, we summerize the findings that authors have reported in the literature when applying graph theory on EEG data for AD detection.

4.2 Brain network parameters

Various graph parameters are used to characterize brain network topology on the basis of several aspects of global and local brain connectivity. In this section, we present in details such parameters that variously detect functional *integration* or *segregation*. Integration refers to the capacity of the network to become interconnected and exchange information. Segregation refers to the degree of which network elements form separate clusters. Other graph parameters quantify importance of individual brain regions or contribute to assess the network's resilience.

4.2.1 Degree

The degree (K) of a node reflects the importance of that node in the network. It corresponds to the number of nodes (electrodes) that still have connection with that node after thresholding. The remaining electrodes are considered as the neighbors of the node (Rubinov and Sporns, 2010; Stam and Van Straaten, 2012; Sporns, 2022). The degree K of a node i is defined as:

$$K_i = \sum_{j=1}^{N} a_{ij} \tag{4.1}$$

where N is the total number of nodes in the network, and a_{ij} is the connection status between nodes i and j: $a_{ij} = 1$ when the link between i and j exists; $a_{ij} = 0$ otherwise.

4.2.2 Clustering coefficient

The clustering coefficient (CC) of a node estimates the density of connections established by its neighbors (Rubinov and Sporns, 2010; Stam and Van Straaten, 2012; Sporns, 2022). It is often considered as a measure of segregation: it reflects the tendency of a network to form topologically local densely circuits (cliques or clusters) presenting high strength intrinsic connectivity.

In case of undirected binary graph, if a node i has k neighbors, the clustering coefficient CC of node i is defined as:

$$CC_i = \frac{\sum_{j,h} a_{ij}.a_{ih}.a_{jh}}{k_i(k_i - 1)} \tag{4.2}$$

where k_i is the number of connections in node i and a_{ij} is the connection status between nodes i and j : $a_{ij} = 1$ when the link (i, j) exists; $a_{ij} = 0$ otherwise.

In case of undirected weighted graph, the weighted clustering coefficient CC^w of node i is defined as:

$$CC_i^w = \frac{\sum_{j,h} (w_{ij}.w_{ih}.w_{jh})^{1/3}}{k_i(k_i - 1)} \tag{4.3}$$

where w_{ij} is the connectivity weight between nodes i and j, and k_i is the number of connections in node i.

To obtain the global clustering coefficient CC_{global} of a network, we average the clustering coefficient values CC_i computed locally over all nodes :

$$\begin{aligned} CC_{global} &= \frac{1}{N} \sum_{i=1}^{N} CC_i \\ CC_{global}^w &= \frac{1}{N} \sum_{i=1}^{N} CC_i^w \end{aligned} \tag{4.4}$$

where N is the total number of nodes.

4.2.3 Shortest path length

The shortest path is a parameter of integration, which quantifies how the information is exchanged or integrated within the brain network (Rubinov and Sporns, 2010; Stam and Van Straaten, 2012; Sporns, 2022). A path is any sequence of edges that connects two nodes and its length is given by the sum of the connection weights that form the shortest weighted path.

The shortest weighted path length $d_{i,j}^w$ between nodes i and j is defined as:

$$d_{i,j}^w = \sum_{w_{ij} \in gi \longleftrightarrow j}^{N} w_{ij} \tag{4.5}$$

where N is the total number of nodes, $gi \longleftrightarrow j$ is the shortest weighted path between nodes i and j, and w_{ij} is the connection weight between nodes i and j. In case of a binary network $w_{ij} = a_{ij}$.

The weighted path length L at node i is generally defined as:

$$L_i = \frac{\sum_{i \neq j} d_{i,j}^w}{(N - 1)} \tag{4.6}$$

where N is the number of nodes and $d_{i,j}^w$ is the shortest path length between nodes i and j, considering all possible paths that have to be spanned from node i to node j.

Note that since path between disconnected nodes is defined to have infinite value, it is usually

recommended to use experimentally the median instead of the mean to compute the shortest path of a node i:

$$L_i = Median(d^w_{i,j}) \tag{4.7}$$

To obtain the characteristic path length of the network, we average all the shortest path over all nodes.

A low value of the shortest path length suggests that information is routed between electrodes with few intermediate steps (edges), which indicates rapid and high efficiency in information transmission across the network.

4.2.4 Local and global efficiency

The local efficiency (E_{loc}) is another measure of network segregation that performs locally at the level of the clusters retrieved with the clustering coefficient.

In the binary case, the local efficiency of the vertex i is defined as:

$$E_{loc,i} = \frac{\sum_{j,h\in N, i\neq j} a_{ij}a_{ih}[d_{jh}]^{-1}}{k_i(k_i-1)} \tag{4.8}$$

where d_{jh} is the shortest path between j and h, which contains only neighbors of i.

In case of a weighted network, the weighted local efficiency of node i is defined as:

$$E^w_{loc,i} = \frac{\sum_{j,h\in N, i\neq j} (w_{ij}w_{ih}[d^w_{jh}]^{-1})^{1/3}}{k_i(k_i-1)} \tag{4.9}$$

Therefore, the local efficiency of a node reports how efficient the communication is between the first neighbors j and h of the node i when this node is removed (Rubinov and Sporns, 2010; Stam and Van Straaten, 2012; Sporns, 2022). High local value indicates better network's resistance to failure on a small scale.

Global efficiency parameter is considered as a measure of network integration. It is equivalent to the average inverse shortest path length and defined as:

$$\begin{aligned} E_{global} &= \frac{1}{N}\frac{\sum^N_{j\neq i}[d_{ij}]^{-1}}{N-1} \\ E^w_{global} &= \frac{1}{N}\frac{\sum^N_{j\neq i}[d^w_{ij}]^{-1}}{N-1} \end{aligned} \tag{4.10}$$

High global efficiency indicates that brain regions are well integrated, which is equivalent to low value of shortest path length. Note that both local and global efficiency can be computed on disconnected nodes, where the associated infinite path length leads to a zero efficiency value.

4.2.5 Small-world index

The concept of small-world networks was introduced by Watts and Strogatz in 1998 (Watts and Strogatz, 1998). The small-world network structure is intermediate between the random graph and the regular graph (see Fig. 4.2). It reflects an optimal balance of efficient information transmission between long range connections (short path length), while maintaining efficient local information processing (high clustering coefficient), as shown in Table 4.1. This occurs due to the existence of relatively few long-term connections (see Fig. 4.2).

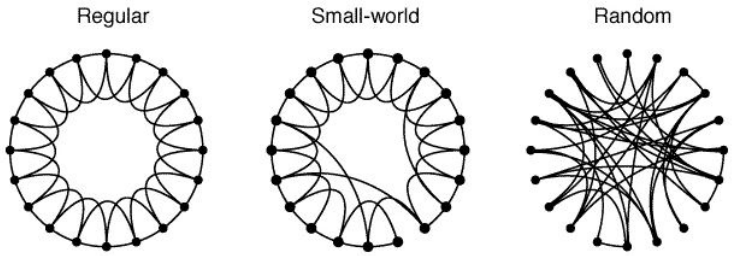

Figure 4.2: Illustration of small-world topology (Watts and Strogatz, 1998).

In fact, small-world index combines the advantages of regular and random networks, ensuring the efficiency of information transmission at both local and global levels. As displayed in Figure 4.2, Small-world networks are formally defined as networks that are significantly more clustered similar to regular networks, with approximately similar path length relatively to random networks, making the network more resistant to damage.

Table 4.1: Small-worldness characteristics.

	Regular	**Random**	**Small-world**
Clustering coefficient	high	Low	high
Shortest path	Long	short	short

Hence, network small-worldness (SW) parameter is calculated by comparing clustering coefficient and path length of a given network to an equivalent random network with same density:

$$SW = \frac{C^w / C^w_{rand}}{L^w / L^w_{rand}} \tag{4.11}$$

where C^w and C^w_{rand} are the clustering coefficients, L^w and L^w_{rand} are the characteristic path lengths of the respective tested network and a random network. Small-world networks often have $SW \gg 1$.

It is worth noticing that this parameter could falsely reflect the small-world topology since it does not give an individual assessment of integration and segregation. Therefore, this measure should not be regarded as a substitute of clustering coefficient and shortest path.

4.2.6 Betweenness

The betweenness of a node (BW) is defined as the number of shortest paths in the network that pass through that node. It reflects the influence that a node has over the flow of information in a graph (Rubinov and Sporns, 2010; Stam and Van Straaten, 2012; Sporns, 2022). The betweenness of node i is defined as:

$$BW_i = \frac{1}{n-1} \sum_{h \neq j, h \neq i, j \neq i} \frac{\rho_{hj}(i)}{\rho_{hj}} \tag{4.12}$$

where ρ_{hj} is the number of shortest paths between h and j, and $\rho_{hj}(i)$ is the number of shortest paths between nodes h and j that pass through node i.

A node with high betweenness value has a high influence on the information transmission through the network.

Betweenness is computed equivalently on weighted and binary networks, provided that path lengths are computed on respective weighted or binary paths.

4.2.7 Modularity

The modularity index reveals a hierarchical structure of a graph network, decomposed into densely intra-connected groups of nodes, referred to as *modules*, that are sparsely inter-connected with nodes in other modules of the network (Rubinov and Sporns, 2010; Stam and Van Straaten, 2012; Sporns, 2022).

This modular structure is organized hierarchically, such that it contains sub-modules over several topological resolution scales. This organization can be consistent with a fractal community structure.

The modular structure, subdividing the network into non-overlapping subnetworks (modules), is achieved by searching for the partition with a maximally possible number of within links, and a minimally possible number of links between modules. The optimal modular structure is typically estimated with an optimization algorithm (Newman and Girvan, 2004), which aims at maximizing the following quantity Q:

$$Q = \frac{1}{L^w} \sum_{ij} [w_{ij} - \frac{k_i k_j}{L^w}] \delta_{m_i m_j} \tag{4.13}$$

where w_{ij} is the connection strength (weight) between nodes i and j; k_i is the number of connections in node i; L^w is the weighted characteristic path length, and $\delta_{m_i m_j}$ is equal to one if nodes i and j belong to the same module and zero otherwise. This ensures that we only count edges between nodes within the same module. In case of a binary network $w_{ij} = a_{ij}$ and $L^w = L$.

Modularity is a general hallmark of complex biological systems. It highlights flexibility and adaptability. Modular architecture naturally arises in networks that can adapt and evolve to changing environmental events, such as the onset of pathology.

4.3 Overview of the literature on brain network analysis

Graph theory is a valuable framework to study the organization of functional connections in normal and altered brain due to AD. Several EEG studies have reported that the network's topology is altered in AD and MCI patients compared to control subjects. There is a robust agreement that the AD group deviates from the optimal small-world topology exhibiting a more random one compared to HC (De Haan et al., 2009; He et al., 2008; Yao et al., 2010). Concerning the other topological parameters, conflicting results emerge in some respect, as it will be shown in the following.

The first application of graph analysis in the context of early AD diagnosis using EEG was published in 2007 (Stam et al., 2007b). Considering EEG data of 15 AD patients and 13 HC, graph theory was applied on functional connectivity matrices computed with synchronization likelihood measure in beta band. Results showed that a loss of small-world network characterizes AD. In fact, it has been found a longer characteristic path length in AD patients with a maintained clustering coefficient, suggesting a less optimal organization.

In (De Haan et al., 2009), the authors also exploited synchronization likelihood as a measure of functional connectivity in different frequency bands. Considering EEG data of 20 patients with mild AD and 23 HC, they found that AD group exhibits a decreased clustering coefficient, especially in lower alpha and beta bands, with a shorter characteristic path length, especially in the lower alpha and gamma bands. According to these results, the authors concluded that the functional brain network organization in AD patients deviates from the optimal small-world network structure towards a more random type. This is associated with less efficient information exchange, supporting the disconnection hypothesis of AD.

In (Poza et al., 2013), graph theory was exploited to discriminate between 32 AD patients and 25 HC. To construct the graph, the authors used Euclidean distance to estimate the similarity between the spectral content of each pair of electrodes. Experiments showed that alterations in brain network organization due to AD is frequency-dependent. Actually, the global clustering coefficient was lower in delta and theta bands for AD patients compared to HC. The inverse was observed in higher alpha and beta bands. The characteristic shortest path was higher in delta and theta bands, and lower in beta and higher alpha bands.

Nevertheless, in another study (Wang et al., 2014), the results revealed that the clustering coefficient was lower and the characteristic shortest path was higher for AD patients in all frequency bands, except delta. Additional graph parameters have been evaluated in this study using coherence measure as functional connectivity. Small-world index, local and global efficiency values were found lower in all frequency bands for AD patients compared to HC.

In (Vecchio et al., 2014), brain network analysis was conducted on a database containing EEG data of 174 AD patients, 154 MCI patients and 50 HC. Results showed a significant increase of both the characteristic shortest path in theta and the clustering coefficient in lower alpha, for AD patients compared to MCI and HC. MCI subjects are find similar to HC.

In (Afshari and Jalili, 2016), local and global efficiency parameters are computed on directed connectivity matrices using Directed Transfer Function, which is based on the Granger causality in frequency domain. Considering EEG signals of 25 AD patients and 26 HC, graph parameters have been investigated to discriminate AD patients from HC at different threshold values applied

to construct the binary graph. The authors pointed out the high sensitivity of the results to the threshold value. Results showed that compared to HC, AD patients exhibit lower global efficiency and higher local efficiency, in a wide range of threshold values in beta and a range of medium thresholds in alpha. Then, these two parameters have been exploited for classification assessment, using LDA classifier with leave-one-out cross-validation protocol. A classification accuracy of 94% was obtained in beta band, at one threshold value keeping the strongest 8% of the connectivity values in the network. According to these results, the authors reported that the decrease of global efficiency could be compensated by an increase of local efficiency, which reflects the wide-spread decline due to AD in the long-range connections.

In (Vecchio et al., 2018), the authors explored a dataset of 145 aMCI, 74 of them still in aMCI stage (Stable S-aMCI as group 1), the other 71 have been converted to AD (C-aMCI as group 2). Coherence has been used as connectivity measure, and small-word (SW) index as graph parameter. Results showed significant SW differences between the two groups in delta, alpha, higher beta, and gamma bands. An accuracy of 61% was obtained when discriminating between the two groups. The same research team have evaluated the small-world index in another study including 59 aMCI subjects with multidomain impairment, divided into S-aMCI and C-aMCI (Miraglia et al., 2020). Patients were further divided in MCI with linguistic domain (LD) impairment and in MCI with executive domain (ED) impairment. It has been found that the small-world index significantly decreases in gamma band in C-MCI compared to S-MCI. Furthermore, in C-MCI with ED impairment, such index decreased in delta and gamma bands and increased in lower alpha.

A similar study (Franciotti et al., 2019) has evaluated Granger causality used as input to graph theory to estimate the strength and the direction of information transmission between electrodes pairs. Different graph parameters (degree, clustering coefficient, efficiency, path length, assortativity) have been investigated on a dataset consisted of 42 HC, 41 AD patients and 42 AD-MCI patients (mild cognitive impairment with at least one positive neurodegeneration biomarker). The number of edges (degree), the number of inward edges (in-degree) and the number of outgoing edges (out-degree) were lower in AD-MCI and AD than the control group for non-hubs and hubs nodes, except the frontal region where AD and AD-MCI showed an additional hub in F3. Clustering coefficient decreases in AD compared with AD-MCI in the right occipital electrode, and it was found positively correlated with the MMSE. Moreover, AD-MCI and AD groups showed lower local and global efficiency compared to control subjects. According to their findings, authors suggest that AD and also its prodromal stage alter the brain network topology, revealed by a reduction of the number of edges and a decrease of the local and global efficiency. Nevertheless, the authors indicated that Granger causality could be sensitive to noise, leading to spurious connection.

In (Chen et al., 2019), authors suggest that global parameters, such as global clustering coefficient and global efficiency, might be exploited as objective markers to assess AD severity. Phase Coherence has been used to construct weighted graphs for 108 AD patients. Results showed significant correlations between the global topological metrics and the severity of AD based on different AD markers, such as verbal fluency and digit-backward tests. In alpha band, clustering coefficient and global efficiency decrease when verbal fluency score decreases. Results also highlighted a topological reorganization of alpha band network in AD patients. The local clustering coefficient at Fz and Pz electrodes seemed to be preserved in AD, whereas it was significantly affected by the disease in frontal and central-parietal regions.

In (Vecchio et al., 2020), the authors investigated the reliability of small-world index to discriminate

between 175 AD patients and 120 HC, based on cortical sources' connectivity. Lagged linear coherence function has been used to construct undirected and weighted networks. Using SVM classifier, they obtained an AUC (Area Under the Curve) value of 0.97 and an accuracy of 95% with a good balance between sensitivity and specificity.

In (Mehraram et al., 2020), weighted phase lag index and weighted graph measures (degree, clustering coefficient, shortest path, small-world and modularity) have been exploited as features to discriminate between 32 patients with AD and 25 patients with Lewy body dementia. Using Random Forest to quantify the feature importance, they found that weighted phase lag index, node degree in beta band, and clustering coefficient in theta, are the most pertinent features. Based on these selected features, a classification accuracy of 66% was obtained. By following the same methodology, an accuracy of 77% was obtained when discriminating the 25 patients with Lewy body dementia from 18 HC. This study also highlighted the problem of network measures dependency on the network density (*i.e.* threshold value), as in (Afshari and Jalili, 2016). Networks were thresholded within a range of percentage values between 3% and 60% in steps of 1%; the optimal threshold was obtained in function of classification accuracy. Comparatively to binary graph framework, results suggested that weighted graph analysis makes the graph measures more consistent across network densities.

In (Jalili, 2017), different graph parameters have been investigated to discriminate 23 AD patients from 25 HC. Pearson's correlation coefficient was used to form the network matrices. To select the most pertinent features, three feature selection methods have been used and compared: Genetic Algorithm (GA), Binary Particle Swarm Optimization (BPSO) and Social Impact Theory based Optimization (SITO). Best accuracy has been obtained in beta band by GA with SVM classifier (accuracy of 83%). The set of optimal features included edge betweenness centrality, global efficiency, modularity and synchronizability.

In (Vecchio et al., 2021), small-worldness was analyzed in 54 normal elderly subjects, 100 AD and 80 MCI patients, as well as in 40 patients suffering from vascular dementia. Graph theory was applied to undirected and weighted networks constructed using lagged linear coherence. It has been found that AD patients presented lower values of small-world index in low frequencies and higher values of such index in alpha, than MCI and normal subjects. MCI patients presented a network organization that is intermediate between normal subjects and AD patients in theta band.

In a MEG study (López-Sanz et al., 2017), MCI showed lower small-worldness, clustering coefficient and transitivity and higher modularity than HC in theta and beta bands. Results on SCI subjects were similar but less significant in clustering and transitivity, while exhibiting alterations in the alpha band in the opposite direction to those shown by MCI for modularity and transitivity. Additionally, an increase in modular partition variability was observable in both SCI and MCI in theta and beta bands, suggesting that SCI subjects exhibit a significant network disruption, showing intermediate values between control and MCI groups in multiple parameters. According to these findings, authors highlighted the relevance of cognitive concerns in the clinical setting and suggest that network disorganization in AD could start in the preclinical stages before the onset of cognitive symptoms. However, in a recent EEG study, no significant changes have been found for AD patients compared to control subjects. Only frontotemporal (FTD) patients showed a derangement in the cortical network modularity (Franciotti et al., 2022).

Another MEG study (Kocagoncu et al., 2020) has highlighted the relationship between Tau protein

and graph parameters and if Tau pathology is associated with functional organization of widespread neurophysiological networks. Results reported that the increase of Tau burden in early AD was associated with a shift away from the optimal small-world organization and a more fragmented network in the beta and gamma bands, whereby parieto-occipital areas were disconnected from the anterior parts of the network. Similarly, higher Tau burden was associated with decreases in both local and global efficiency, especially in the gamma band. Pearson's correlation coefficient has been used to construct weighted graphs.

In (Tait et al., 2019), the authors have evaluated the correlation between graph parameters and clinical markers. Functional networks were constructed by calculating the phase locking factor on EEG data of 21 AD patients and 26 HC. Findings reported positive correlation between small-worldness and both of MMSE and language sub-score in theta band. This positive correlation is due to negative correlation with shortest path length, particularly in the temporal region that plays an important role in the language impairments of AD subjects. Authors concluded that temporal lobe disconnection plays a key role in cognitive impairment in AD.

In order to facilitate the comparison between the above-mentioned studies, we summarize the majority of these works in Table 4.2, reporting the most pertinent information.

Table 4.2: Summary of the literature addressing brain network analysis with graph theory.

Reference	Dataset	Connectivity measure	Graph type	Graph parameters	Main Results
(Stam et al., 2007b)	15 HC 13 AD	Euclidean distance	binary	CC L	• $L(AD) > L(HC)$ in beta • Negative correlation between L and MMSE in beta • CC: no significant change
(De Haan et al., 2009)	23 HC 20 AD	Synchronization likelihood	binary	CC L	• $CC(AD) < CC(HC)$ in alpha1 and gamma • $L(AD) < L(HC)$ in alpha1 and gamma
(Poza et al., 2013)	32 HC 25 AD	Euclidean distance	binary	CC L	• $CC(AD) > CC(HC)$ in delta and theta • $CC(AD) < CC(HC)$ in alpha2 and beta • $L(AD) < L(HC)$ in theta • $L(AD) > L(HC)$ in alpha2 and beta

(Wang et al., 2014)	32 HC 25 AD	Coherence	binary	CC L $Eloc$ E_{global}	• $CC(AD) < CC(HC)$ in all frequency band exexpt delta • $L(AD) > L(HC)$ in all frequency band exexpt delta • $E_{loc}(AD) < E_{loc}(HC)$ in all frequency bands • $E_{global}(AD) < E_{global}(HC)$ in all frequency bands • $SW(AD) < SW(HC)$ in all frequency bands
(Vecchio et al., 2014)	50 HC 154 MCI 174 AD	Coherence	weighted	CC L SW	• $CC(AD) > CC(MCI) > CC(HC)$ in delta, and especially in theta • $L(AD) < L(HC)$ in theta while $L(MCI) \approx L(HC)$ • $SW(AD) > SW(MCI) > SW(HC)$ in theta
(Afshari and Jalili, 2016)	26 HC 25 AD	Directed transfer function	binary	E_{loc} E_{global}	• $E_{loc}(AD) > E_{loc}(HC)$ in alpha and especially in beta • $E_{global}(AD) < E_{global}(HC)$ in alpha and beta • Classification: best accuracy = 94% (0.08 as threshold value) • Accuracy was very sensitive to threshold value
(Vecchio et al., 2018)	74 S-aMSI 71 C-aMCI	Coherence	weighted	SW	• Significant differences in SW in delta, alpha1, alpha2, beta2, gamma bands. • SW values (in each band) were not sufficient to obtain a good classification between the two groups (acc = 61%).
(Miraglia et al., 2020)	59 aMCI	Default mode network	weighted	SW E_{global}	• $SW(C-aMCI) < SW(S-aMCI)$ in gamma • SW of C-aMCI with LD impairment decreased in delta • SW of C-aMCI with ED impairment decreased in delta and gamma • SW of C-aMCI with ED impairment decreased in alpha1
(Franciotti et al., 2019)	42 HC 42 AD-MCI 41 AD	Granger causality	binary (directed)	K, K_{in}, K_{out} CC L E_{loc} E_{global} $assortivity$	• $K_{in,out}(patients) < K_{in,out}(HC)$ for non-hubs and hubs nodes, exept the frontal region where patients groups showed an additional hub in F3. • $CC(AD) < CC(AD-MCI)$ in the right occipital electrode • CC of right occipital electrode was positively correlated with MMSE • $E_{loc}(patients) < E_{loc}(HC)$ • $E_{global}(patients) < E_{global}(HC)$
(Chen et al., 2019)	109 AD	Pearson's correlation coefficient	weighted	CC_{global} E_{global} CC	• Poitive correlation between both of CC_{global} and E_{global} with verbal fluency score • CC(F3,F4,C3,Cz,C4,P3,P4) is affected significantly due to AD.

(Li et al., 2019)	8 HC 6 AD	weighted phase lag index	weighted	K CC BW	• $K_{in,out}(patients) < K_{in,out}(HC)$ for non-hubs and hubs nodes, exept the frontal region where patients' groups showed an additional hub in F3. • $[K, CC, BW](AD) < [K, CC, BW](HC)$ in prefrontal and parietal regions in alpha 2 and beta • $[K, CC, BW](AD) < [K, CC, BW](HC)$ in frontal region in all frequeny bands • $[K, CC, BW](AD) > [K, CC, BW](HC)$ in temporal region in all frequeny bands
(Vecchio et al., 2020)	120 HC 175 AD	Coherence	wei	SW	• Optimal classification accuracy on an individual basis (AUC = 0.97)
(Mehraram et al., 2020)	18 HC 32 AD 25 DLB	weighted phase lag index	weighted	K CC L SW Q	• classification accuracy AD vs DLB : accuracy = 66% • classification accuracy HC vs DLB : accuracy = 77%
(Jalili, 2017)	25 HC 23 AD	Pearson's correlation coefficient	binary	L E_{loc} E_{global} BW T ast Q	• GA was the best method of feature selection compared to BPSO and SITO in term of classification accuracy (acc= 83% in beta) • Optimal features included BW, E_{global}, Q, assortivity.
(Cecchetti et al., 2021)	33 HC 86 aMCI 39 AD	Pearson's correlation coefficient & Coherence	weighted	CC L	Especially in occipital and temporal regions : • $CC(AD) > CC(aMCI) > CC(HC)$ in theta • $CC(AD) < CC(aMCI) < CC(HC)$ in alpha2 • $L(AD) < L(aMCI) < L(HC)$ in theta • $L(AD) > L(aMCI) > L(HC)$ in alpha2
(Vecchio et al., 2021)	54 HC 80 aMCI 100 AD 40 VaD	Coherence	weighted	SW	• $SW(AD) < SW(MCI) < CC(HC)$ in theta • $SW(AD) > CC(HC)$ in alpha • $SW(VaD) \approx SW(AD)$
(Tait et al., 2019)	26 HC 21 AD	Coherence	weighted	SW L	Especially in temporal region : • Poitive correlation between SW and both of MMSE and language sub-score in theta band • Negative correlation between L and both of MMSE and language sub-score in theta band

4.4 Conclusion

In this chapter, we first explained how graph theory is exploited for brain network construction based on functional connectivity measurement. Then, we summarized the main results of the literature exploiting graph theory for brain network analysis in AD, MCI and healthy subjects. In

spite of the fact that the majority of studies have reported that the network's topology is altered in AD and MCI patients compared to HC, Table 4.2 shows that contradictory results are observed in the literature.

In this thesis, we will exploit graph theory to analyze the cortical brain network over three stages of cognitive decline, namely SCI, MCI and AD stages. One of our goals is to clarify the use of the topological parameters in our framework, by proposing a deep interpretation of such parameters. We will also conduct comparative studies exploiting different functional connectivity measures to evaluate their effectiveness in characterizing the brain topologies in the three stages of cognitive decline.

Chapter 5

EEG signal analysis with a statistical connectivity measure for AD detection

5.1 Objective of the study

As earlier mentioned in Chapter 1, we conducted a first study to evaluate the potential use of *EpEn*, already introduced and published in (Houmani et al., 2013, 2015, 2018), to estimate the functional connectivity between brain regions.

As explained in Section 3.4.1, *EpEn* stems from a refined characterization of the local statistical properties of EEG signals using Hidden Markov Models (HMM). It has been shown that this measure estimates the disorder of EEG signals locally over time (as done by classical complexity measures), and spatially by estimating the inter-channel disorder.

The present study addresses the problem of AD detection based on the analysis of a database containing EEG time series acquired in real clinical conditions at Charles-Foix Hospital in France. This database contains EEG data from subjects with Subjective Cognitive Impairment (SCI), patients with Mild Cognitive Impairment (MCI), and AD patients.

The objective of the study is to extend our previous results and demonstrate the effectiveness of *EpEn* measure for AD detection comparatively to other functional connectivity measures. In this way, four alternative connectivity measures are thus used as ground truth to assess the effectiveness of our method: phase synchrony, Granger causality, coherence and mutual information. We will show that the proposed statistical measure allows a better characterization of the underlying neuronal dynamics in the context of AD detection, since it relies on the refined statistical modeling of EEG signal considering its complete spatio-temporal nature.

5.2 Charles-Foix database

5.2.1 Study population

All experimental studies conducted in this thesis are retrospective, and exploit a database containing EEG signals recorded in real clinical conditions between 2009 and 2013 at Charles-Foix Hospital

(Ivry-sur-Seine, France). The particularity of such database relies on the fact that it reflects what medical practitioners are facing in reality, as opposed to databases used in the literature that are prone to experimental constraints that do not match the reality on the ground.

The retrospective studies were approved by the institutional review board of the local Ethics Committee Paris 6, on May 16th, 2013 (France). All data were fully anonymized before exploiting them in our research work. An information letter on the research work was sent to the patients, with possibility of opposing to the use of their collected data. Informed consent was thus waived in this context. There are legal and ethical restrictions on sharing these data. The French law requires patients to be duly informed of any use of their data. We did not get patients' permission to share their data publicly. We are not able to ask for their consent today because the data was collected some time ago, between 2009 and 2013.

The database contains EEG data of 102 patients (mean age 75.38 ± 10.66 years old, range 42 ± 97 years old; 69 women), including 22 SCI subjects, 52 MCI patients and 28 mild to moderate AD patients. Table 5.1 reports information about demographic and clinical characteristics of the patients.

Table 5.1: Clinical characteristics of the cohort.

Characteristics	**SCI (n=22)**	**MCI (n=52)**	**AD (n=28)**
Age (mean ± SD)	68.9 ± 10.3	75.2 ± 10.8	80.8 ± 10.5
Female	81.8%	61.5%	67.8%
MMSE (mean ± SD)	28.3 ± 1.6	24.5 ± 4.9	18.3 ± 6.1
BREF (mean ± SD)	15 ± 1.6	13 ± 2.1 (n=21)	10,8 ± 2,9
Hippocampal memory disorders	0%	25% (n=20)	88.9%
Hippocampal atrophy	14,3% (n=7)	46,7% (n=15)	80% (n=15)
Benzodiazepine use	18.28%	9.6%	28.6%
Antidepressant use	9%	19.2%	42.8%
Neuroleptic use	0%	3.8%	17.8%
Hypnotic use	22.7%	23.1%	25%

The patients who complained of memory impairment were referred to the outpatient memory clinic of the Charles-Foix Hospital to undergo a battery of clinical tests for brain disorders, including neuropsychological test, brain imaging and blood samplings. For each patient, a diagnosis was established at the memory clinic on the basis of the clinical assessment, brain imaging, psychometric findings, interviews and neuropsychological tests, conducted by a multidisciplinary medical staff, according to the standard diagnostic criteria: DSM-IV, NINDS, Jessen criteria for SCI, Mc Keith criteria for Lewy body dementia (Jessen et al., 2014; Mitchell et al., 2014; McKeith et al., 2005). Patients with epilepsy were excluded. Of note, EEG was not used to establish the diagnosis.

5.2.2 EEG recordings

The EEG recordings were obtained at rest and with closed eyes using a Deltamed digital EEG acquisition system with scalp electrodes, positioned over the whole head according to the 10–20 international system, in a common reference montage. Thirty electrodes were considered: Fp1,

Fp2, F7, F3, Fz, F4, F8, FT7, FC3, FC7, FC4, FT8, T3, C3, Cz, C4, T4, TP7, CP3, CPz, CP4, TP8, T5, P3, Pz, P4, T6, O1, Oz, and O2 as displayed in Figure 5.1.

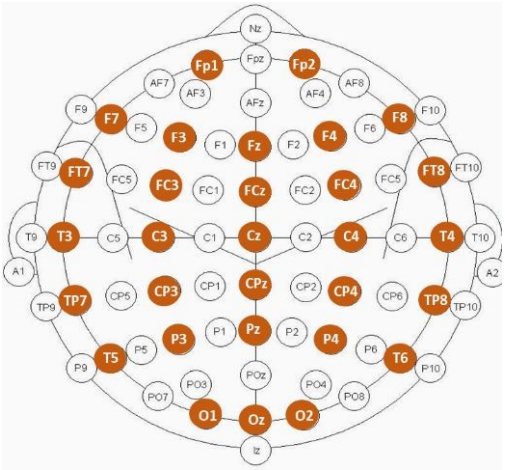

Figure 5.1: Placement of the 30 electrodes used for EEG signal recordings (marked in red).

All data were digitalized in a continuous recording mode for a minimum of 20 min with a 256 Hz sampling frequency.

The EEG recordings were pre-processed off-line on MATLAB software. For each subject in the database, continuous epochs of 20 seconds, free from artifacts (eye movements, eye blinks, muscular activity, instrumental noise etc.), were manually selected. To do that, an EEG expert visually inspected the EEG signals and discarded the parts of the signals presenting artifacts. The extracted clean 20 seconds segments were then kept for the study. Note that the EEG expert was blinded from the results of the experimental studies.

Then, the obtained free artifact 20s EEG signals were notch filtered at 50 Hz to eliminate possible artifacts caused by power line interference. Finally, the obtained EEG signals were band pass filtered with a third-order digital Butterworth filter in the four conventional frequency bands of interest: delta (1–4 Hz), theta (4–8 Hz), alpha (8–12 Hz) and beta (12–30 Hz).

5.3 Study design

The first study of the thesis was performed considering EEG recordings of the 22 SCI subjects, the 28 AD patients and 22 MCI patients (among the 52 MCI available in the database).

In this work, we investigate the reliability of *EpEn* measure for the discrimination of AD patients from SCI and MCI patients. We confront this statistical measure to coherence, phase synchrony, mutual information and Granger causality measures, in terms of classification performance using Support Vector Machine (SVM) classifier. Note that all these measures are presented in Section 3.3.1. The comparison of the five measures will allow a better understanding on the mechanisms of *EpEn* in the framework of AD detection.

To this end, we computed for each person all the EEG measures (hereafter referred to as features)

on the four frequency bands (delta, theta, alpha and beta) considering different brain regions, using sets of channels located in regions susceptible to be sensitive to changes due to AD. Hence, we defined seven regions of interest: prefrontal (Fp1, Fp2), occipital (O1, O2), frontal (F7, F3, Fz, F4, F8), temporal (T6, T4, F8, T5, T3, F7), central (FCz, C3, CPz, C4), occipito-prefrontal (Fp1, Fp2, O1, O2) and parieto-occipital (T6, P4, Pz, P3, T5, O1, O2).

In order to compute for each person the four classical EEG features (coherence, phase synchrony, mutual information and Granger causality), we first calculated such measures between all pairs of electrodes belonging to the considered brain region. Then, we averaged over all those signal pairs to obtain a functional connectivity measure per region.

By contrast, *EpEn* computes in one single step the information content conveyed by coupling different EEG signals of a given region, by means of the statistical modeling of the multidimensional EEG signal with HMM. Note that the optimal values of the hyperparameters needed for a reliable estimation of the *EpEn* measure, such as number of Gaussians and epochs (states of the HMM), were fixed based on our experimental findings in previous works (Houmani et al., 2013, 2015, 2018).

Then, to distinguish automatically between each pair of classes, i.e. AD vs. SCI, SCI vs. MCI and AD vs. MCI, a linear single-feature SVM classifier was first used with a leave-one-out procedure, and the threshold that gave the best correct classification rate was selected. The performance was assessed for each brain region and each frequency band. Then, in order to improve the performance, we estimated the classification performance per frequency band using a linear SVM combining two brain regions.

5.4 Experimental results

5.4.1 Discriminating AD patients from SCI subjects

Table 5.2 shows the correct classification rate for the five measures per brain region and frequency band. We report the configurations that led to the best classification performance in terms of accuracy.

Table 5.2: Best classification performance when discriminating AD from SCI with each EEG feature.

AD vs. SCI	**Coherence**	**Phase synchrony**	**Granger causality**	**Mutual information**	**EpEn**
Brain region	Parieto-occipital	Prefrontal	Frontal	Temporal	Occipital
Frequency band	Delta	Alpha	/	Alpha	Theta
Accuracy	70%	66%	68%	68%	70%
Sensitivity (AD)	59.1%	68.2%	41%	89.3%	59.1%
Specificity (SCI)	78.6%	64.3%	85.7%	40.9%	78.6%

To obtain an *EpEn* value for each subject, per brain region and frequency band, the HMM was trained on a set of EEG signals captured by the electrodes of the considered brain region, as explained in the previous section. The other measures were computed for each person, per brain region and frequency band, by averaging all the connectivity values computed between pairs of electrodes of the considered region. Note that Granger causality measure is computed on the complete EEG time series in the time domain.

Results show that the five EEG features are not reliable to discriminate AD patients from SCI subjects, when computed per brain region and per frequency band. Coherence and *EpEn* are those giving the best accuracy value of 70% but with an unbalanced performance in terms of sensitivity (percentage of AD well classified) and specificity (percentage of SCI well classified).

Besides, Table 5.2 highlights different brain regions of interest and frequency bands when discriminating AD from SCI, dependent on the functional connectivity measure under consideration. This finding reflects in part the disparity of the conclusions in the literature on the brain regions and frequency bands that could be considered in the framework of AD.

For a refined comparative analysis, Figure 5.2 shows the boxplots of the five features considering the brain regions and the frequency band that gave the best accuracy value to distinguish AD patients from SCI. Figure 5.2.a and Figure 5.2.e show that AD patients have lower values of coherence and *EpEn* than control subjects, respectively, in low frequency bands. AD induces a decreased coherence on delta band in parieto-occipital regions (Mann-Whitney $p = 1.42 * 10^{-2}$), and a decreased information content conveyed by the multidimensional EEG time series on theta band in the occipital region (Mann-Whitney $p = 5.22 * 10^{-4}$).

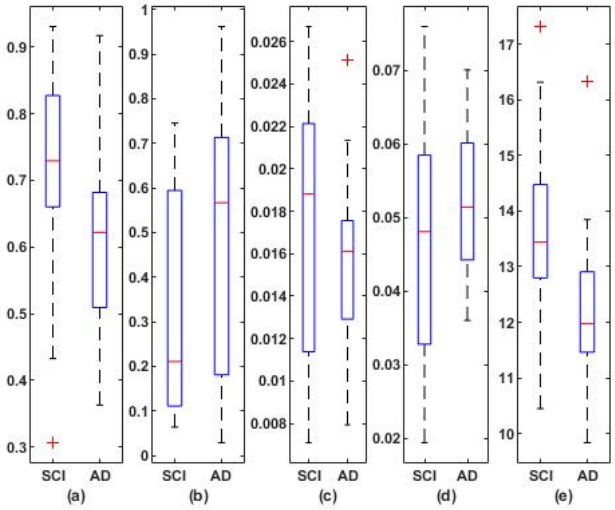

Figure 5.2: Boxplots of the five EEG features when discriminating AD patients from SCI subjects with: (a) coherence, (b) phase synchrony, (c) Granger causality, (d) mutual information, and (e) *EpEn* measure, computed on the region and the frequency band reported in Table 5.2.

Table 5.3 shows the classification performance when discriminating AD from SCI with each measure,

considering the functional connectivity values of two brain regions as input to the linear SVM classifier. We performed experiments on different combinations of brain regions and reported in Table 5.3 only those leading to the best accuracy value.

Table 5.3: Best classification performance when discriminating AD from SCI with each EEG feature, considering a combination of two brain regions.

AD vs. SCI	**Coherence**	**Phase synchrony**	**Granger causality**	**Mutual information**	**EpEn**
Brain regions	Temporal & Parieto-occipital	Central & Occipito-prefrontal	Frontal & Temporal Frontal & occipital	Temporal & Occipito-prefrontal	Temporal & Parieto-occipital Frontal & occipital Central & Occipital Central & Prefrontal
Frequency band	Delta	Theta	/	Alpha	Theta
Accuracy	70%	72%	74%	70%	98%
Sensitivity (AD)	59.1%	63.6%	54.5%	89.3%	95.5%
Specificity (SCI)	78.6%	78.6%	89.3%	45.5%	100%

Results clearly show that, except for coherence measure, the performance are improved for all measures when combining different brain regions. However, we observe that for the four widely used measures, an unbalanced specificity and sensitivity values remains.

The improvement of performance is significant with *EpEn* measure. A correct classification rate of 98% is reached with a specificity of 100% and a sensitivity of 95.5%. This result shows the reliability of the used feature to detect AD, even the control subjects of this database are not healthy subjects since they have some memory complaints.

Also, we observe that this good discrimination of AD from SCI is obtained with different combinations of brain regions (temporal & parieto-occipital, frontal & occipital, central & occipital, central & prefrontal). This finding suggests that *EpEn* is less sensitive to brain regions changes, and thus is more stable and reliable comparatively to the other measures.

In addition, the selected frequency band and brain regions with *EpEn* are in accordance with some results reported in the literature (Jelic et al., 2000; Locatelli et al., 1998; Adler et al., 2003; Jelic et al., 1997; Knott et al., 2000) and clinical knowledge (Braak and Braak, 1991; Pantel et al., 2004; Brun and Englund, 1981): on the one hand, AD detection has been shown on theta band; on the other hand, temporo-parieto-occipital regions are the first affected regions in the early stage of AD.

Another interesting finding emerge with *EpEn*: the central region is informative for AD detection considering long-range dynamics with distant regions, *i.e.* the extreme posterior (occipital) or the extreme anterior (prefrontal) regions. Actually, we notice that the discrimination between AD and SCI with *EpEn* relies on the quantification of the long-range information transmission among regions of the brain, as displayed in Figure 5.3.

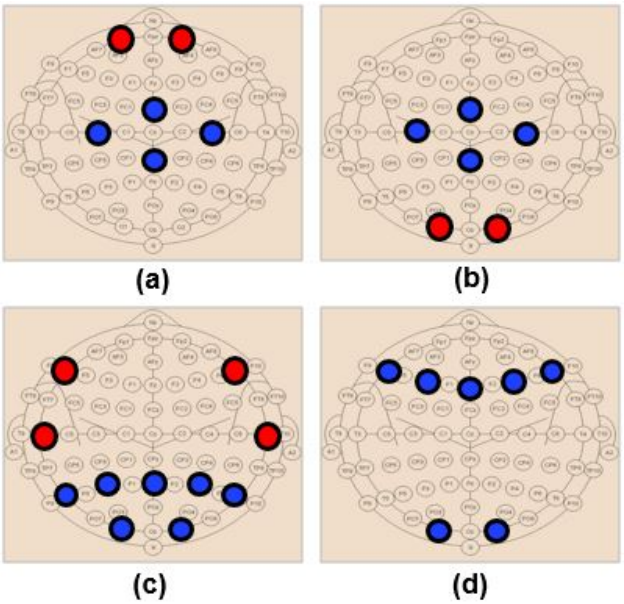

Figure 5.3: The electrodes that belong to the regions leading to the best discrimination between AD and SCI with *EpEn* in theta band: (a) central & prefrontal, (b) central & occipital, (c) temporal & parieto-occipital, and (d) frontal & occipital regions.

In order to go deeper in our understanding, Figure 5.4 and Figure 5.5 show the distribution of *EpEn* values in theta band for the two populations (AD and SCI) considering the two combinations of two regions among those reported in Table 5.3 (frontal & occipital regions, central & occipital regions, respectively). A linear separation between the two populations appears clearly in both cases; this result highlights the discrimination efficiency of *EpEn* measure.

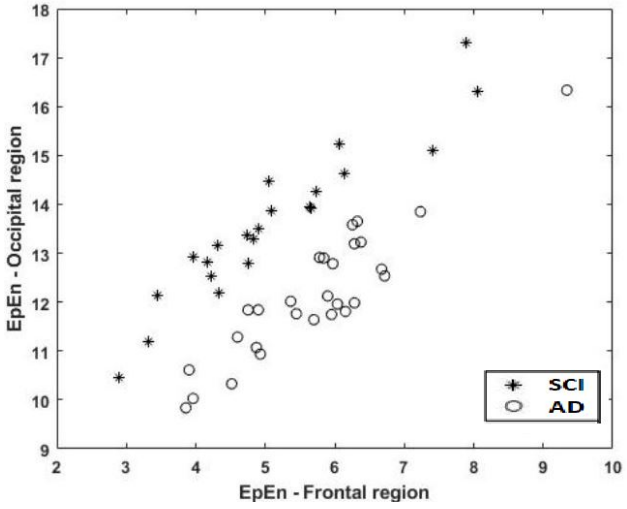

Figure 5.4: The distribution of *EpEn* values of AD patients and SCI subjects computed on theta band considering frontal & occipital regions.

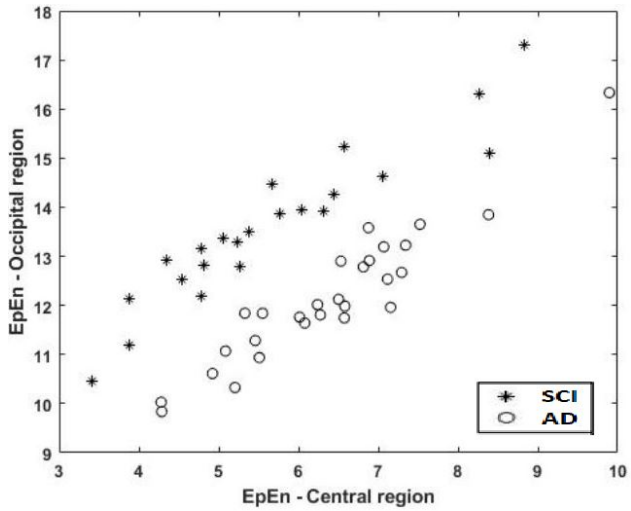

Figure 5.5: The distribution of *EpEn* values of AD patients and SCI subjects computed on theta band considering central & occipital regions.

5.4.2 Discriminating AD patients from MCI patients

Table 5.4 shows the performance of the linear SVM classifier when discriminating AD patients from MCI patients, with a leave-one-out procedure. We report the best classification performance obtained for each EEG feature.

Table 5.4: Best classification performance when discriminating AD from MCI with each EEG feature.

AD vs. MCI	**Coherence**	**Phase synchrony**	**Granger causality**	**Mutual information**	**EpEn**
Brain region	Central	Parieto-occipital	Occipital	Temporal	Occipital
Frequency band	Delta	Delta	/	Beta	Theta
Accuracy	66 %	60 %	54 %	70 %	70 %
Sensitivity (AD)	60.7 %	75 %	100 %	57.1 %	64.3 %
Specificity (MCI)	72.7 %	40.9 %	0 %	86.4 %	77.3 %

Mutual information and *EpEn* measures are those giving the best accuracy of 70% when discriminating AD patients from MCI patients. However, *EpEn* offers a better balance between sensitivity (percentage of AD well classified) and specificity (percentage of MCI well classified).

When comparing the obtained results with *EpEn* in Table 5.4 (AD vs. MCI) to those reported in Table 5.2 (AD vs. SCI), we notice that the occipital region and theta band are selected in both cases. This means that computing *EpEn* in the occipital region on theta band allows discriminating

AD from the two first stages of the disease, *i.e.* SCI and MCI. This behavior is not observed for the other measures.

We display in Figure 5.6 the boxplots for each EEG features considering the brain regions and the frequency band that gave the best accuracy value to distinguish AD patients from MCI. Figure 5.6.b and Figure 5.6.e show that AD patients have lower values of phase synchrony and *EpEn* than MCI subjects, respectively. Moreover, it appears clearly that the *EpEn* values of AD patients are significantly lower than those of MCI patients (Mann Whitney $p = 1.22 * 10^{-4}$). This result is coherent with those reported in the literature (Pijnenburg et al., 2004; Stam and Van Dijk, 2002; Stam et al., 2003; Babiloni et al., 2004b): AD induces a reduction of synchronization and information transmission in AD compared with MCI.

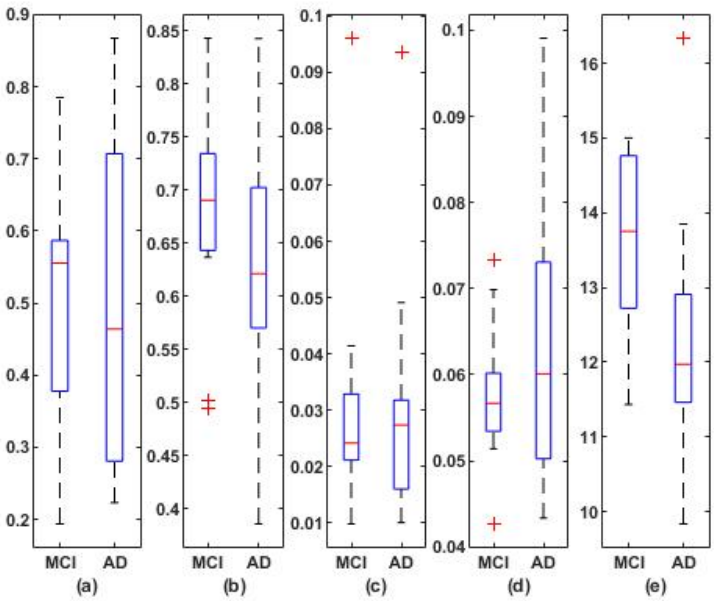

Figure 5.6: Boxplots of the five EEG features when discriminating AD patients from MCI subjects with: (a) coherence; (b) phase synchrony, (c) Granger causality, (d) mutual information, and (e) *EpEn* measure, computed on the region and the frequency band reported in Table 5.4.

Table 5.5 reports the classification performance for each measure, when combining two brain regions. We carried out experiments on different combinations of brain regions per frequency band and reported only those leading to the best accuracy value.

The *EpEn* measure outperforms significantly all the other functional connectivity measures: an accuracy of 100% is reached in the theta band when considering occipital and frontal regions.

Table 5.5: Best classification performance when discriminating AD from MCI with each EEG feature, considering a combination of two brain regions.

AD vs. MCI	**Coherence**	**Phase synchrony**	**Granger causality**	**Mutual information**	**EpEn**
Brain regions	Occipital & Parieto-Occipital	Temporal & Frontal	Temporal & Parieto-Occipital	Temporal & Occipito-prefrontal	Occipital & Frontal
Frequency band	Alpha	Delta	/	Alpha	Theta
Accuracy	68%	64%	58%	74%	100%
Sensitivity (AD)	60.7%	85.7%	60.7%	96.4%	100%
Specificity (MCI)	77.3%	36.4%	54.6%	45.5%	100%

Compared to the previous results obtained in Table 5.3 (AD vs. SCI), we notice that *EpEn* is the best feature for AD detection (versus SCI or MCI) when computed on theta band in the occipital and frontal regions.

Figure 5.7 displays the distribution of *EpEn* values in theta band for AD and MCI patients considering the combinations of the occipital and frontal regions. We clearly observe a linear separation between the two populations, which indicates the discrimination efficiency of *EpEn* measure.

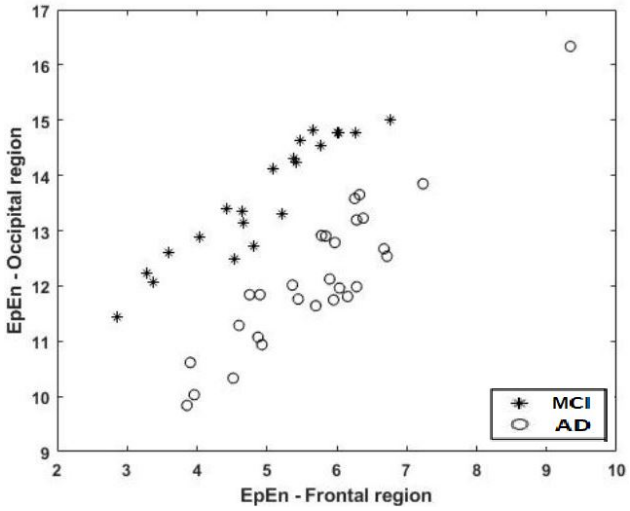

Figure 5.7: The distribution of *EpEn* values of AD and MCI patients computed on theta band considering the frontal and occipital regions.

5.4.3 Discriminating SCI subjects from MCI patients

To go deeper in our analysis, we carried out additional experiments to discriminate SCI subjects from MCI patients considering only *EpEn* measure, since it outperforms the other measures for AD detection.

As shown in Table 5.6, a classification accuracy of 77.3% is obtained with a specificity of 77.3% and a sensitivity of 77.3%, considering all frequency bands and the combination of *EpEn* values computed on the occipital region and the occipito-parietal region. A polynomial SVM of order two was used for this two-class classification using eight features as input to the SVM. This result proves the difficulty to differentiate these two populations (SCI and MCI), which are both at the first stage of the disease.

Table 5.6: Best classification performance when discriminating SCI from MCI with EpEn measure.

SCI vs. MCI	**EpEn**
Brain regions	Occipital & Parieto- Occipital
Frequency band	Delta-Alpha-Beta-Theta
Accuracy	77.3%
Sensitivity (MCI)	77.3%
Specificity (SCI)	77.3%

Interestingly, we observe that the selected brain region to distinguish MCI from SCI subjects with *EpEn* is localized in the posterior brain area, *i.e.* in the parietal and the occipital regions. This result is in contrast with the obtained results on AD patients (AD vs. SCI or AD vs. MCI), where long-range connectivity is taken into account to detect the disease.

5.5 Discussion and conclusion

The utility of rsEEG in Alzheimer's disease (AD) research has been demonstrated over several decades in numerous studies. The major EEG changes that have been reported in AD are the reduction of EEG complexity and the perturbations of EEG functional connectivity. Several EEG markers have been employed successfully to investigate these two AD-related alterations, based on sophisticated signal processing techniques.

However, three main drawbacks emerge from the research works in the state-of-the-art. First, complexity and functional connectivity were commonly quantified separately. Second, the majority of the extracted EEG markers did not consider the EEG signal as a multidimensional time series. Third, such measures were computed on the whole EEG time series without addressing the problem of their non-stationarity, even it is well known that most physiological signals, such as EEG are non-stationary.

The purpose of this study (referred to as Study 1) was to review a recently proposed entropy-based functional connectivity measure, called *Epoch-based Entropy*, and to investigate its potential

application to the detection of AD patients based on multi-channel EEG signals. This entropy measure is computed on piecewise stationary epochs using a HMM, which performs local density estimation at the epoch level. The use of HMM is motivated by the fact that its structure is suitable for modeling neural dynamics underlying the observed EEG signals. In addition, HMM can manage multidimensional signals by applying multivariate probability density functions on the signals.

The originality of this statistical measure lies on the fact that it estimates the information content or the disorder in EEG signals on piecewise stationary epochs over time; and at the spatial level, by quantifying the functional connectivity in terms of the heterogeneity of piecewise stationary epochs between multi-channel EEG signals. This will allow a better estimation of the spatio-temporal characteristics of EEG signals merged into a single figure.

By comparing Epoch-based Entropy to four alternative functional connectivity measures, namely coherence, phase synchrony, Granger causality and mutual information, we showed that the statistical measure is by far a more reliable feature for AD detection, on our experimental data. We obtained a high accuracy for the classification of AD vs. SCI (98% accuracy, 100% specificity, 95.5% sensitivity). Then, by comparing AD and MCI, we reached an accuracy of 100%. In both cases, a common finding was observed: computing the Epoch-based Entropy on theta in frontal and occipital regions allows a good discrimination between AD and its early stages (SCI and MCI).

In conclusion, our study demonstrates the effectiveness of the statistical modeling of EEG with HMM for analyzing the dynamics of neural activity in patients with AD. However, by comparing SCI and MCI patients, we obtained an accuracy of 77.3% due to the similarities between SCI patients and MCI patients. Indeed, a proportion of SCI patients are actually at an early stage of MCI (**?**). Based on these findings, we conducted further experiments to improve classification performance when comparing SCI, MCI and AD. In the following chapter, we will present a new framework based on graph theory that allows a better discrimination between the three populations.

Chapter 6

Weighted brain network analysis on different stages of clinical cognitive decline

6.1 Problem and objective of the study

In spite the fact that the majority of studies have reported that the network's topology is altered in AD and MCI patients compared to HC, contradictory results are observed in the literature, as reported in Section 4.3 and shown in Table 4.2. This is mainly due to the use of data sets with different characteristics as well as methodological differences. More precisely, EEG databases with different characteristics are used in the literature for comparing AD patients to HC and MCI. In addition, they are prone to experimental constraints that do not match the reality on the ground, such as including strict patient's inclusion and exclusion criteria and considering normal healthy subjects as controls.

Besides, most studies consider undirected binary networks, which require the application of an arbitrary threshold on adjacency connectivity matrices. This factor affects directly the resulting network. Also, the choice of using weighted or binary matrices to estimate network graph has mostly been arbitrary to date. Recently, some studies addressing this issue (Chen et al., 2019; Mehraram et al., 2020) found that preserving real-valued weights produces consistent results by exploiting additional topological information that is stored in the weights.

Moreover, several measures are exploited to quantify the connectivity in brain networks. These measures may reflect different processes, which lead to different network topologies. The majority of studies motivated the use of a specific connectivity measure, without comparing it to others on the same database, and without studying the contribution of graph analysis with respect to classical connectivity analysis. The variability in calculation routines leads to a difficulty in comparing the results between studies that are sometime contradictory. In addition, all graph-based studies characterizes links in graph networks using only the degree of signal synchronization between electrodes, without considering the other EEG abnormalities in AD, such as reduction of EEG complexity.

By contrast to the above-mentioned investigations, the present study relates to the analysis of the functional connectivity network in SCI, MCI and AD stages, based on rsEEG data acquired in real-life clinical conditions. To this aim, we exploited *EpEn* as a spatiotemporal connectivity

measure, to perform a weighted graph analysis of SCI, MCI and AD brain networks.

In the previous study presented in Chapter 5, *EpEn* was computed per brain region on a set of EEG signals belonging to the considered region (Houmani et al., 2013, 2015, 2018). In this work, we propose to compute *EpEn* on all possible pairwise electrodes for a refined characterization of the functional connectivity, which will be exploited for the network topology analysis.

By means of graph theory analysis on the obtained adjacency matrices, we assess the hypothesis that the refined characterization of EEG signals based on our statistical spatiotemporal entropy measure combined to the topological characterization of the brain network, could allow a better understanding of the global connectivity organization between SCI, MCI and AD populations.

The novelty of this study is twofold. First, this is the first study addressing EEG brain network analysis over the three SCI, MCI and AD stages. Second, to our knowledge, this is the first study combining an entropy-based measure to graph theory. We show that this new framework allows conducting a refined brain network analysis, which highly contributes to a better understanding on the evolution of AD from the SCI to dementia, through the MCI stage.

6.2 Study design and methodology

The present study was conducted considering the rsEEG data of the 22 SCI, the 52 MCI and the 28 AD patients of Charles-Foix database. Details about the characteristics of the three populations are given in Section 5.2.1.

In order to investigate differences between SCI, MCI and AD, we first studied the functional connectivity in the three groups using *EpEn*. To assess the effectiveness of our entropy metric, we compared it to two alternative measures, commonly used in the literature: Magnitude Square Coherence (*MSC*) and Phase Lag Index (*PLI*), which are described in Section 3.3.1. Then, by means of graph theory analysis on the obtained adjacency matrices, we studied the organizational properties of brain networks in SCI, MCI and AD based on three topological parameters: clustering coefficient, shortest path and modularity. The description of these topological parameters was given in Section 4.2.

To analyse the difference between SCI, AD and MCI populations, we carried out a statistical analyses using MATLAB R2020a software. We compared characteristics between the SCI, MCI and AD groups using the Kruskal–Wallis test. This statistical test is a nonparametric version of the one-way ANOVA and is an extension of the Wilcoxon rank sum test to more than two groups. The results with a p-value lower than 0.05 are considered to be statistically significant. To evaluate the differences among the three groups in terms of functional connectivity measures, the statistical test was applied in Section 6.3.1 on each of the 30 electrodes and at each frequency band.

We also assessed the significant difference between groups in terms of the graph parameters computed on the average connectivity matrices. The Kruskal–Wallis test was performed on each frequency band considering, for each group, the 30 clustering coefficient values associated to the 30 electrodes. For the shortest path comparisons, the statistical analysis between the three groups was conducted on each electrode and each frequency band.

6.3 Experimental results

6.3.1 Functional connectivity assessment with three metrics

We computed the three functional connectivity measures between all pairs of the 30 electrodes for each person, and then averaged across subjects of SCI, MCI and AD group.

Figures 6.1, 6.2 and 6.3 show the average adjacency matrices (30x30) with *MSC*, *PLI* and *EpEn*, respectively, for the three populations in the four frequency bands. The electrodes are positioned on the matrices from left to right, anterior-posteriorly, as follows: (Fp1, Fp2, F7, F3, Fz, F4, F8, FT7, FC3, FCz, FC4, FT8, T3, C3, Cz, C4, T4, TP7, CP3, CPz, CP4, TP8, T5, P3, Pz, P4, T6, O1, Oz, O2). The diagonal elements of such matrices represent the connectivity of each electrode with itself. Thus, we ignored the diagonal elements in our analysis to consider only pairwise dynamics.

We visually notice that Figures 6.1, 6.2 and 6.3 exhibit different patterns in the average adjacency matrices between SCI, MCI and AD, in function of the functional connectivity measure and the frequency band. For a precise comparison between the three groups, we performed the Kruskal-Wallis test to detect the significant differences between matrices on each electrode and at each frequency band, as presented in Section 6.2.

We notice a significant difference between SCI, MCI and AD groups with *MSC* in delta band for all electrodes ($\rho < 0.05$) except TP7, in theta band at (FP1, FP2, F7, FT7, FC3, FCz, T3, CP3, CPz, P4, T6) and in beta band at (FT7, CP3). No significant difference was observed with MSC in alpha band. Concerning *PLI*, we observe a significant difference between the three groups in delta at (Fp1, Fp2, F3, FT7, CP3, CPz, TP8, T5, P4, O1, Oz), in theta at several electrodes except (Fp2, F8, FT8, C3, C4, T4, TPz, TP8, T5, P3, P4, O2), in alpha band at all electrodes, and beta band at (Fp1, Fp2, FT7, CP3, T6).

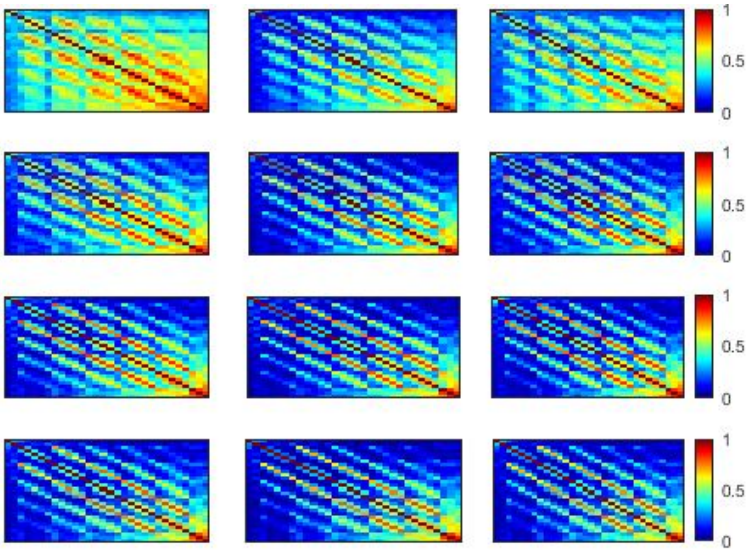

Figure 6.1: Average *MSC* across subjects in SCI (left), MCI (middle) and AD (right) groups for (a) delta, (b) theta, (c) alpha, and (d) beta bands. The 30 electrodes are shown from left to right side, anterior-posteriorly (up to bottom). The color bar indicates the values of *MSC*.

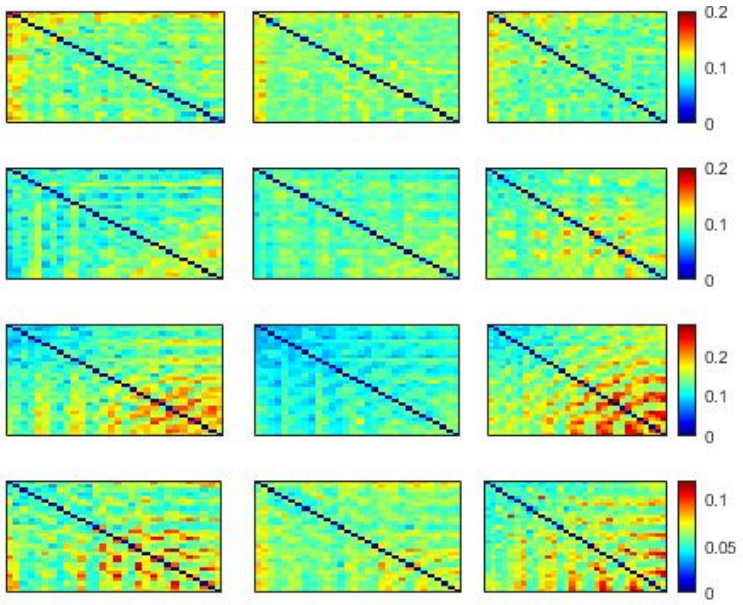

Figure 6.2: Average *PLI* across subjects in SCI (left), MCI (middle) and AD (right) groups for (a) delta, (b) theta, (c) alpha, and (d) beta bands. The 30 electrodes are shown from left to right side, anterior-posteriorly (up to bottom). The color bar indicates the values of *PLI*.

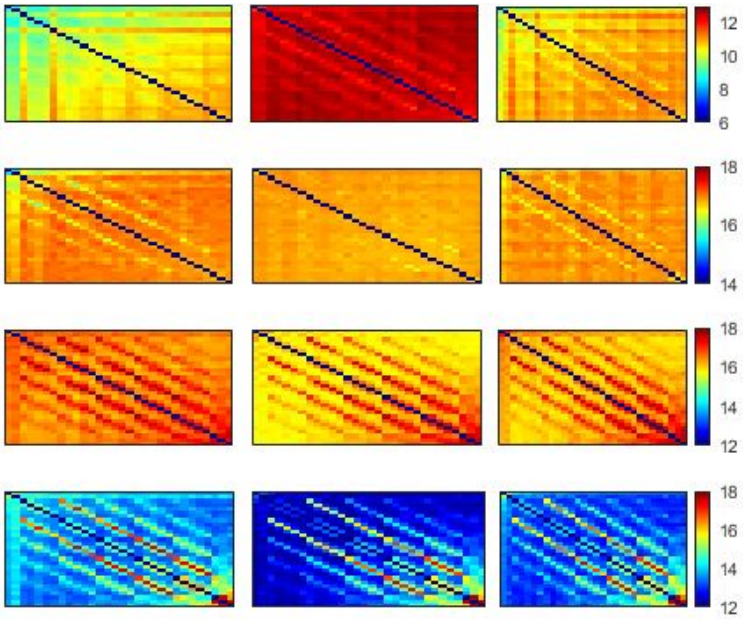

Figure 6.3: Average *EpEn* across subjects in SCI (left), MCI (middle) and AD (right) groups for (a) delta, (b) theta, (c) alpha, and (d) beta bands. The 30 electrodes are shown from left to right side, anterior-posteriorly (up to bottom). The color bar indicates the values of *EpEn*.

Regarding *EpEn* measure, Figure 6.3 shows a clear difference in the global functional connectivity organization between the three groups in all frequency bands. In delta, a significant difference is

obtained between the three groups at all electrodes ($\rho < 1e-12$). Besides, in Figure 6.3.a, we clearly observe a very high information content in MCI between all pairs of electrodes, which reduces in AD and even more in SCI, especially in the prefrontal and frontal regions. In theta, the difference between the three groups is less pronounced visually (see Fig.6.3.b); however the statistical analysis reveals a significant difference at all electrodes, except at (F3, P4). In high frequencies (Fig.6.3.c and Fig.6.3.d), the information content between all pairs of electrodes quantified by *EpEn* is higher for SCI and reduces for AD and even more for MCI. A significant difference between the three groups ($\rho < 0.05$) is observed in alpha and beta bands at all electrodes.

Figures 6.4, 6.5 and 6.6 display the distribution of the connectivity values computed between all pairs of the 30 electrodes, for the three groups in the four frequency bands. These connectivity values (435 values) correspond to those of the upper triangular part of the average matrices in Figures 6.1, 6.2 and 6.3, since these matrices are symmetric.

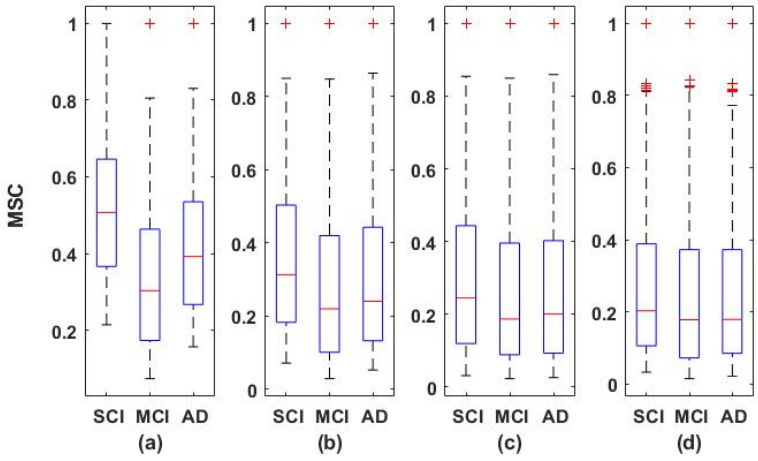

Figure 6.4: Boxplots of *MSC* values averaged over all subjects of SCI, MCI and AD groups, on (a) delta, (b) theta, (c) alpha and (d) beta bands.

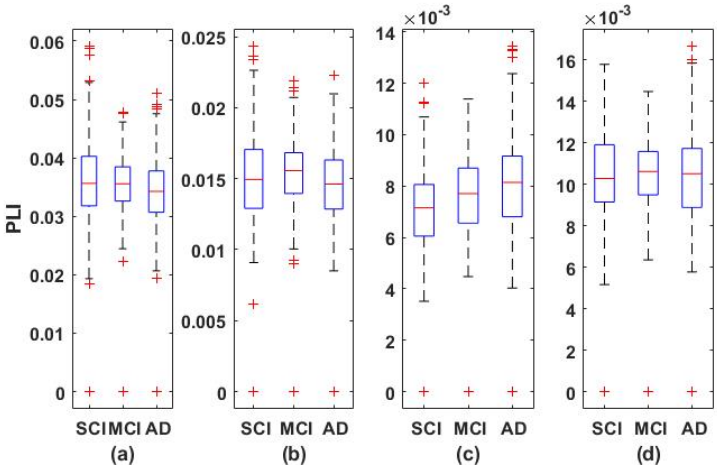

Figure 6.5: Boxplots of *PLI* values averaged over all subjects of SCI, MCI and AD groups, on (a) delta, (b) theta, (c) alpha and (d) beta bands.

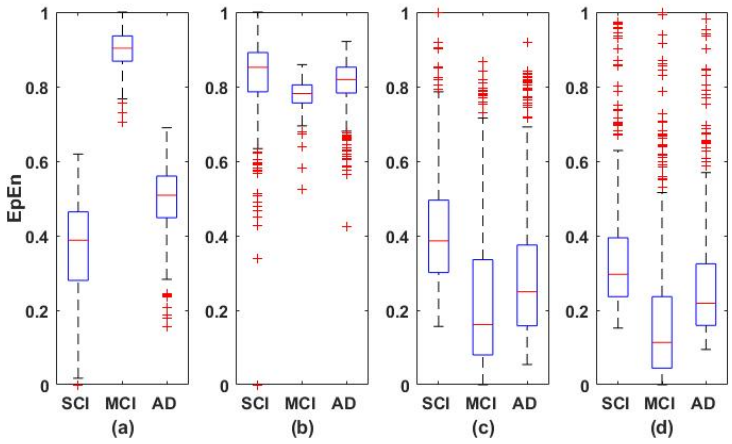

Figure 6.6: Boxplots of *EpEn* values averaged over all subjects of SCI, MCI and AD groups, on (a) delta, (b) theta, (c) alpha and (d) beta bands.

Overall, the statistical spatiotemporal entropy measure appears as the EEG marker that highlights a better distinction between the three groups compared to the two other deterministic measures. The contrast between SCI, MCI and AD is observed with *EpEn* at different frequency bands and almost all electrodes. When comparing *EpEn* values between AD and SCI, AD group presents higher values in delta and lower values in alpha and beta (Fig. 6.6). This result is in accordance with previously published studies: AD leads to an increased activity in delta and decreased activity in alpha and beta bands (Babiloni et al., 2020; Dauwels et al., 2010a; Babiloni et al., 2016; Jelic et al., 2000; Brassen and Adler, 2003; Onofrj et al., 2003; Ponomareva et al., 2003; Jeong, 2004).

Regarding the MCI group, it exhibits the highest *EpEn* values in delta and the lowest values in alpha and beta. Actually, MCI group shows a more accentuated behavior than AD relatively to SCI. In theta, the difference between the three groups with *EpEn* is less pronounced compared to the other frequency bands.

In addition, *EpEn* shows more differentiation between the three cognitive decline stages, at all electrodes, compared to the two other classical measures. Since we exploit local clustering coefficient and local shortest path parameters, in the rest of the paper, we investigate brain networks of SCI, MCI and AD using only *EpEn* to represent the connectivity between nodes. Figure 6.7 illustrates the network connectivity between the 30 electrodes using *EpEn* measure.

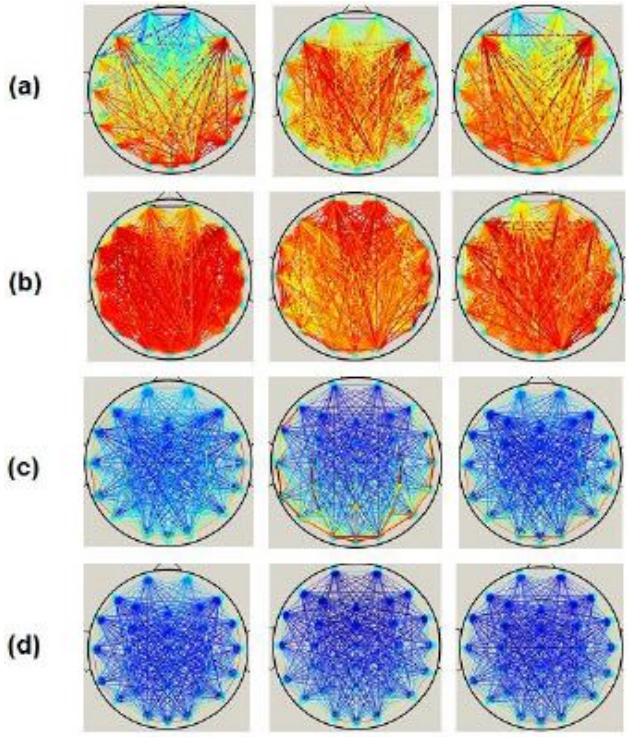

Figure 6.7: *EpEn* connectivity network of SCI (left), MCI (middle) and AD (right) groups, on (a) delta, (b) theta, (c) alpha and (d) beta bands.

6.3.2 Clustering coefficient

Figure 6.8 represents the distribution of clustering coefficient values computed for each average EpEn matrix of each group, in the four frequency bands. Each boxplot contains 30 local clustering coefficient values associated to the 30 nodes (electrodes).

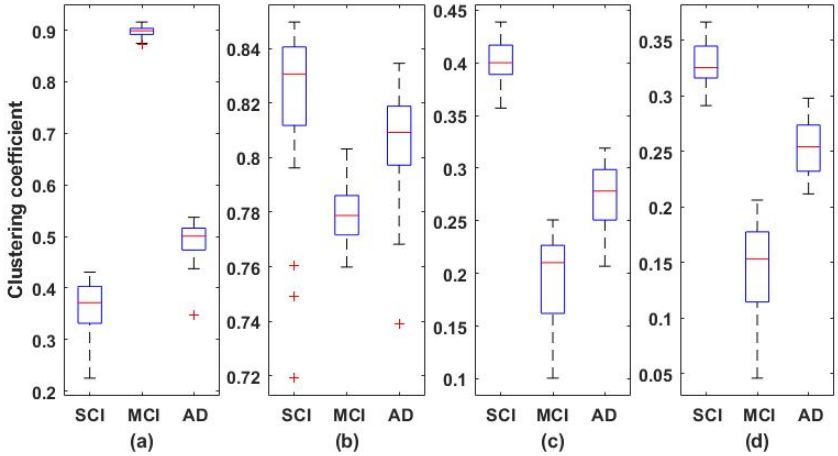

Figure 6.8: Boxplots of the local clustering coefficient values computed for each average *EpEn* matrix of SCI, MCI and AD, on (a) delta, (b) theta, (c) alpha and (d) beta bands.

When comparing Figure 6.8 and Figure 6.6, we notice that the clustering coefficient is correlated to *EpEn*: the relative positioning of the three populations, in the four frequency bands, is almost similar. Nevertheless, the clustering coefficient leads to a better characterization of the three populations than *EpEn*. The difference between SCI, MCI and AD is significant ($\rho < 1e-10$) in all frequency bands.

In theta, alpha and beta, the clustering coefficient presents the same tendency across the three groups; the opposite behavior is observed in delta.

In order to provide deeper insights on the topological organization in SCI, MCI and AD, in terms of clustering coefficient, we analyzed such parameter locally at each electrode (Fig. 6.9). We notice that, except for theta, there is no overlap between the three populations in delta, alpha and beta; but the behavior of this graph parameter across the three populations is frequency band-dependent.

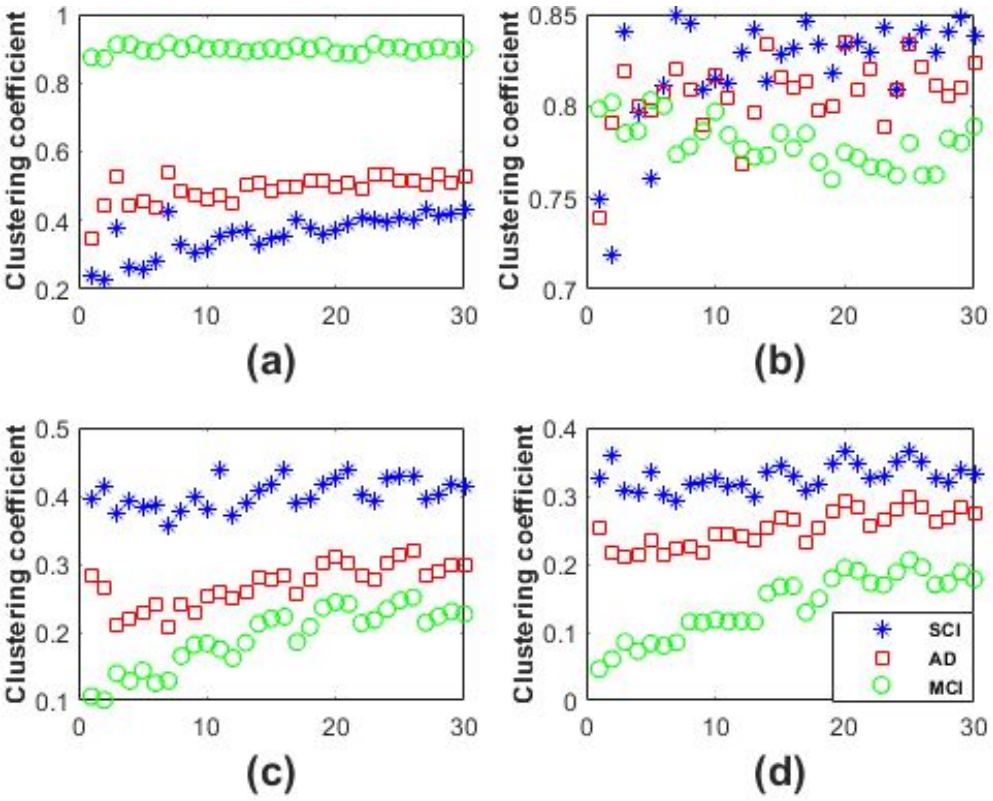

Figure 6.9: Clustering coefficient values over the 30 electrodes for SCI, MCI and AD, on (a) delta, (b) theta, (c) alpha, and (d) beta bands.

In delta, the MCI group shows the highest values of the clustering coefficient for all nodes; the SCI group shows the lowest values. The opposite is observed in the other frequency ranges, especially alpha and beta. Finally, the clustering coefficient values of AD group are in between those of SCI and MCI, whatever the frequency band.

Therefore, it is clear that the local clustering coefficient allows a better separation between SCI, MCI and AD, and thus a better characterization of the three stages of the disease.

6.3.3 Shortest path

At each node, we computed all the shortest paths between such node and the other 29 nodes, as explained in Section 4.2.3. For each shortest path, we calculated the number of edges composing the obtained path. Figure 6.10 reports the average number of edges in the obtained shortest paths at each node for the SCI, MCI and AD groups in delta, alpha and beta. In theta, the results do not show difference between the three groups in terms of number of edges in each electrode, as confirmed by the statistical test conducted on each frequency band and each electrode ($\rho > 0.05$).

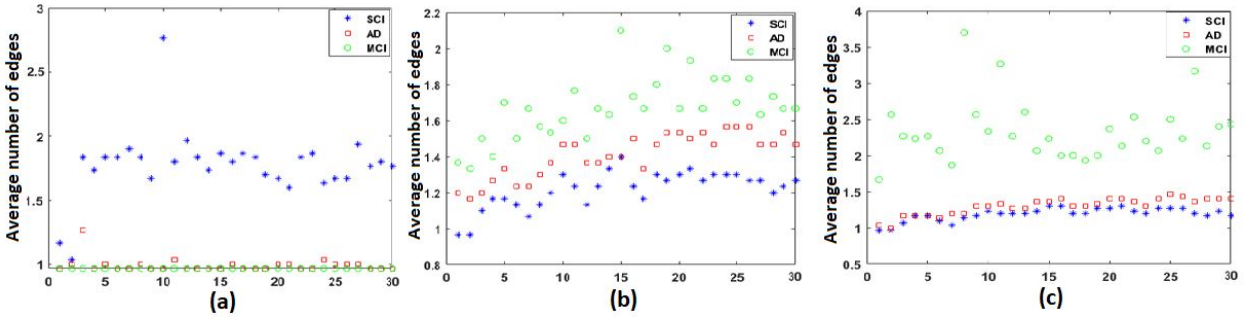

Figure 6.10: Average number of edges in the shortest path at each node for SCI, MCI and AD, on (a) delta, (b) alpha, and (c) beta bands.

Note that electrodes are positioned in Figure 6.10 following the same order as in the adjacency matrices: Fp1, Fp2, F7, F3, Fz, F4, F8, FT7, FC3, FCz, FC4, FT8, T3, C3, Cz, C4, T4, TP7, CP3, CPz, CP4, TP8, T5, P3, Pz, P4, T6, O1, Oz, O2. We recall that a low value of edges in the shortest path indicates that information exchange is rapid and efficient in the whole network.

In delta, the SCI group is by far the one with the longest shortest path in terms of intermediate steps (see Figure 6.10.a). MCI and AD groups are almost similar, except on F7 (electrode n°3), for which MCI group shows the lowest average shortest path that increases on AD and even more on SCI. The opposite behavior appears in alpha and beta bands: MCI and SCI groups exhibit, respectively, the highest and the lowest values of average shortest path; AD group is in between. However, we notice that the separation between the three groups is better in alpha band on almost all nodes (Fig. 6.10.b).

For a better understanding on the functioning of this graph parameter, we observed the shortest path for SCI group in delta between F7 and FCz for example. We found that the shortest path is not the direct link between such electrodes, as it is the case for AD and MCI. Actually, the information is routed via two other nodes Fp2 and Fz ($F7 \rightarrow Fp2 \rightarrow Fz \rightarrow FCz$). This result reveals that many short-term connections are set up in SCI to transmit the information between two electrodes in delta band.

Besides, regarding the shortest path of MCI group on beta for example, in order to transmit the information from FT7 to FT8, the brain network displays the following path $FT7 \rightarrow FC4 \rightarrow T3 \rightarrow Fz \rightarrow T4 \rightarrow F3 \rightarrow FT8$; while the direct connection between FT7 and FT8 is observed for SCI group. This result suggests that MCI group exhibits many short-term connections for information exchange in high frequencies.

6.3.4 Modularity

Figures 6.11 and 6.12 show the obtained modules in alpha and beta for the three populations. In delta and theta, results showed that all electrodes belong to only one module (Q=1), meaning that there is absence of sub-networks (no modular structure) in our framework that considers fully connected matrices, i.e. all the connections in the network are maintained. Note that a sub-network refers to a group of nodes having denser relations with each other than with the rest of the network.

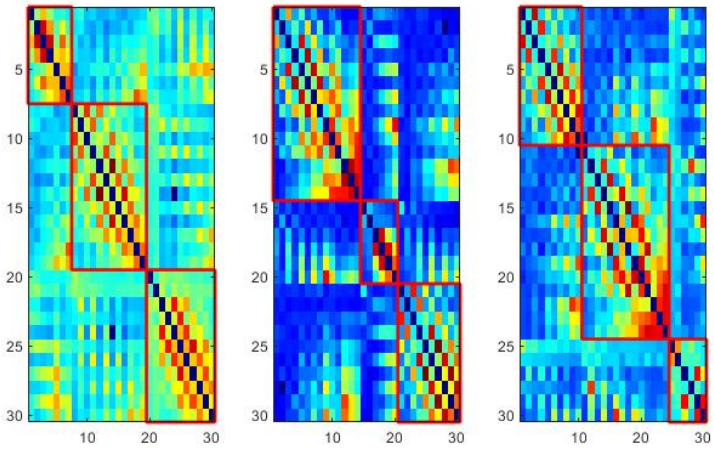

Figure 6.11: The obtained modules for SCI (left), MCI (middle) and AD (right), in alpha band.

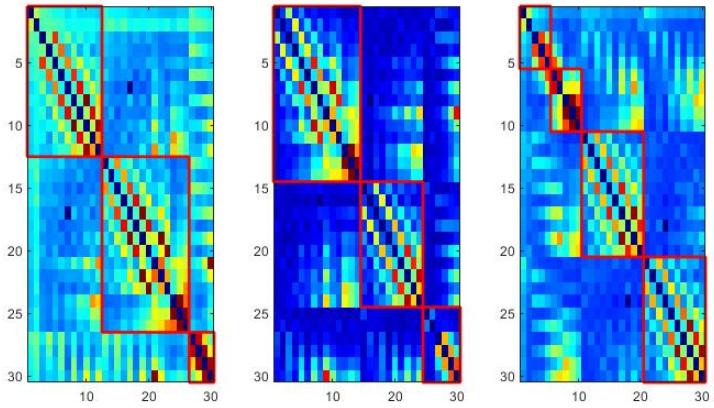

Figure 6.12: The obtained modules for SCI (left), MCI (middle) and AD (right), in beta band.

Figures 6.13 and 6.14 display the composition of the obtained modules in the three populations, in alpha and beta respectively.

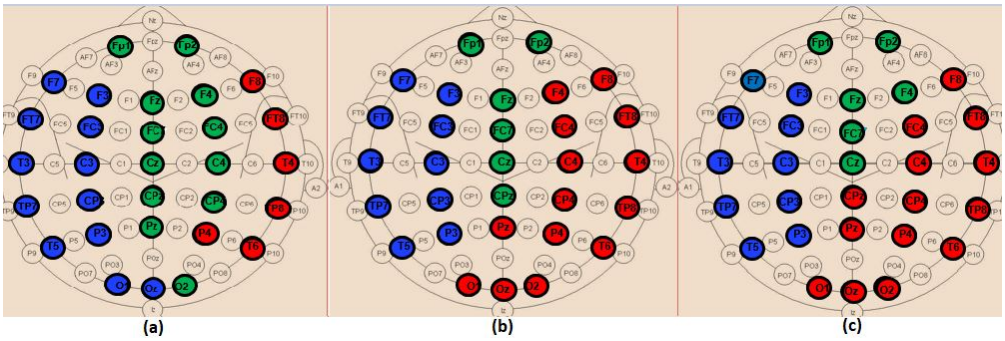

Figure 6.13: The distribution of the nodes in each module in alpha band for (a) SCI, (b) MCI and (c) AD groups.

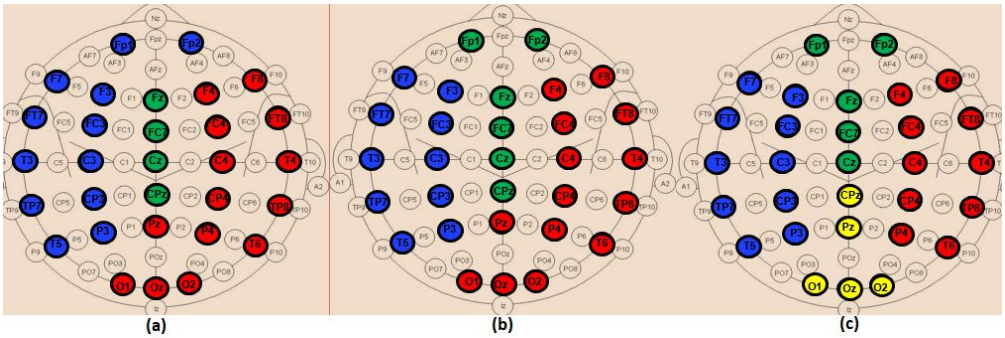

Figure 6.14: The distribution of the nodes in each module in beta band for (a) SCI, (b) MCI and (c) AD groups.

When comparing the spatial distribution of the obtained modules in alpha band for SCI and AD groups (Fig. 6.13.a and Fig. 6.13.c), we first notice that two modules among the three ones observed in SCI extend from anterior to posterior regions. More precisely, in Figure 6.13.a, the module in green color contains electrodes from prefrontal (FP1, FP2) to occipital (O2) regions passing by frontal, central and parietal regions. The blue one contains electrodes from frontal to occipital regions. In addition, we notice that the electrodes of the same brain region are distributed over several modules, particularly electrodes of the occipital region.

These findings may indicate a strong dynamic interaction between different brain areas for SCI group, which facilitates the long-term information transmission. Indeed, the interaction between electrodes belonging to the same module is relatively strong according to the definition of the modularity. More precisely, we observe a clear difference between SCI and AD in the occipital area (Fig. 6.13). SCI group presents a strong interaction between the occipital region and the left anterior regions since O1, Oz exist in the same module as (F7, F3, FT7, FC3, T3, C3, TP7, CP3, T5, P3). In parallel, (O2) exists in the same module as (Fp1,Fp2, Fz, FCz, CPz, Pz, F4, FC4, C4, CP4), so the occipital region has also a strong interaction with anterior regions by another way. This is not the case of AD group, where the interaction of the occipital region is limited to the right area of the brain (Fig. 6.13.c). In addition, the prefrontal region in AD interacts only with some electrodes from frontal and central regions (Fz, F4, FCz, Cz).

In beta, we also observe a stronger long-term connectivity between brain regions for SCI compared to AD (Fig. 6.14). Actually, for SCI group (Fig. 6.14.a), the occipital region has a strong connectivity with the right brain area, including parietal, central, temporal and frontal electrodes. However, for AD group (Fig. 6.14.c), the occipital electrodes (O1, Oz, O2) are grouped in one module with Pz and CPz; which reflects the weak interaction of the occipital area with the other regions.

Regarding MCI group, their topology in alpha band is closer to that of AD compared to SCI (Fig. 6.13.b). In beta band, the topology of MCI (Fig. 6.14.b) is closer to that of SCI; nevertheless, the prefrontal region (Fp1,Fp2) has a relatively weak connectivity with the left part of the brain as for AD. These results support the fact that MCI group has an intermediate behavior between SCI and AD groups.

6.4 Discussion

Previous rsEEG studies on functional organization of the brain network in the context of AD reported conflicting results (refer to Table 4.2 and Section 4.3). These discrepancies among studies could be related to methodological differences and the use of databases with different characteristics and which are sometimes prone to experimental constraints that do not match the reality on the ground.

In light of this, in the present study (Study 2), we used a real-life clinical database containing rsEEG data of 102 patients, at SCI, MCI and AD stages. To our knowledge, this is the first study to date employing graph theory to characterize the evolution of brain networks throughout different clinical stages of cognitive decline, including at once healthy elders with subjective cognitive impairments (SCI), MCI patients and patients with AD. In the literature, many studies investigated network topology on different cognitive profiles (Vecchio et al., 2014; Franciotti et al., 2019; Chen et al., 2019; Das and Puthankattil, 2020; Gaubert et al., 2019; Dattola et al., 2021). Nevertheless, the majority of studies considered normal aged-matched healthy subjects as controls to study the evolution of EEG markers through MCI and AD stages. When SCI subjects have been considered in (Gaubert et al., 2019), the authors studied different cognitive phenotype profiles in such population to predict the evolution towards dementia.

In addition, we performed a graph theory analysis based on functional connectivity values quantified with *EpEn*. This choice was made after comparing such a measure to two widely used metrics, coherence and phase lag index, relying on different mathematical concepts. The experimental study was carried out in the four frequency bands (delta, theta, alpha and beta), considering all the 30 rsEEG channels available in our data.

Experiments showed that a statistical modeling of EEG with a spatiotemporal entropy measure (*EpEn*) allows a better differentiation between SCI, MCI and AD stages, compared to coherence and phase lag index, which are deterministic measures. This result is in accordance with those obtained in Study 1, presented in Chapter 5. The average adjacency matrices of the three groups show a different connectivity organization with *EpEn* in the four frequency bands (Fig. 6.3).

In delta, AD group presents higher EpEn values compared to SCI group, especially in the prefrontal and frontal regions (Fig. 6.3 and Fig. 6.6). In alpha and beta, an opposite behaviour appears: AD

group shows lower EpEn values compared to SCI group. EpEn measures the information content related to the dynamics of brain activity, conveyed by a couple of EEG time series. This finding shows that SCI subjects, considered as controls, present a high information content in their rsEEG, with brain dynamics between 8 and 30 Hz, while AD group shows a slower rsEEG activity between 1 and 4Hz.

This result is in accordance with previously published studies: compared to the controls, AD patients show an increase in slow rsEEG activities (delta and theta) and a decrease in fast rsEEG activities (alpha and beta) (Babiloni et al., 2020; Dauwels et al., 2010a; Babiloni et al., 2016; Jelic et al., 2000; Brassen and Adler, 2003; Onofrj et al., 2003; Ponomareva et al., 2003; Jeong, 2004; Bennys et al., 2001). It is interesting to notice that these results are still valid although the control subjects in the present study are not considered as healthy subjects since they suffer from SCI with memory complaints, with an increased risk of future objective cognitive decline.

Regarding the MCI group, it exhibits the highest *EpEn* values in delta and the lowest *EpEn* values in alpha and beta (Fig. 6.3 and Fig. 6.6). These results show the slowing of rsEEG activity (low information content) in both MCI and AD relatively to SCI, since the activity is concentrated in low frequency range, between 1 and 4Hz. However, MCI group displays a stronger activity compared to AD (Fig. 6.3 and Fig. 6.6), which may reveal a compensatory mechanism underpinning the cognitive activity of MCI.

These findings with *EpEn* measure show that MCI group is intermediate between SCI and AD, which fits with some results of the literature reporting that MCI is considered to be the transitional stage between normal aging and AD (Dauwels et al., 2010a; Yao et al., 2010; Vecchio et al., 2014; Dattola et al., 2021).

Graph theory was then applied on *EpEn* functional connectivity matrices, using three core and complementary topological parameters: clustering coefficient, shortest path and modularity. By contrast to majority of works in the literature, we adopted in the present study a weighted graph analysis based on fully connected matrices. This allows preserving all the available information. Moreover, it has been shown that weighted graph analysis could provide a richer topological information than a classical binary one (Chen et al., 2019; Mehraram et al., 2020; Rubinov and Sporns, 2011).

Experiments show that the analysis of functional connectivity in terms of its topological organization in the brain network, and not only in terms of its values, allows a better understanding on the evolution of functional connectivity networks throughout SCI, MCI and AD.

The clustering coefficient (Fig. 6.8) shows the same behaviour as *EpEn* (Fig. 6.6): AD group presents higher values in delta and lower values in alpha and beta compared to SCI group. However, we notice that the clustering coefficient leads to a better distinction between the three populations compared to *EpEn*, especially in theta band. This result shows the improvement brought by a global network analysis, in addition to a local functional connectivity estimation, already efficient in characterizing the three populations.

Previous studies reported increased (He et al., 2008; Yao et al., 2010; Vecchio et al., 2014), decreased (Tijms et al., 2013; De Haan et al., 2009; Franciotti et al., 2019; Chen et al., 2019; Stam et al., 2009) or unmodified (Sporns, 2022) clustering coefficient in AD compared to control group. In the present

study, the clustering coefficient was instead increased in AD and even more in MCI compared with SCI in delta band, and that at all electrode locations. The opposite is observed in alpha and beta, with reduced clustering coefficient in AD and even more in MCI. In theta, we observe the same tendency as in alpha and beta, except in prefrontal and some part of frontal region (Fig. 6.9.b). In alpha, for which a consensus appears in the literature, our study confirms that AD leads to a reduction of the clustering coefficient.

The topological network analysis with clustering coefficient is found frequency band dependent; this could explain partially the divergent results in the state-of-the-art, additionally to data characteristics and methodological differences. This finding leads to interpret the parameter differently depending on the frequency band.

In delta, the results indicate the ability of AD and MCI networks to form locally dense cliques (high clustering coefficient); but MCI group presents a predominance of high strength intrinsic connectivity. This may reflect the compensatory response to the neuronal damage occurring early in the disease process. Nevertheless, typically, the literature reports that a high value of the clustering coefficient reflects the robustness of a network in case of cognitive impairments or damage. This phenomenon is observed in our study, particularly in alpha and beta for the SCI group, since their rsEEG activity is contained in such high frequencies.

Regarding the shortest path, SCI group shows by far the highest values of shortest path in delta and no difference was observed between MCI and AD (Figure 6.10.a). In alpha and beta, MCI group exhibits the highest shortest path values, which decreases in AD and SCI (Fig. 6.10.b and Fig. 6.10.c). The difference between the three populations in terms of shortest path is more notable in alpha for almost all EEG channels.

The information transfer in AD and MCI networks seems to be more fluent compared to SCI in delta. This suggests the establishment of more short-term connections in SCI at very low frequencies. On the contrary, in high frequency ranges, especially in alpha, the low values of the shortest path indicate rapid and high efficiency in information transmission across the SCI network, reflecting more long-term connections in SCI compared to MCI and AD. This is in accordance with some studies reporting that AD leads to a decrease of the path length (Tijms et al., 2013; De Haan et al., 2009).

Besides, in high frequencies (Figures 6.10.b and 6.10.c), MCI group shows higher shortest path values than AD, meaning that the information is processed throughout more short term connections in MCI. This interesting result could also reflect the compensation mechanism in MCI: it could be thus postulated that MCI patients may exploit additional neural resources to compensate the loss of cognitive functions occurring early in the disease process.

This postulate is consistent with the high variance of local clustering coefficient values across electrodes, observed in MCI in alpha and beta (Fig. 6.9.c and Fig. 6.9.d), also observed with EpEn in Figure 6.6. In fact, when the homogeneity in the functional connectivity between nodes decreases, there is a high chance to transmit the information by means of several electrodes, leading to an increased shortest path.

Based on both segregation and integration parameters, we notice that in high frequencies, SCI group observes simultaneously high clustering coefficient and low shortest path, meaning that SCI

network tends to have a small world topology. Indeed, small-world topology presents an optimal balance between local connected structure and global distributed information processing (Bullmore and Sporns, 2009; Rubinov and Sporns, 2010). This occurs due to the existence of relatively few long-term connections, making the network more resistant to damage. Some studies have investigated the small-worldness of the brain network in AD context; they found that AD group exhibits a more random overall network structure (De Haan et al., 2009; Stam et al., 2007b; Stam and Reijneveld, 2007) than HC; which corresponds to our results in high frequencies.

Finally, when investigating the modular structure of the retrieved networks, we did not find differences between the three populations in terms of modularity value. This may be due to the use of fully connected matrices. The majority of studies in the literature reported increased modularity in HC compared to AD, which indicates that the brain dynamics is organized into sub-autonomous networks that interact with one another through relatively short and long-term pathways. This brain structure is more resilient to neuronal damage.

Nevertheless, when investigating the composition of the obtained modules, we found a difference between the three populations in alpha and beta (Fig. 6.13 and Fig. 6.14). When comparing SCI and AD in terms of the composition of the sub-networks (modules), results show that on the one hand, the electrodes of the same brain region are distributed over several modules in SCI; on the other hand, some obtained modules in SCI are extended from anterior to posterior brain regions. This result may indicate the strong interaction between different brain regions for SCI group compared to AD, hence facilitating the information transfer and process. These findings show that in case of damage, the network is more resilient in SCI compared to MCI and even more compared to AD. This result corresponds to our conclusions with the clustering coefficient and the shortest path.

Furthermore, the spatial distribution of the obtained modules for MCI is found intermediate between that of SCI and AD. This result confirms our previous finding: MCI is a transitional stage between normal aging and dementia stage.

6.5 Limitations

Our study presents some limitations. The obtained results should be considered limited to the context of resting-state and scalp-level EEG connectivity analysis. It is largely acknowledged that sensor-level analysis is prone to the effects of volume conduction and poor signal-to-noise ratio. Currently, there is no method that guarantees to discard volume conduction effects (Lai et al., 2018).

One way to manage this issue consists in using connectivity measures that are relatively insensitive to these effects. In our study, we used different connectivity metrics, in particular *PLI* measure, which is relatively insensitive to this effect, since it discards the zero lag component of the interaction (Babiloni et al., 2020; Kasakawa et al., 2016; Stam et al., 2007a; Bastos and Schoffelen, 2016). Besides, *EpEn* measure exploits HMM, whose structure is adapted for modeling neural dynamics underlying the observed EEG signal. In fact, HMM is a probabilistic model used to describe the evolution of observable events or signal realizations, which depend on internal factors that are not directly observed, called "hidden states". The statistical modeling of multidimensional EEG signals

allows obtaining a functional connectivity measure that is more robust to noise, as demonstrated in (Houmani et al., 2015). In addition, the non-linear interaction between pairwise signals is modeled by a mixture of Gaussians at the level of an epoch, to address the problem of zero lag correlations. However, further investigation should be performed using EEG source estimation approach, which is merging as a potential method that addresses the effects of volume conduction (Tait et al., 2019; Gaubert et al., 2019; Lai et al., 2018; Hassan and Wendling, 2018). In our study, the use of low-density EEG recordings did not allow performing a correct source connectivity analysis. Actually, there is evidence that increasing the number of electrodes provides greater accuracy in source estimation. Many studies exploited at least 64 electrodes to obtain satisfactory results (Tait et al., 2019; Gaubert et al., 2019; Hassan and Wendling, 2018), as also reported in (Franciotti et al., 2019). The main aim of our study was to investigate differences between different clinical stages, using EEG data acquired on elderly and impaired patients in real-life clinical conditions. In such context, it is difficult to use EEG recordings with high-density electrodes for cost, practical and comfort reasons. In another study, it would be of great interest to assess the effectiveness of EpEn considering scalp and source reconstructed EEG networks on highly dense EEG data and to compare with outcomes of the present work.

In addition, our results are based on weighted graphs in which all nodes are connected. Majority of works in the literature performed a graph analysis after applying a thresholding to maintain only the strongest connections. It is thus important in the future to confront our study to different topological scales and analyze the topological organization between the three groups at different resolution scales. This is of high interest since topological parameters and group contrasts may differ across thresholds (Chen et al., 2019; Dattola et al., 2021; Garrison et al., 2015).

Furthermore, the presented results were reported on a clinical database that includes 102 subjects acquired in real-life conditions. However, our findings need to be validated on other data in order to be confirmed. This study is therefore a preliminary work that requires conducting an in-depth research, which should involve more patients. One of the objectives of this forthcoming research will also be to go further in our analysis by confronting our EEG-based results to the available neuropsychological and clinical markers.

6.6 Conclusion

The present study on rsEEG has investigated brain network analysis over different stages of cognitive decline, from SCI to AD passing through MCI. We proposed a new framework to study the topological brain networks based on a refined spatiotemporal entropy measure (*EpEn*), relying on a statistical modeling of EEG time series using HMM. This modeling approach is suitable to the analysis of the underlying neuronal dynamics, since it quantifies on piecewise stationary epochs, the information content conveyed by EEG signals locally over time and spatially by estimating inter-channels relationship.

Our results add some evidence in the comprehension of the progression of cognitive severity towards dementia.

Experiments have shown that functional connectivity and graph analysis are frequency band-

dependent and functional alterations starts at the MCI stage with a specific scheme. In delta, SCI group exhibits a reduction of brain activity quantified by *EpEn*, a decrease of clustering coefficient and an increase of the path length compared to MCI and AD. This indicates the ability of AD and MCI networks to form locally dense cliques. In high frequencies, especially in alpha, opposite behaviour appears, suggesting a rapid and high efficiency in information transmission across the SCI network. We concluded that the brain network at SCI stage tends to have a small world topology compared to MCI and AD stages. Moreover, the modular structure of brain networks has revealed that in case of damage, the SCI network is more resilient to neuronal damage compared to that of MCI and even more compared to that of AD stage.

Finally, our results add new pieces of evidence in the understanding of the early brain changes, confirming that MCI is a transitional stage between SCI and AD. In addition, all the results pointed the predominance of high strength intrinsic connectivity that appears at the MCI stage, which may reflect the compensatory response to the neuronal damage occurring early in the disease process.

Chapter 7

A comparative study of functional connectivity measures for brain network analysis

7.1 Objective of the study

In the present study, we also extend the use of *EpEn* to brain network assessment with graph theory. In contrast to the previous study (Study 2), this work aims at discriminating AD patients from SCI and MCI patients, using different graph parameters computed from binary graph.

We also conduct a comparative study by investigating the classification performance of the graph parameters based on *EpEn* as well as three additional connectivity measures, namely phase lag index, coherence and mutual information, when exploited to quantify the connectivity links in brain networks.

7.2 Study design

The present study was conducted considering rsEEG data of the 22 SCI subjects, the 28 mild to moderate AD patients and 28 MCI patients, from Charles-Foix database. The characteristics of such database are given in Section 5.2.1.

In order to discriminate between SCI, MCI and AD, we first computed the functional connectivity in the three groups using Epoch-based Entropy (*EpEn*) measure, and that for each frequency band (1–4 Hz delta, 4-8 Hz theta, 8–12 Hz alpha, 12–30 Hz beta). The connectivity measure was computed between all pairs of the 30 electrodes for each person.

Then, we applied a thresholding on the obtained real-valued connectivity matrices to generate their binary form keeping only the highest connectivity values. We considered 9 proportional threshold values from 10% to 90% with steps of 10%. Therefore, for each threshold value (among the nine), a person had four binary matrices (in the four frequency bands), on which we computed a local graph parameter to characterize the topology of the binary network. A vector of 30 values was thus obtained for each matrix, where each element is the graph parameter value of a node (electrode).

After that, a feature selection procedure was applied to identify the most relevant nodes in each

frequency band for a given threshold. To do that, we used the Orthogonal Forward Regression (OFR) algorithm and the random probe technique (Chen et al., 1989; Dreyfus, 2005). Then, by merging the selected features of the four frequency bands, we applied an additional feature selection procedure to combine the extracted information at different frequency bands. At the end, the selected features represented the graph parameter value for the selected nodes and the selected frequency bands.

Finally, such selected combination of features was given as input to a linear SVM classifier (Campbell and Ying, 2011; Boser et al., 1992) to evaluate the discrimination capability between SCI, MCI and AD at different threshold values. To assess the effectiveness of *EpEn*, we compared it to three alternative measures, commonly used in the literature: phase lag index (PLI), magnitude squared coherence (MSC), and mutual information (MI). These measures are presented in Section 3.3.1. Additionally, we considered five local graph parameters for the brain network analysis in the binary framework: degree, clustering coefficient, shortest path length, local efficiency and betweenness. These parameters are defined and presented in Section 4.3.

7.3 Brain network analysis

In the present study, we conducted the graph analysis on binary functional connectivity matrices, by applying a thresholding approach on the generated connectivity matrices, which are originally real-valued. This allows obtaining a sparse and a binary form. Thresholding is commonly used in the literature to remove weaker connections, which are most affected by experimental noise, and to reduce the density of the graph for lower computational cost (Bullmore and Sporns, 2009; Rubinov and Sporns, 2010; Stam and Van Straaten, 2012; Bassett and Bullmore, 2009).

Absolute or proportional threshold approaches can be used. The absolute threshold approach consists of the selection of edges with a connectivity value higher than the absolute threshold value, setting all surviving connections to 1 and the others to 0 in the binary case. This leads to different density networks across subjects. To overcome this issue, we adopted in this work a proportional threshold (PT), which consists of the selection of the strongest percentage of connections in each network, setting all surviving connections to 1 and the others to 0.

7.4 Feature selection method

In this study, we computed the functional connectivity measures of the three populations in the four frequency bands, and computed the associated local graph parameters for each node ($n = 30$ electrodes). This induces the availability of a large number of candidate input features to the linear SVM classifier. It is, thus, necessary to perform a feature selection procedure in order to reduce the number of features by determining, upstream of the classification step, the most relevant features to discriminate between SCI, MCI and AD.

To select the most pertinent input features for the SVM classifier, we used the Orthogonal Forward Regression (OFR) algorithm and the random probe technique: the OFR algorithm allows ranking all the candidate features in decreasing order of relevance (Chen et al., 1989; Dreyfus, 2005); the random probe serves as a decision criterion to keep the most relevant features. For feature ranking with the OFR algorithm, we applied the procedure hereinafter:

a Select the feature that best correlates to the output of the process to be modeled. For example, in case of SCI vs. AD, the output vector contains 22 true values and 28 false values;

b Project the output vector onto the null space of the selected feature. Orthogonalize the remaining candidate features using Gram–Schmidt orthogonalization method;

c Discard the selected feature from the list of candidate features;

d Return to (a) and repeat the procedure until a stopping criterion is met based on the random probe technique, described below.

In order to select the most relevant features, we applied the random probe technique (Stoppiglia et al., 2003). In the set of candidate features, we considered an additional feature, called "*probe*" feature, which is a realization of a random variable. This probe feature is ranked as all other candidate features by the procedure described above. It would be obvious to discard all features that are ranked after the probe.

More precisely, 1000 random realizations of the probe feature are generated. Each random realization of the probe is concatenated to the set of real candidate features, and all features (real and probe) are ranked with the OFR algorithm as above-mentioned. Once the cumulative distribution of the rank of the probe was computed, we defined an acceptable risk value that a random variable can explain the output process more reliably than one of the selected real features. In this study, we chose the value 0.1 (10%) as an acceptable risk value, as carried out in (Houmani et al., 2018). Therefore, at each step of the OFR procedure, we followed this procedure:

a Identify a candidate feature with OFR;

b Compute the value of the cumulative distribution function of the rank of the probe. If the value is smaller than the risk (0.1), keep the feature and return to step (b) of the OFR algorithm; otherwise, reject the feature under consideration and finish the procedure.

7.5 Experimental results

To discriminate between each pair of classes, *i.e.*, SCI vs. AD, SCI vs. MCI and AD vs. MCI, we generated for each person in the four frequency bands, the connectivity matrix between all pairs of electrodes, with the four connectivity measures separately. Then, we applied on each connectivity matrix a PT value to have a binary form of such matrix, on which we calculated the five graph parameters. In this study, we used 9 PT values, from 10% to 90% (with steps of 10%). Therefore, for each PT value, in each frequency band, a graph parameter vector of dimension 30 characterizes each person in the cohort.

For performance assessment with the SVM, we selected for each PT the most relevant input features to discriminate each pair of class. To do that, we first applied the feature selection algorithm in each frequency band to select the most pertinent combination of electrodes that distinguish between each pair of classes. We considered an acceptable risk of 10% to fix the number of features that we had to keep using the probe method. Then, by combining all the selected features obtained on each frequency band, we applied a second feature selection to have, at the end, a combination of features fusing different frequency bands. Then, we evaluated the SVM performance by considering,

progressively, the 3 most relevant features to a maximum of 10, and retained the combination of features that gave the best performance in terms of accuracy.

We report in the following sections only the performance associated to the optimal PT and the best number of relevant features, which give the best accuracy value with the linear SVM classifier.

7.5.1 Discriminating AD patients from SCI subjects

Tables 7.1 to 7.4 show the performance of the SVM classifier when discriminating SCI subjects from AD patients with the five graph parameters: clustering coefficient (CC), degree (K), shortest path (L), local efficiency (E_{loc}) and betweenness (BW). Each table reports performance using a given functional connectivity measure to quantify the connectivity links in the network.

Table 7.1: Classification performance when discriminating SCI from AD with different graph parameters, using *EpEn* to quantify the connectivity links in the network.

EpEn	**CC**	**K**	**L**	E_{loc}	**BW**
Accuracy	94%	90%	90%	94%	92%
Specificity	90.91%	90.91%	90.91%	95.45%	86.36%
Sensitivity	96.43%	89.28%	89.28%	92.86%	96.43%

Table 7.2: Classification performance when discriminating SCI from AD with different graph parameters, using *PLI* to quantify the connectivity links in the network.

PLI	**CC**	**K**	**L**	E_{loc}	**BW**
Accuracy	96%	84%	84%	94%	86%
Specificity	95.45%	81.82%	77.27%	95.45%	77.27%
Sensitivity	96.43%	85.71%	89.28%	92.86%	92.86%

Table 7.3: Classification performance when discriminating SCI from AD with different graph parameters, using *MSC* to quantify the connectivity links in the network.

MSC	**CC**	**K**	**L**	E_{loc}	**BW**
Accuracy	84%	86%	88%	94%	90%
Specificity	81.82%	77.27%	86.36%	90.91%	86.36%
Sensitivity	85.71%	92.85%	89.28%	96.43%	92.86%

We first observe that *EpEn* measure allows achieving a very good classification performance when discriminating SCI from AD. Indeed, the accuracy value is between 90% and 94% considering the five graph parameters. We reach 94% of accuracy with a good balance of specificity (proportion of well classified SCI patients) and sensitivity (proportion of well classified AD patients), considering the clustering coefficient and the efficiency. Besides, in the case of *PLI* and *MSC* measures, we notice that the accuracy value is 84% or 86% for three graph parameters with *PLI*, and for four graph parameters with *MSC*.

Table 7.4: Classification performance when discriminating SCI from AD with different graph parameters, using *MI* to quantify the connectivity links in the network.

MI	**CC**	**K**	**L**	E_{loc}	**BW**
Accuracy	92%	92%	82%	92%	92%
Specificity	90.91%	90.91%	81.82%	90.91%	86.36%
Sensitivity	92.86%	92.86%	82.14%	92.86%	96.43%

In the case of *MI* measures, the accuracy reaches 92% with a good balance of specificity and sensitivity for almost all graph parameters, except for the shortest path for which the accuracy is 82% with a specificity of 81.82% and a sensitivity of 81.14%.

Compared to the three classical measures, we notice that *EpEn* allows obtaining the best performance, when the brain network is characterized by the following four graph parameters: clustering coefficient, shortest path, efficiency and betweenness. Concerning the degree parameter, *EpEn* is ranked in the second position after *MI* due to a difference in sensitivity: 92.86% with *MI* and 89.28% with *EpEn*.

Finally, we can observe that, contrary to the *EpEn* measure, *PLI*, *MSC* and *MI* give, in some cases, the worst results for some graph parameters.

For a better understanding of the results of the feature selection step, the best combination of features obtained with *EpEn*, considering the clustering coefficient graph parameter combines eight clustering coefficient values computed at: delta (T6), delta (CP3), delta (FP1), beta (T6), delta (FCz), beta (Pz), beta (FC3), and beta (F3). This best combination of features was obtained in the case of binary matrices binarized with a proportional threshold of 70%.

7.5.2 Discriminating MCI patients from SCI subjects

Tables 7.5 to 7.8 show that the four measures allow reaching good classification performance when discriminating SCI subjects from MCI patients. This is observed especially with *MI* measure that allows achieving an accuracy value between 90% and 96%, and *EpEn* measure, which leads to an accuracy value between 92% and 100%. We notice that *EpEn* outperforms the other measures, especially for the degree, the shortest path and the betweenness parameters, reaching sometimes 100% of specificity (proportion of well classified SCI patients) and 100% of sensitivity (proportion of well classified MCI patients). The results again pointed out the reliability of the *EpEn* measure whatever the graph parameter used.

Table 7.5: Classification performance when discriminating SCI from MCI with different graph parameters, using EpEn to quantify the connectivity links in the network.

EpEn	**CC**	**K**	**L**	E_{loc}	**BW**
Accuracy	94%	100%	96%	92%	100%
Specificity	90.91%	100%	95.45%	81.82%	100%
Sensitivity	96.43%	100%	96.43%	100%	100%

Table 7.6: Classification performance when discriminating SCI from MCI with different graph parameters, using PLI to quantify the connectivity links in the network.

PLI	**CC**	**K**	**L**	E_{loc}	**BW**
Accuracy	88%	86%	94%	88%	90%
Specificity	77.27%	72.72%	86.36%	81.82%	95.45%
Sensitivity	96.43%	96.43%	100%	92.86%	85.71%

Table 7.7: Classification performance when discriminating SCI from MCI with different graph parameters, using MSC to quantify the connectivity links in the network.

MSC	**CC**	**K**	**L**	E_{loc}	**BW**
Accuracy	90%	88%	94%	94%	90%
Specificity	81.82%	81.82%	90.91%	90.91%	86.36%
Sensitivity	96.43%	92.86%	96.43%	96.43%	92.86%

Table 7.8: Classification performance when discriminating SCI from MCI with different graph parameters, using MI to quantify the connectivity links in the network.

MI	**CC**	**K**	**L**	E_{loc}	**BW**
Accuracy	94%	90%	90%	96%	92%
Specificity	95.45%	86.36%	90.91%	90.91%	86.36%
Sensitivity	92.86%	92.86%	89.28%	100%	96.43%

Additionally, we observe that *PLI* and *MSC* measures do not give the best results, whatever the graph parameter used, even though the performance is still correct.

7.5.3 Discriminating AD patients from MCI patients

Tables 7.9 to 7.12 report the classification performance of the SVM classifier when discriminating AD patients from MCI patients. Specificity and sensitivity correspond, respectively, to the proportion of AD patients and MCI patients well classified.

Table 7.9: Classification performance when discriminating AD from MCI with different graph parameters, using EpEn to quantify the connectivity links in the network.

EpEn	**CC**	**K**	**L**	E_{loc}	**BW**
Accuracy	87.5%	92.86%	83.93%	91.07%	89.28%
Specificity	89.28%	86.36%	89.28%	89.28%	85.71%
Sensitivity	85.71%	85.71%	78.57%	92.86%	92.86%

Table 7.10: Classification performance when discriminating AD from MCI with different graph parameters, using PLI to quantify the connectivity links in the network.

PLI	**CC**	**K**	**L**	E_{loc}	**BW**
Accuracy	87.5%	89.28%	83.93%	85.71%	85.71%
Specificity	85.71%	89.28%	89.28%	89.28%	85.71%
Sensitivity	89.28%	89.28%	78.57%	82.15%	89.28%

Table 7.11: Classification performance when discriminating AD from MCI with different graph parameters, using MSC to quantify the connectivity links in the network.

MSC	**CC**	**K**	**L**	E_{loc}	**BW**
Accuracy	80.36%	83.93%	80.36%	83.93%	87.5%
Specificity	71.43%	89.28%	75%	82.14%	89.28%
Sensitivity	89.28%	78.57%	85.71%	85.71%	85.71%

Table 7.12: Classification performance when discriminating AD from MCI with different graph parameters, using MI to quantify the connectivity links in the network.

MI	**CC**	**K**	**L**	E_{loc}	**BW**
Accuracy	85.71%	92.86%	89.28%	89.28%	87.5%
Specificity	82.14%	92.86%	92.86%	92.86%	85.71%
Sensitivity	89.28%	92.86%	85.71%	89.28%	85.71%

We first notice that all measures reach worst results compared to the other cases comparing SCI to AD or SCI to MCI. This reflects the difficulty of discriminating the AD group from the MCI group. Moreover, we notice that PLI and MSC measures give the worst results compared to MI and EpEn. When comparing *MI* and *EpEn*, we observe that their classification performance depends on the graph parameter.

Finally, compared to the three classical measures, we notice that the *EpEn* measure is ranked either in the first or the second position; while the others can give the worst results for some graph parameters.

7.5.4 Global Comparison of the four functional connectivity measures

Figure 7.1 shows the global rank of each connectivity measure in terms of accuracy, considering all the graph parameters together and all two-class comparisons (SCI vs. AD, SCI vs. MCI and AD vs. MCI). We report the number of times each connectivity measure is ranked in position 1, 2, 3 or 4. Each connectivity measure is evaluated 15 times (5 graph parameters * 3 class pairs comparisons). We clearly show the discriminative potential of the *EpEn* measure compared to the other classical measures. Indeed, *EpEn* is ranked ten times in the first position, four times in the second position and only one time in the third position. In addition, it was never ranked in the last position, contrary to the other connectivity measures.

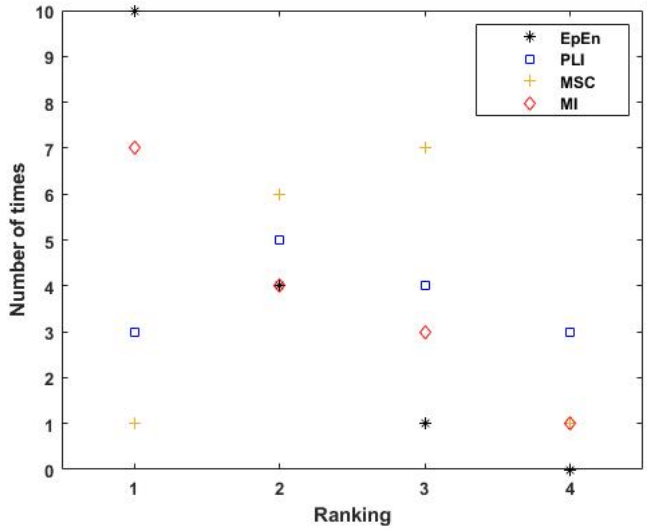

Figure 7.1: The global ranking of the four connectivity measures in terms of accuracy considering the graph parameters and class comparison.

We go more deeply in this comparative study by computing the average SVM posterior probability that one person is classified into the positive class for each connectivity measure and graph parameter (see Figures 7.2 to 7.4). The results show that the probability outcome for decision making with the SVM on the positive class is higher in general when considering the *EpEn* measure.

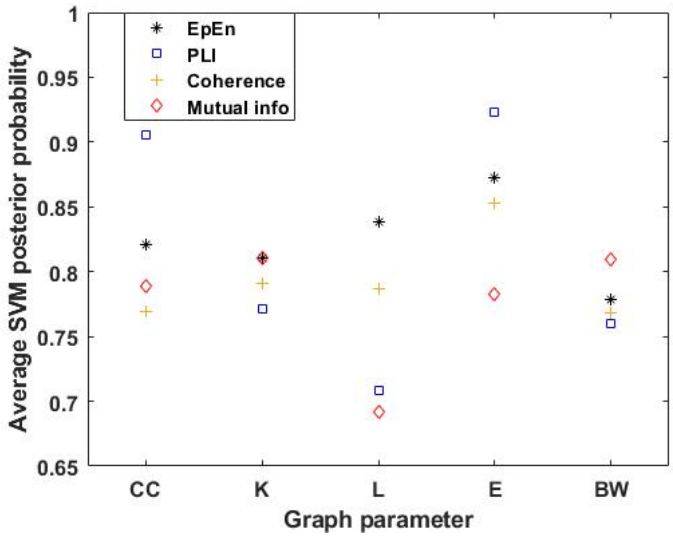

Figure 7.2: The average SVM posterior probability that one person is classified into the positive class for the four connectivity measures and the five graph parameters, when comparing SCI vs. AD.

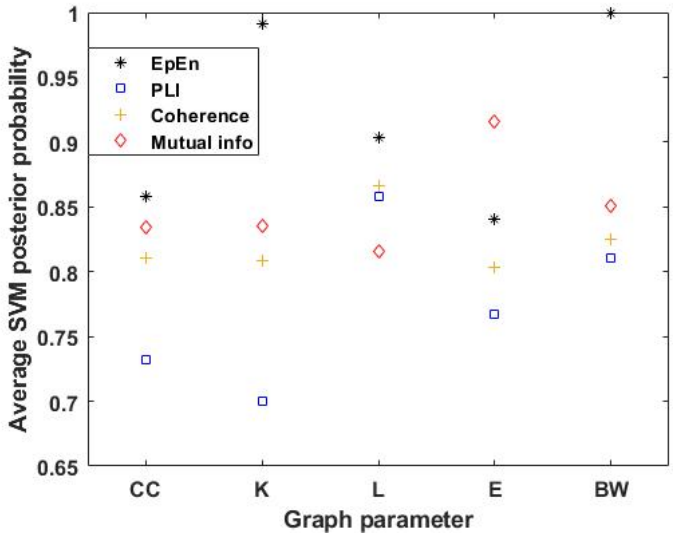

Figure 7.3: The average SVM posterior probability that one person is classified into the positive class for the four connectivity measures and the five graph parameters, when comparing SCI vs. MCI.

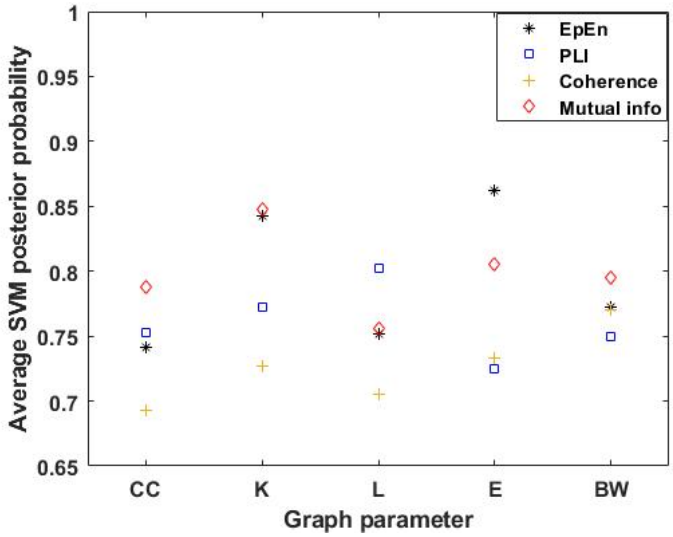

Figure 7.4: The average SVM posterior probability that one person is classified into the positive class for the four connectivity measures and the five graph parameters, when comparing AD vs. MCI.

7.5.5 Differential AD diagnosis with the three groups of patients

This study exploits a multiclass database that includes three classes of patients: SCI, MCI and AD patients. We are, thus, left confronting a K-class classification problem *(K = 3)* that was turned into a set of *(K(K-1)/2)* two-class problems (Knerr et al., 1990), as carried out in the previous sections.

In the following, we present the results of further experiments, targeting a differential AD diagnosis with the three groups of patients simultaneously, using the previous results obtained with the two-class problems.

Therefore, to assess the performance of a three-class SVM classifier, we exploited the previous linear SVM classifiers used to discriminate between each pair of classes, considering the same number N of selected variables. We recall that, for each PT value, we evaluated the two-class SVM classifiers by considering progressively the 3 to 10 most relevant features, and reported only the performance associated to the optimal PT and the best number of relevant features that give the best accuracy value. We follow the same methodology for the three-class problem.

To estimate pairwise posterior probabilities of the three-class SVM classifier, *N*(K(K-1)/2)* two-class classifiers are trained for each PT ($N = 8$ since we evaluated the performance considering progressively the 3 to 10 most relevant features leading to 8 cases for each PT value).

The global probability that a patient described by the feature vector x belongs to the class C_i is computed as in (Knerr et al., 1990):

$$Pr(C_i|x) = 1 \Big/ \sum_{j=1, j\neq i}^{K} \frac{1}{Pr_{ij}} - (K-2) \tag{7.1}$$

where K is the number of classes and Pr_{ij} is the probability of the patients belonging to the class i, estimated by the SVM classifier separating the class C_i from the class C_{ij}.

Tables 7.13 to 7.17 report the best classification performance of the three-class classifier for each graph parameter using the four connectivity measures.

Table 7.13: Confusion matrices for differential AD diagnosis with the three groups of patients, using the clustering coefficient (CC) parameter with the four connectivity measures.

CC		**SCI**	**MCI**	**AD**	**Total accuracy**
EpEn	SCI (n = 22)	20	2	0	92.31%
	MCI (n = 28)	0	25	3	
	AD (n = 28)	0	1	27	
PLI	SCI (n = 22)	21	1	0	91.03%
	MCI (n = 28)	0	26	2	
	AD (n = 28)	1	3	24	
MSC	SCI (n = 22)	19	2	1	87.18%
	MCI (n = 28)	3	24	1	
	AD (n = 28)	0	4	24	
MI	SCI (n = 22)	19	0	3	87.18%
	MCI (n = 28)	0	26	2	
	AD (n = 28)	1	3	24	

Table 7.14: Confusion matrices for differential AD diagnosis with the three groups of patients, using the degree (K) parameter with the four connectivity measures.

K		SCI	MCI	AD	Total accuracy
EpEn	SCI (n = 22)	21	0	1	94.87%
	MCI (n = 28)	0	26	2	
	AD (n = 28)	1	0	27	
PLI	SCI (n = 22)	17	1	4	88.46%
	MCI (n = 28)	0	25	3	
	AD (n = 28)	1	0	27	
MSC	SCI (n = 22)	20	2	0	89.74%
	MCI (n = 28)	2	23	3	
	AD (n = 28)	0	2	26	
MI	SCI (n = 22)	20	1	1	89.74%
	MCI (n = 28)	5	22	1	
	AD (n = 28)	0	1	27	

Table 7.15: Confusion matrices for differential AD diagnosis with the three groups of patients, using the shortest path (L) parameter with the four connectivity measures.

L		SCI	MCI	AD	Total accuracy
EpEn	SCI (n = 22)	20	2	2	91.03%
	MCI (n = 28)	2	24	0	
	AD (n = 28)	1	1	26	
PLI	SCI (n = 22)	19	2	1	85.90%
	MCI (n = 28)	0	25	3	
	AD (n = 28)	2	3	23	
MSC	SCI (n = 22)	20	1	1	87.18%
	MCI (n = 28)	2	23	3	
	AD (n = 28)	1	3	24	
MI	SCI (n = 22)	20	0	2	91.03%
	MCI (n = 28)	3	23	2	
	AD (n = 28)	0	1	27	

We notice that *EpEn* measure gives the best results in terms of classification performance compared to the other connectivity measures, reaching a total accuracy between 91.02% with betweenness and 94.87% with degree and efficiency parameters.

Additionally, we notice that the misclassification errors obtained with *EpEn* have more sense than the other measures. More precisely, most of the misclassified SCI and AD patients are classified as MCI patients, which is in accordance with the fact that MCI is an intermediate stage in the evolution towards AD.

Table 7.16: Confusion matrices for differential AD diagnosis with the three groups of patients, using the local efficiency E_{loc} parameter with the four connectivity measures.

E_{loc}		**SCI**	**MCI**	**AD**	**Total accuracy**
EpEn	SCI (n = 22)	21	1	0	94.87%
	MCI (n = 28)	0	27	1	
	AD (n = 28)	0	2	26	
PLI	SCI (n = 22)	16	5	1	89.74%
	MCI (n = 28)	2	25	1	
	AD (n = 28)	0	0	28	
MSC	SCI (n = 22)	17	5	0	89.74%
	MCI (n = 28)	2	25	1	
	AD (n = 28)	0	1	27	
MI	SCI (n = 22)	19	1	2	89.74%
	MCI (n = 28)	2	25	1	
	AD (n = 28)	1	2	25	

Table 7.17: Confusion matrices for differential AD diagnosis with the three groups of patients, using the betweenness (BW) parameter with the four connectivity measures.

BW		**SCI**	**MCI**	**AD**	**Total accuracy**
EpEn	SCI (n = 22)	19	2	1	91.02%
	MCI (n = 28)	0	28	0	
	AD (n = 28)	1	3	24	
PLI	SCI (n = 22)	17	1	4	85.90%
	MCI (n = 28)	2	24	2	
	AD (n = 28)	3	0	25	
MSC	SCI (n = 22)	19	2	1	91.03%
	MCI (n = 28)	0	28	0	
	AD (n = 28)	3	1	24	
MI	SCI (n = 22)	18	1	3	89.74%
	MCI (n = 28)	0	27	1	
	AD (n = 28)	1	2	25	

For a better insight on the selected features, we report in Tables 7.18 to 7.20 the best combination of features obtained for the multiclass classification, with the *EpEn* measure since it gave the best performance. We can see that with the clustering coefficient, for example, the three two-classifiers (SCI vs. AD, SCI vs. MCI and AD vs. MCI) have the same number of selected features (eight features) as above-mentioned. The same is observed for the other graph parameters.

Table 7.18: Best combination of features for discriminating SCI from AD patients using different graph parameters with EpEn.

Selected Features for SCI vs. AD										
CC	θ_T6	β_P4	α_P3	θ_F4	δ_F8	δ_FC4	δ_F4	δ_T5		
K	α_FC4	δ_T6	β_CPz	β_FP2	δ_P3	δ_C3	α_TP8	θ_TP8	δ_FC3	
L	δ_F3	α_FP2	δ_T6	δ_P4	θ_Oz	α_FC4	β_FC4	β_FP2	β_Oz	
E_{loc}	δ_T6	δ_F3	α_CP3	δ_FT8	θ_TP7	α_FT8	α_Fz	β_FC4	β_FC3	β_P4
BW	δ_T6	δ_P3	β_FC4	β_FC3	β_FCz	δ_C4	β_T6	θ_T5		

Table 7.19: Best combination of features for discriminating SCI from MCI patients using different graph parameters with EpEn.

Selected Features for SCI vs. MCI										
CC	α_P3	δ_FP1	δ_CPz	θ_T6	α_C3	θ_TP7	δ_F3	α_TP8		
K	β_O2	θ_F8	α_FC4	δ_T6	δ_F8	δ_T3	δ_Oz	θ_T4	δ_FC4	
L	δ_Oz	β_Oz	β_FP2	β_C4	β_CP3	β_F8	β_T3	β_Pz	α_FC4	
E_{loc}	δ_F3	β_TP7	θ_FT7	α_P3	θ_TP7	β_FC4	β_O1	α_Fz	α_FT8	α_C4
BW	β_T6	δ_FC3	δ_Fz	α_F8	δ_FT8	β_F4	β_O2	β_Fz		

Table 7.20: Best combination of features for discriminating AD from MCI patients using different graph parameters with *EpEn*.

Selected Features for AD vs. MCI										
CC	δ_FP1	δ_T3	δ_FC4	δ_F4	β_P3	θ_Fz	θ_FT8	α_FP2		
K	δ_F3	θ_Fz	δ_Fz	δ_Cz	δ_F4	δ_FC3	δ_FT8	β_T4	θ_TP7	
L	β_F8	δ_FP1	β_O2	δ_T3	θ_Cz	β_CP4	β_T4	θ_FT8	δ_P3	
E_{loc}	δ_FP1	δ_T3	α_T3	θ_Fz	α_FP1	β_C4	β_Cz	δ_CPz	α_F8	β_F7
BW	β_FP1	β_Fz	θ_CPz	β_P4	β_TP7	δ_Fz	δ_T6	β_O2		

We clearly show that the selected combinations of features include different frequency bands and different electrodes. Additionally, we observe that the selected features depend on the exploited graph parameter. However, we observe a certain homogeneity between graph parameters when looking to the first selected feature, which is considered by the OFR algorithm as the best feature explaining the output. Note that the advantage of our feature selection method is to retrieve the most relevant combination of features sharing complementary information.

The electrode (T6) that is located in the right side of the parieto-temporal region emerges as a relevant channel to discriminate SCI from AD with three graph parameters. Such an electrode also appears in the second position with degree parameter and in the third position with the shortest path. We also notice that the delta and theta bands are relevant to distinguish SCI from AD. For SCI vs. MCI, the first features belong in general to the posterior brain region, while for AD vs. MCI, the first features belong to the frontal brain region.

7.6 Conclusion

Experiments showed that the statistical modeling of EEG signals with *EpEn* allows a better differentiation between SCI, MCI and AD stages, compared to phase lag index, coherence and mutual information, which are deterministic measures. When discriminating SCI from AD, the accuracy value with *EpEn* is between 90% and 94% considering the five graph parameters. We reached 94% of accuracy with a high specificity (90.91% of well classified SCI patients) and a high sensitivity (96.43% of well classified AD patients), considering the clustering coefficient and the efficiency. Contrary to *EpEn*, *PLI*, *MSC* and *MI* give in some cases the worst results for some graph parameters.

When discriminating SCI from MCI, the results indicated that *MI* and *EpEn* lead to good classification performance: we achieved an accuracy value between 90% and 96% with *MI* and an accuracy value between 92% and 100% with *EpEn*. Nevertheless, *EpEn* outperforms by far the other measures, reaching sometimes 100% of specificity and sensitivity. When discriminating AD from MCI group, the results showed that *PLI* and *MSC* measures give the worst results compared to *MI* and *EpEn*. When comparing *MI* and *EpEn*, we found that their classification performance depends on the graph parameter.

After that, when summarizing all of the obtained results, we clearly showed the discriminative potential of EpEn compared to the other measures: EpEn is ranked ten times in the first position, four times in the second position, and only one time in the third position (see Fig. 7.1). In addition, contrary to the other connectivity measures, EpEn was never ranked in the last position.

Finally, when conducting a multiclass classification to discriminate SCI, MCI and AD simultaneously, results show again that EpEn outperforms the other measures, reaching a total accuracy between 91.02% and 94.87% depending on the used graph parameter.

Additionally, we noticed that the misclassification errors obtained with EpEn have more sense compared to the other measures: most of the misclassified SCI and AD patients are classified as MCI patients, which is more coherent with the evolution stages of cognitive impairment. MCI being an intermediate stage in the evolution towards AD.

In conclusion, this study (referred to as Study 3) demonstrates the effectiveness of the statistical modeling of EEG with an HMM for analyzing the brain network in patients with different clinical severity stages of cognitive dysfunction. However, our study presents with some limitations. We performed our experiments based on a methodology that selects automatically the most relevant input features for classification performance assessment. A deeper analysis should be performed to interpret more finely our results in terms of the selected features in relation with brain disorder detection. In addition, we reported in this study only the performance of the optimal proportional threshold value that gave the best accuracy.

However, we noticed that the obtained proportional threshold value varied across the graph parameters and across the connectivity measures. It would be interesting in the future to compare all of the measures at different proportional threshold values in order to study the stability of the measures. The assumption is that some measures could be more stable to threshold changes. This could be investigated in future work.

Chapter 8

A multi-scale density analysis of EEG signals for AD diagnosis

8.1 Problem and objective of the study

As presented in Chapter 2, EEG signals are multidimensional time series captured through several cortical electrodes (EEG channels). In addition, EEG signals are analyzed either in the time domain or in specific standard frequency bands, namely delta, theta, alpha, and beta bands. Further divisions in these bands are considered (low alpha, high alpha, low beta, etc). Each frequency band conveys different information about brain functionality and synchronization.

Conventionally, different EEG markers are extracted to quantify changes in brain activity based on several aspects: frequency band, synchronization, coherence, time-frequency analysis, complexity measurement based on fractal dimension and information theory, and functional graphs. These EEG markers are commonly studied in different frequency ranges. Thus, owing the huge amount of information embedded in EEG signals, there is a serious difficulty about how to choose relevant EEG markers for AD diagnosis and how to exploit them because often several EEG markers can be informative. In general, it is necessary to combine different EEG markers to reach good classification performance.

Besides, the literature suffers from some limitations. First, the prevailing paradigm in the literature extracts information from EEG signals by averaging them over electrodes; this leads to a smoothing of the inter-channel relationships. Second, the majority of works identify brain regions of interest by specifying a group of electrodes belonging to the considered region. However, it is not obvious to state the spatial limits of a brain area. This latest point can explain in part the difficulty to achieve common conclusions in the literature.

In addition, as stated in Chapter 4, many works of the literature have focused on the analysis of brain functional connectivity using graph theory, which allows conducting a topological study of the brain functional organization. Most studies in the literature have used undirected binary networks leading to promising insights on the characterization of the underlying brain dynamics in AD. However, conflicting results emerge in some respect, related to methodological differences in particular. Actually, most current studies applied a thresholding approach on dense and weighted complex networks to obtain sparse and binary form. Although studies have suggested that this operation may ignore potentially valuable information during network construction, thresholding

is commonly applied to remove weaker connections, which are most affected by experimental noise (Van Den Heuvel and Fornito, 2014), and to reduce the density of the graph, thus making it computationally more tractable.

Absolute or proportional threshold approaches can be applied. The first approach consists in the selection of edges with a connectivity value higher than the absolute threshold value, setting all surviving connections to 1 and the others to 0 in the binary case. This leads to different density networks across subjects. Graph density, corresponding to the proportion of all connections that are present in the network, has been shown to have an impact on the computation of graph metrics (Van Wijk et al., 2010). Indeed, the potential differences in network topology between two populations, in terms of graph metrics, could be related to the differences in number of network connections and not directly to disease.

To overcome this issue, other studies have used a proportional threshold (PT) (Bassett and Bullmore, 2009; Achard and Bullmore, 2007; van den Broek et al., 1998), which consists in the selection of the strongest percentage of connections in each individual network, setting all surviving connections to 1 and others to 0. Such approach ensures equal graph density across populations, making it a commonly used approach for network analysis in disease studies (Garrison et al., 2015; Braun, 2012; Ginestet et al., 2011).

The crucial aspect in functional networks studies is how the threshold value is fixed in order to obtain a graph from a connectivity matrix, where the non-relevant connections are pruned off and the connections whose weights are above the threshold are preserved. In the literature, a common adopted strategy is to use different PT values in an arbitrary interval, from which graph parameters are calculated. Then, we keep the threshold value for which we observe a significant statistical difference between populations in terms of topological parameters.

However, the effect of the threshold choice in not completely understood and it could lead to different study conclusions. As we will show in the present work, small variations of the proportional threshold may lead to high variability of classification performance. Thus, it is necessary to consider other reasoning options behind the choice of the threshold.

The present study (referred to as Study 4) relates to an automatic hierarchical method for EEG analysis, which allows the extraction of a big amount of information based on a single EEG marker. The analysis of functional connectivity is carried out for different brain network densities, based on multi-scale density analysis (combination of different threshold values). Actually, our proposal provides a refined analysis of EEG dynamics at different network density scales. It also proposes an automatic selection of the frequency band, the spatial location of the pertinent electrode, and the density scale of brain network that we have to consider for discriminating AD patients from SCI and MCI patients.

8.2 Study design and methodology

This study is carried out on Charles-Foix database, considering EEG signals of the 22 SCI subjects, the 28 AD patients and 28 MCI patients among the 52 available in the dataset. A detailed description of the database is given in Section 5.2.1.

For each subject in the cohort, we computed functional connectivity between all pairs of electrodes, leading to a connectivity matrix 30x30. Then, we applied a proportional threshold (PT) to the generated connectivity matrices to preserve the connections with the highest connectivity values. The matrices were computed in each frequency band (delta, theta, alpha and beta), and thresholded within a range of percentage values (PT%) between 10% and 100% in step of 10%. Hence, each subject is finally characterized by 40 weighted adjacency matrices (10 thresholded matrices per frequency band).

Figure 8.1 shows the obtained weighted brain network at different proportional threshold values. The proportional threshold conserves the edges (the connections) with the highest values.

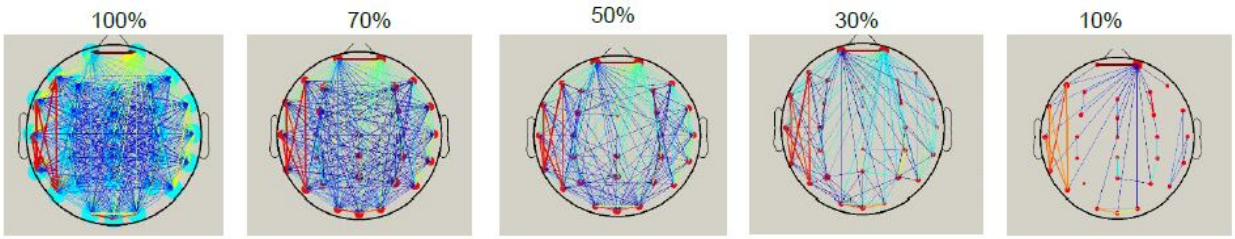

Figure 8.1: Weighted brain network at different proportional threshold values.

Then, from each adjacency matrix, we compute a local graph parameter associated to each electrode. Thus, a vector of 30 components characterizes each person (in each frequency band and each PT value), where each component represents the graph parameter value at the considered electrode (step 1 in Fig. 8.2). In the end, each person is represented by a graph parameter vector of 30 components, computed in the four frequency bands and the 10 PT values.

After that, in order to discriminate between two populations (*e.g.* AD patients from SCI subjects), we applied a first feature selection procedure to identify the most relevant electrode discriminating the two populations, at a given frequency band and a given PT value (step 2 in Fig. 8.2). To do that, we used the Orthogonal Forward Regression (OFR) algorithm, previously presented in Section 7.4, following a leave-one-out protocol.

Note that this procedure is repeated 40 times in the case of a weighted graph (4 frequency bands and 10 PT values), in order to select only the most pertinent electrode, at a given frequency band and a given network density. In case of a binary graph, we can not exploit the whole network (100%) since all values would be assigned to one. Thus, the matrices were thresholded between 10% and 90% in step of 10%, and the feature selection procedure is repeated 36 times (four frequency bands and 9 PT values).

Then, by merging the 40 selected features in case of weighted graph (36 features in case of binary graph), we applied an additional feature selection procedure to combine the extracted information mixing different electrodes, frequency bands, and network densities (step 3 in Fig. 8.2). To choose the features to be kept, we applied the random probe method with an acceptable risk level defined at 5% (as presented in Section 7.4). Finally, a feature vector is selected for classification performance assessment combining different triplets in this form (frequency, PT, electrode). For example, $\alpha 10(FC4)$ corresponds to the thresholded values obtained for an EEG signal acquired with an elec-

trode positioned on the FC4 location, filtered on the frequency band alpha and thresholded with a PT of 10%.

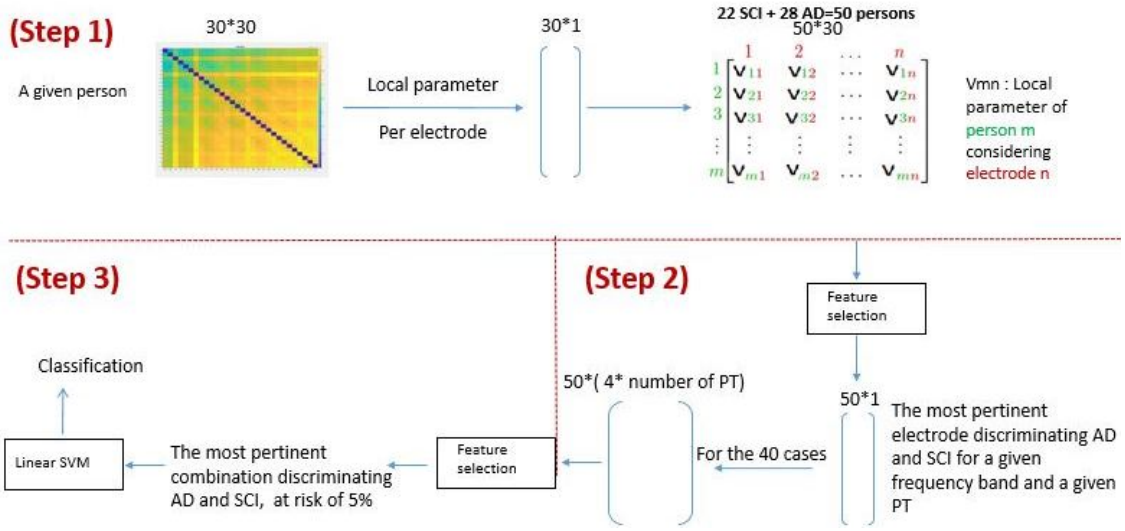

Figure 8.2: Scheme of the proposed methodology for analyzing weighted brain network between SCI and AD patients.

Since feature selection results depend on the range of the PT interval considered, we applied our methodology for different PT intervals (10% to 100%, 10% to 90%,..., 10% to 20%). At each interval, different combinations of features could emerge. When considering a wide range of PT interval (10%-100%), 40 cases emerge for feature selection. When considering lower ranges, low cases emerge for feature selection. For example, for 10%-60% interval, 24 cases emerge for feature selection (6 PT values x 4 frequency bands).

To evaluate the discriminative power of our methodology, we used both linear SVM and LDA classifiers, and we considered *different connectivity measures* to compute the functional connectivity: Epoch-based Entropy ($EpEn$), phase lag index (PLI), and mutual information (MI). In addition, we considered different graph parameters computed on both binary and weighted graphs: clustering coefficient (CC), degree (K), shortest path (L), local efficiency (E_{loc}) and betweenness (BW). A detailed description of such parameters is given in Section 4.2.

8.3 Experimental results

8.3.1 Influence of the proportional threshold

For a better insight on the effect of the threshold choice on the discrimination between populations, we report in Table 8.1 the obtained SVM classification performance between SCI and AD groups with clustering coefficient. We conducted the experiments considering the binary graph framework and used $EpEn$ as a connectivity measure. The reported results consider a combination of the four frequency bands, following the approach presented in the previous section, without combining PT values.

Table 8.1: SVM classification performance (in %) when discriminating SCI from AD with the clustering coefficient, using *EpEn* to quantify the connectivity links in the binary network, considering different threshold (PT) values.

PT value	**90**	**80**	**70**	**60**	**50**	**40**	**30**	**20**	**10**
Accuracy	72	66	76	74	78	76	74	62	70
Specificity	72.73	50	63.64	68.18	72.73	63.64	63.64	50	59.09
Sensitivity	71.34	78.57	85.71	78.57	82.14	85.71	82.14	71.34	78.57

We clearly observe that the classification performance is very sensitive to the chosen threshold and there is no correlation between the obtained accuracy values and the variation of the density network. Also, we notice that the accuracy is not very good and reaches 78% when preserving the highest 50% connectivity values. In addition, we notice that there is no balance between specificity (SCI subjects well classified) and sensitivity (AD patients well classified). However, when mixing different PT values, following exactly the same methodology presented in the previous section and considering different PT ranges, we obtain the results reported in Table 8.2.

Table 8.2: SVM classification performance (in %) with our methodology when discriminating SCI from AD with the clustering coefficient, using *EpEn* to quantify the connectivity links in the binary network, considering different ranges of threshold (PT) values.

PT interval	**10-90**	**10-80**	**10-70**	**10-60**	**10-50**	**10-40**	**10-30**	**10-20**
Accuracy	100	100	100	94	94	74	74	70
Specificity	100	100	100	90.91	90.91	68.12	68.12	59.09
Sensitivity	100	100	100	96.43	96.43	78.57	78.57	78.57

We first notice that the performance is better than that obtained in Table 8.1, reaching an accuracy of 100% when considering 7 levels of network densities, *i.e.* when considering PT interval 10%-70%. The same results are obtained with larger ranges (10-80 and 10-90). Indeed, for the three PT intervals, the same feature vector is obtained: [$\delta 50(T6)$, $\beta 70(T6)$, $\theta 50(F4)$, $\theta 30(T6)$, $\beta 50(FCz)$, $\alpha 50(Fp2)$]. Moreover, we observe a better balance between specificity and sensitivity, as well as a better stability of the performance across the PT intervals. These results demonstrate the effectiveness of our proposal in terms of performance improvement and stability of the results.

The observations are found similar when discriminating between AD and MCI patients (see Tables 8.3 and 8.4), and between SCI and MCI patients (see Tables 8.5 and 8.6).

Table 8.3: SVM classification performance (in %) when discriminating SCI from MCI with the clustering coefficient, using *EpEn* to quantify the connectivity links in the binary network, considering different threshold (PT) values.

PT	**90**	**80**	**70**	**60**	**50**	**40**	**30**	**20**	**10**
Accuracy	76	84	80	66	70	80	72	72	84
Specificity	63.64	72.73	81.82	50	59.09	68.18	63.64	54.54	81.82
Sensitivity	85.71	92.86	78.57	78.57	78.57	89.29	75	85.71	85.71

Table 8.4: SVM classification performance (in %) with our methodology when discriminating SCI from MCI with the clustering coefficient, using *EpEn* to quantify the connectivity links in the binary network, considering different ranges of threshold (PT) values.

PT interval	**10-90**	**10-80**	**10-70**	**10-60**	**10-50**	**10-40**	**10-30**	**10-20**
Accuracy	92	92	92	90	92	90	84	82
Specificity	95.46	95.46	90.91	86.36	86.36	86.36	77.27	72.73
Sensitivity	89.29	89.29	92.85	92.85	96.43	92.85	89.29	89.29

Table 8.5: SVM classification performance (in %) when discriminating AD from MCI with the clustering coefficient, using *EpEn* to quantify the connectivity links in the binary network, considering different threshold (PT) values.

PT	**90**	**80**	**70**	**60**	**50**	**40**	**30**	**20**	**10**
Accuracy	75	69.64	75	66.07	67.86	62.5	71.43	62.5	66.07
Specificity	82.14	64.28	71.43	50	60.71	53.57	67.85	64.29	46.43
Sensitivity	67.86	75	78.57	82.14	75	71.43	75	60.71	85.71

Table 8.6: SVM classification performance (in %) with our methodology when discriminating AD from MCI with the clustering coefficient, using *EpEn* to quantify the connectivity links in the binary network, considering different ranges of threshold (PT) values.

PT interval	**10-90**	**10-80**	**10-70**	**10-60**	**10-50**	**10-40**	**10-30**	**10-20**
Accuracy	78.57	80.35	80.35	80.35	80.35	82.14	82.14	75
Specificity	75	78.57	78.57	78.57	78.57	82.14	82.14	53.57
Sensitivity	82.14	82.14	82.14	82.14	82.14	82.14	82.14	96.43

In the following section, we present the classification performance obtained with our proposal, using different graph parameters and different connectivity measures. Indeed, we aim to answer to the following question: *is the methodology efficient whatever the considered connectivity measure and the graph parameter?*

8.3.2 Binary graph framework

8.3.2.1 Discriminating AD patients from SCI subjects

Tables 8.7 to 8.9 show the performance of the SVM classifier when discriminating SCI subjects from AD patients, with the five graph parameters and the three functional connectivity measures: *EpEn*, *PLI* and *MI*, respectively. To facilitate the readability of the results, we report only the PT intervals for which the selected combination of features gives the best accuracy.

Note that we put in supplementary materials (Section 8.5) all the obtained results with LDA classifier and with weighted graph framework.

Table 8.7: SVM classification performance (in %) when discriminating SCI from AD with different graph parameters, using *EpEn* to quantify the connectivity links in the binary network.

EpEn	**CC**	**K**	**L**	E_{loc}	**BW**
PT interval	10-70	10-80	10-50	10-70	10-80
Accuracy	100	86	94	94	88
Specificity	100	81.82	95.45	86.36	86.36
Sensitivity	100	89.28	92.86	100	89.28

Table 8.8: SVM classification performance (in %) when discriminating SCI from AD with different graph parameters, using *PLI* to quantify the connectivity links in the binary network.

PLI	**CC**	**K**	**L**	E_{loc}	**BW**
PT interval	10-60	10-90	10-50	10-40	10-90
Accuracy	86	86	84	90	98
Specificity	77.27	81.82	81.82	86.36	100
Sensitivity	92.86	89.28	85.71	96.43	96.46

Table 8.9: SVM classification performance (in %) when discriminating SCI from AD with different graph parameters, using *MI* to quantify the connectivity links in the binary network.

MI	**CC**	**K**	**L**	E_{loc}	**BW**
PT interval	10-60	10-90	10-50	10-40	10-90
Accuracy	94	82	88	88	88
Specificity	95.45	81.82	81.82	86.36	86.36
Sensitivity	92.86	82.14	92.86	89.29	89.29

When comparing the results obtained with the three functional connectivity measures, we globally notice that our methodology allows reaching good classification performance for all connectivity measures and graph parameters. Actually, the performance ranges between 82% and 100% with a very good balance between specificity and sensitivity. Nevertheless, *EpEn* measure allows a better

discrimination between AD and SCI groups, for all graph parameters except betweenness. The best discrimination between AD and SCI using the betweenness parameter has been obtained with PLI measure, reaching an accuracy of 98% (see Table 8.8).

In the sequel, we will conduct a preliminary analysis of the selected features for a better understanding on the behavior of the topological parameters in both AD and SCI groups. We display in Figures 8.3 to 8.7 the distribution of the graph parameters for SCI and AD patients, considering the best combination of features leading to the best accuracy.

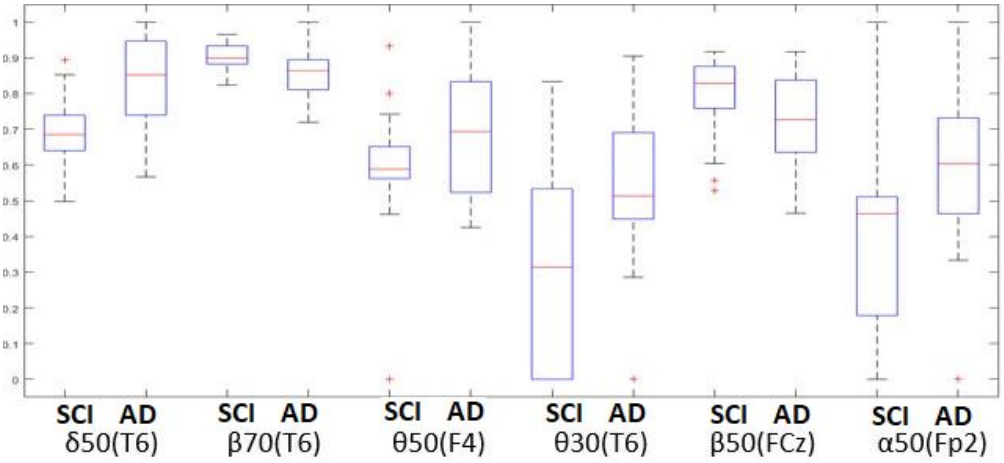

Figure 8.3: Boxplots of the local clustering coefficient values computed on *EpEn* binary graph for SCI subjects and AD patients.

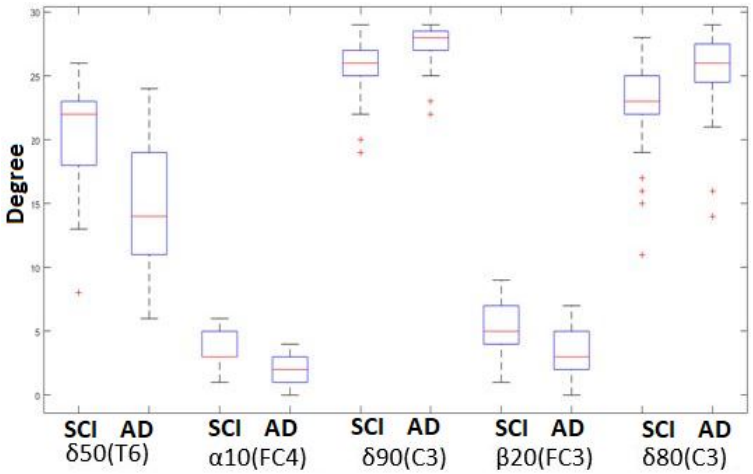

Figure 8.4: Boxplots of the degree values computed on *EpEn* binary graph for SCI subjects and AD patients.

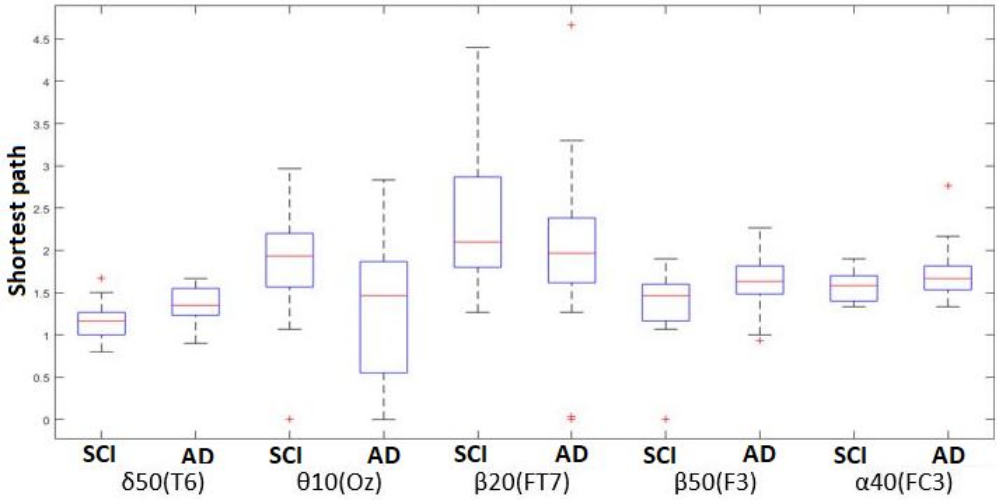

Figure 8.5: Boxplots of the shortest path values computed on *EpEn* binary graph for SCI subjects and AD patients.

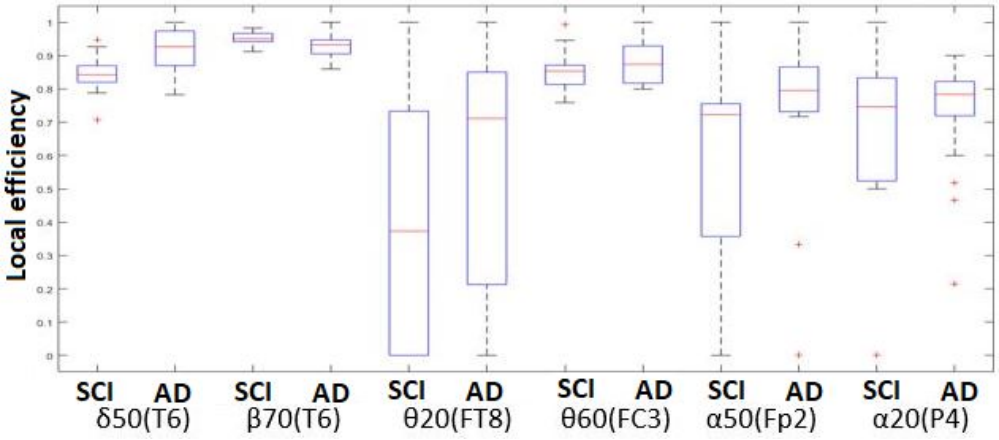

Figure 8.6: Boxplots of the local efficiency values computed on *EpEn* binary graph for SCI subjects and AD patients.

First, we observe that the right temporal region represented by (*T6*) is a very relevant feature to distinguish between SCI and AD groups. This electrode is found to be pertinent for several graph parameters (*CC*, *K*, *L*, and $_{loc}$), in delta and beta bands with a PT value of 50% and 70%. The frontal region plays an additional role to improve classification accuracy.

Moreover, by analyzing the values of boxplots in Figure 8.3, we find that the clustering coefficient values of the right temporal region (*T6*) are greater in AD patients than in SCI subjects in low frequency bands and especially in delta. This indicates that the neighbors in right temporal region are well connected to each other in the network of AD patients compared to SCI subjects. The opposite behavior is observed in beta band (see Figure 8.3).

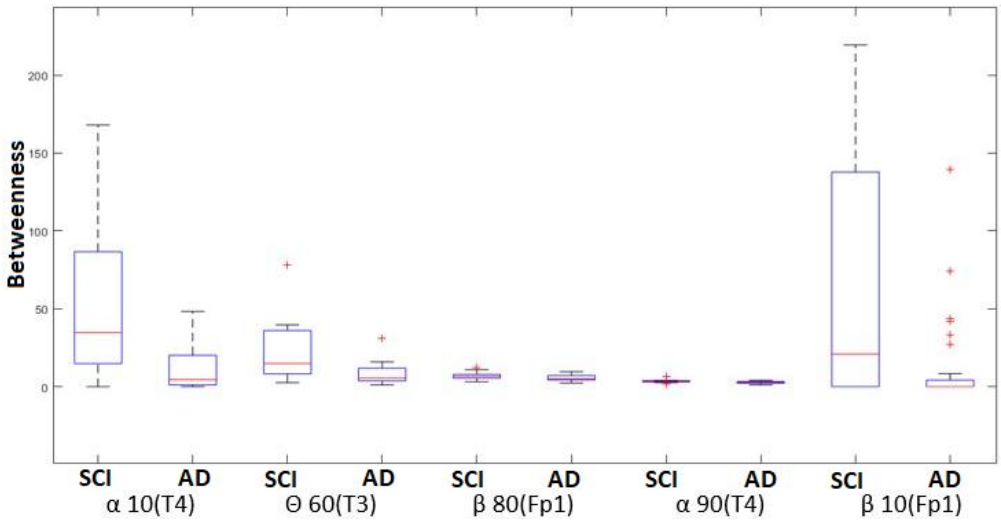

Figure 8.7: Boxplots of the betweenness values (BW) computed on PLI binary graph for SCI subjects and AD patients.

This behavior of clustering coefficient is in accordance with the literature statements. It can be explained by the slowing of EEG signals in AD, leading to the concentration of AD-related activity in the low frequency bands. Our finding is in line with (Cecchetti et al., 2021), where the authors reported that the clustering coefficient gradually increases in theta band as the disease progresses, and gradually decreases in alpha2 band especially in temporal and occipital regions.

In Figure 8.4, we notice that $T6$ has few neighbors (lower degree) in the network of AD patients compared to SCI group in delta band. Nevertheless, since $T6$ is very connected with its neighbors (high clustering coefficient), the low degree value highlights that $T6$ forms a clique with its neighbors.

Furthermore, Figure 8.5 shows that AD patients have longer shortest path than SCI subjects, in the right temporal region in delta band. This result reflects a lack of fluidity in the transmission of information in this region for AD group.

Regarding the clustering coefficient (Fig. 8.3) and local efficiency (Fig. 8.6), we observe a similar behavior between AD and SCI patients based on the first two features: $\delta 50(T6)$ and $\beta 70(T6)$. This same behavior can be explained by the fact that when the neighbors of $T6$ are well connected (high clustering coefficient), there will be more chance that these neighbors can compensate the functioning of this electrode in case of damage, which increases the efficiency of this electrode. Therefore, AD network seems to be more resistant in delta band.

Also, we observe in Figure 8.7 that the betweenness with (PLI) at $T4$ (neighbor of $T6$ and belongs to the right temporal region) is lower for AD patients in alpha band. This indicates that the right temporal region in SCI subjects highly contribute in the transmission of information between regions in alpha band compared to AD patients.

8.3.2.2 Discriminating MCI patients from SCI subjects

Tables 8.10 to 8.12 show the SVM classifier performance when discriminating SCI subjects from MCI patients, with the five binary graph parameters. Each table reports the performance using a specific functional connectivity measure to quantify the connectivity links in the binary network.

Table 8.10: SVM classification performance (in %) when discriminating SCI from MCI with different binary graph parameters, using *EpEn* to quantify the connectivity links in the network.

EpEn	**CC**	**K**	**L**	E_{loc}	**BW**
PT interval	10-50	10-50	10-50	10-70	10-80
Accuracy	92	90	96	90	88
Specificity	86.36	90.91	95.45	95.45	86.36
Sensitivity	96.43	89.28	96.43	89.28	89.28

Table 8.11: SVM classification performance (in %) when discriminating SCI from MCI with different binary graph parameters, using *PLI* to quantify the connectivity links in the network.

PLI	**CC**	**K**	**L**	E_{loc}	**BW**
PT interval	10-80	10-70	10-50	10-80	10-80
Accuracy	92	88	82	90	90
Specificity	90.91	90.91	86.36	86.36	90.91
Sensitivity	92.86	85.71	78.57	92.86	89.28

Table 8.12: SVM classification performance (in %) when discriminating SCI from MCI with different binary graph parameters, using *MI* to quantify the connectivity links in the network.

EpEn	**CC**	**K**	**L**	E_{loc}	**BW**
PT interval	10-90	10-50	10-90	10-80	10-90
Accuracy	90	88	86	88	94
Specificity	81.82	86.36	81.82	86.36	86.36
Sensitivity	96.43	89.29	89.29	89.29	100

Again, a better discrimination between SCI and MCI is observed with *EpEn* measure, for all graph parameters, except betweenness. The obtained accuracy values range from 88% to 96%. We also notice the good balance between sensitivity (MCI well classified) and specificity (SCI well classified).

Regarding *EpEn* measure, when comparing the selected PT intervals in Table 8.7 related to SCI vs. AD to those obtained in Table 8.10 related to SCI vs. MCI, we notice that the density network is smaller to distinguish reliably between SCI and MCI (10%-50%), compared to SCI vs. AD (10%-70% or 10%-80%).

8.3.2.3 Discriminating AD patients from MCI patients

Tables 8.13 to 8.15 show the performance of the SVM classifier when discriminating AD patients from MCI patients with the five binary graph parameters and the three functional connectivity measures.

Table 8.13: SVM classification performance (in %) when discriminating AD from MCI with different binary graph parameters using *EpEn*.

EpEn	**CC**	**K**	**L**	E_{loc}	**BW**
PT interval	10-30	10-50	10-50	10-80	10-50
Accuracy	82.14	87.5	80.36	87.5	89.29
Specificity	82.14	89.29	75	85.71	89.29
Sensitivity	82.14	85.17	85.71	89.28	89.28

Table 8.14: SVM classification performance (in %) when discriminating AD from MCI with different binary graph parameters using *PLI*.

PLI	**CC**	**K**	**L**	E_{loc}	**BW**
PT interval	10-80	10-80	10-50	10-70	10-90
Accuracy	98.21	83.93	82.14	91.07	92.86
Specificity	96.43	82.14	82.14	92.86	96.43
Sensitivity	100	85.17	82.14	89.28	89.28

Table 8.15: SVM classification performance (in %) when discriminating AD from MCI with different binary graph parameters using *MI*.

MI	**CC**	**K**	**L**	E_{loc}	**BW**
PT interval	10-50	10-90	10-60	10-80	10-90
Accuracy	82.14	80.36	91.07	89.29	82.14
Specificity	78.57	78.57	92.86	85.71	75
Sensitivity	85.71	82.14	89.29	92.86	89.28

Regarding *EpEn* measure, when comparing the selected PT intervals in Table 8.13 related to AD vs. MCI to those previously obtained in Table 8.10 related to SCI vs. MCI and in Table 8.7 related to SCI vs. AD, we notice that the density network ranges are even smaller to distinguish reliably between AD and MCI. In fact, with *EpEn* measure, it is necessary to go deeper and focus on the very high *EpEn* values to better discriminate between the two groups.

We note that the best classification performance has been obtained with *PLI* for most graph parameters. The accuracy values range from 82.14% with the shortest path to 98.21% with clustering coefficient. A good balance between sensitivity and specificity is still maintained with our methodology. Note that such performance is reached with *PLI* considering wide density network ranges, contrary to *EpEn* measure.

8.3.2.4 Differential AD diagnosis with the three groups

To assess the effectiveness of our methodology, we also performed a multi-class classification considering the three groups of patients simultaneously. As explained in Section 7.5.5, we are thus confronting to a K-class classification problem *(K = 3)* that we turned into a set of *(K(K-1)/2)* two-class problems.

In the sequel, we report the obtained results for a differential AD diagnosis with the three groups of patients simultaneously, using the results previously obtained with the two-class problems. Therefore, to evaluate the performance of a three-class SVM classifier, we exploit the previous SVM classifiers used to discriminate between each pair of classes.

Table 8.16: Confusion matrices for differential AD diagnosis with the three groups of patients, using the clustering coefficient (CC) with the three connectivity measures.

CC		**SCI**	**MCI**	**AD**	**Total accuracy**
EpEn	SCI (n = 22)	21	1	0	89.47%
	MCI (n = 28)	0	24	4	
	AD (n = 28)	1	2	25	
PLI	SCI (n = 22)	20	0	2	96.15%
	MCI (n = 28)	0	28	0	
	AD (n = 28)	1	0	27	
MI	SCI (n = 22)	19	3	0	83.33%
	MCI (n = 28)	1	23	4	
	AD (n = 28)	1	4	23	

Table 8.17: Confusion matrices for differential AD diagnosis with the three groups of patients, using the degree (K) with the three connectivity measures.

K		**SCI**	**MCI**	**AD**	**Total accuracy**
EpEn	SCI (n = 22)	18	1	3	85.9%
	MCI (n = 28)	0	25	3	
	AD (n = 28)	1	3	24	
PLI	SCI (n = 22)	19	1	2	82.05%
	MCI (n = 28)	3	21	4	
	AD (n = 28)	2	2	24	
MI	SCI (n = 22)	16	3	3	75.64%
	MCI (n = 28)	1	23	4	
	AD (n = 28)	3	5	20	

Table 8.18: Confusion matrices for differential AD diagnosis with the three groups of patients, using the shortest path (L) with the three connectivity measures.

L		**SCI**	**MCI**	**AD**	**Total accuracy**
EpEn	SCI (n = 22)	19	3	0	85.9%
	MCI (n = 28)	2	23	3	
	AD (n = 28)	0	3	25	
PLI	SCI (n = 22)	15	3	4	70.51%
	MCI (n = 28)	3	20	5	
	AD (n = 28)	3	5	20	
MI	SCI (n = 22)	15	3	4	70.51%
	MCI (n = 28)	3	20	5	
	AD (n = 28)	3	5	20	

Table 8.19: Confusion matrices for differential AD diagnosis with the three groups of patients, using the local efficiency E_{loc} with the three connectivity measures.

E_{loc}		**SCI**	**MCI**	**AD**	**Total accuracy**
EpEn	SCI (n = 22)	20	1	1	88.64%
	MCI (n = 28)	0	25	3	
	AD (n = 28)	1	3	24	
PLI	SCI (n = 22)	21	1	0	93.59%
	MCI (n = 28)	0	27	1	
	AD (n = 28)	1	2	25	
MI	SCI (n = 22)	19	1	2	85.9%
	MCI (n = 28)	1	24	3	
	AD (n = 28)	2	2	24	

Table 8.20: Confusion matrices for differential AD diagnosis with the three groups of patients, using the betweenness (BW) with the three connectivity measures.

BW		**SCI**	**MCI**	**AD**	**Total accuracy**
EpEn	SCI (n = 22)	21	1	0	92.31%
	MCI (n = 28)	1	26	1	
	AD (n = 28)	2	1	25	
PLI	SCI (n = 22)	20	2	0	92.31%
	MCI (n = 28)	2	25	1	
	AD (n = 28)	1	0	27	
MI	SCI (n = 22)	17	1	4	82.05%
	MCI (n = 28)	0	26	2	
	AD (n = 28)	1	6	21	

Results show the effectiveness of our proposed methodology even for a multi-class classification, especially with *EpEn* and *PLI* connectivity measures. Note that even if the performance shows slight degradation for some graph parameters, it reaches in the worst case 85.9% with *EpEn* and 70.51% with *PLI*.

Table 8.21 shows the three-class classification performance taking into account the combination of the selected features obtained with the five graph parameters. In fact, an additional feature selection procedure is applied to select the relevant features considered as inputs for the two-class classifiers. Note that in this case, the obtained relevant features may mix different frequency bands, density network values, electrode locations, as well as different graph parameters.

Table 8.21: Confusion matrices for differential AD diagnosis with the three groups of patients, using binary graph parameters combination with the three connectivity measures.

Binary graph		**SCI**	**MCI**	**AD**	**Total accuracy**
EpEn	SCI (n = 22)	22	0	0	98.72%
	MCI (n = 28)	0	27	1	
	AD (n = 28)	0	0	28	
PLI	SCI (n = 22)	22	0	0	96.15%
	MCI (n = 28)	0	26	2	
	AD (n = 28)	0	1	27	
MI	SCI (n = 22)	22	0	0	98.72%
	MCI (n = 28)	0	28	0	
	AD (n = 28)	0	1	27	

We clearly observe an improvement of performance when fusing graph parameters for the three connectivity measures considered in the present study. To have a better insight on the results, we report in Table 8.22 the obtained features when considering *EpEn* as a connectivity measure. We notice that all graph parameters, all frequency bands, different electrode locations and different density scales contribute to the discrimination between populations.

Table 8.22: The selected features with *EpEn* when combining all graph parameters.

Groups	Frequency band_ Threshold value_ Local graph parameter(electrode)
SCI .vs AD	δ_50_$CC(T6)$; α_40_$L(FC3)$; θ_80_$K(T6)$; β_70_$CC(T6)$ θ_20_E_{loc}(FT8); θ_40_$L(Pz)$; δ_30_$L(F3)$; β_20_$K(FC3)$; β_50_$CC(FCz)$; β_20_$L(CP3)$; δ_20_$L(F8)$; α_30_$BW(FC3)$
SCI .vs MCI	β_20_$K(Oz)$; β_40_$CC(TP7)$; δ_90_$BW(Fz)$; α_30_$CC(P3)$; β_30_$L(Oz)$; β_20_$L(F3)$ θ_40_$K(F8)$; δ_30_$L(Oz)$; α_30_$K(FC4)$
AD .vs MCI	β_20_$BW(C4)$; δ_30_$CC(FP1)$; β_30_$L(F8)$; δ_20_E_{loc}(T5); θ_30_$L(Cz)$; β_10_$CC(F4)$; α_10_$BW(F8)$

8.3.3 Correlation study between EEG digital markers and clinical data

We recall that EEG was not exploited to establish the diagnosis of the patients included in the Charles-Foix database. To realize the clinical relevance of using EEG as an additional diagnostic tool, we investigated the existence of correlation between the extracted EEG markers and clinical data.

In the database, three clinical tests are available:

- The MMSE test, which assesses cognitive functions, including attention, arithmetic, recall, language, the ability to follow simple commands, and orientation.
- The RL/RI-16 test, which is used to assess the presence of verbal episodic memory difficulties and detect progression to dementia. More precisely, it permits to determine whether the memory disorder comes from stage 2 of memorization, namely storage, which is the stage affected in AD. If the RL/RI-16 value is low, this indicates a problem during this storage step.
- The BREF (Batterie Rapide d'Efficience Frontale), which is commonly used as a clinical test to evaluate the alteration in the executive functions.

We assessed the correlation between MMSE, RL/RI-16, BREF tests and the final EEG markers reported in Table 8.22. We reported in Tables 8.23 to 8.25 all the EEG markers that have a correlation value higher than *0.5* with one of three clinical tests.

Table 8.23: Correlation between EEG markers and markers for SCI subject. Graph marker is presented as band_ PT_ graph parameter(electrode)

Connectivity measure	**Graph type**	**Graph marker**	**MMSE** n=21	**BREF** n=9	**RLRI** n=17
EpEn	weighted	α_70_$CC(FP2)$	0.53	/	/
	binary	β_20_$K(FC3)$	-0.53	/	/
	binary	α_30_$BW(FC3)$	/	0.53	/
	binary	δ_90_$BW(Fz)$	/	0.55	/
	weighted	α_40_$CC(Fz)$	/	0.71	/
	weighted	θ_80_$E(Cz)$	/	0.60	/
	binary	θ_40_$K(F8)$	/	0.79	/
	weighted	β_70_$BW(F8)$	/	0.60	/
	binary	β_10_$CC(F4)$	/	-0.63	/
	binary	β_20_$BW(C4)$	/	0.71	/
	weighted	β_20_$BW(C4)$	/	0.73	/
	binary	α_30_$CC(P3)$	/	0.64	/
	weighted	α_30_$CC(P3)$	/	0.53	/
	weighted	β_50_$K(P4)$	/	0.62	/
	weighted	θ_80_$K(T6)$	/	-0,60	/
	weighted	δ_60_$BW(O2)$	/	/	-0,61
PLI	weighted	α_80_$BW(FC3)$	/	-0.8	/
	binary	α_70_$K(FC3)$	0.51	/	/
	binary	α_70_$E(Fz)$	/	0.53	/
	binary	δ_10_$E(C3)$	/	-0.8	/
	binary	δ_20_$CC(CPz)$	/	0.69	/
	weighted	δ_40_$BW(Pz)$	/	-0.50	/
	weighted	θ_80_$BW(CP3)$	/	0.52	/
	binary	θ_60_$BW(T3)$	/	-0.50	/
	binary	δ_40_$E(T3)$	/	0.69	/
	weighted	β_50_$BW(T6)$	/	0.69	/
MI	binary	β_10_$BW(F8)$	/	-0.68	/
	binary	β_20_$BW(F4)$	0.51	/	/
	weighted	β_30_$E(TP7)$	/	-0.57	/
	weighted	α_30_$E(TP8)$	/	0.73	/
	binary	β_20_$CC(O1)$	/	0.56	/
	weighted	θ_20_$E(O1)$	/	0.59	/

Table 8.24: Correlation between EEG markers and markers for MCI subject. Graph marker is presented as band_ PT_ graph parameter(electrode)

Connectivity measure	**Graph type**	**Graph marker**	**MMSE** n=42	**BREF** n=24	**RLRI** n=31
EpEn	weighted	α_40_$CC(Fz)$	/	-0.59	/
	weighted	θ_80_$E(Cz)$	/	0.55	/
PLI	weighted	α_70_$CC(FP2)$	/	0.53	/
	binary	β_30_$CC(F3)$	/	-0.57	/
	weighted	β_40_$BW(F8)$	/	-0.54	/
	binary	α_80_$CC(FCz)$	/	-0.54	/
	binary	α_10_$K(C3)$	/	-0.57	/

Table 8.25: Correlation between EEG markers and markers for AD subject. Graph marker is presented as band_ PT_ graph parameter(electrode)

Connectivity measure	**Graph type**	**Graph marker**	**MMSE** n=26	**BREF** n=17	**RLRI** n=13
EpEn	weighted	θ_40_$K(F8)$	/	/	0.53
	binary	α_30_$CC(P3)$	/	0.57	/
	weighted	α_30_$CC(P3)$	/	0.57	/
	weighted	β_40_$CC(TP7)$	/	/	0.51
PLI	weighted	θ_40_$K(F8)$	/	/	0.53
	weighted	α_70_$CC(FP2)$	/	/	-0.66
	binary	α_70_$BW(F7)$	/	/	0.60
	binary	θ_40_$E(Fz)$	/	0.80	/
	weighted	α_80_$BW(FC3)$	/	/	0.52
	binary	δ_10_$E(C3)$	/	/	0.52
	weighted	θ_50_$BW(P4)$	/	0.80	/
	binary	β_30_$E(O2)$	/	/	0.6
MI	weighted	α_20_$E(F7)$	/	/	0.59
	binary	α_10_$BW(FC3)$	/	/	0.55

We first observe that there is no correlation between the EEG markers and the MMSE. In addition, regarding the SCI group, we notice that several EEG markers are correlated with the BREF, especially with *EpEn*. However, the correlation has been assessed only on 9 SCI subjects for whome the BREF is available in our database.

On MCI group, the same behavior is observed: a correlation emerges with the BREF test, especially with *PLI*, considering the 24 persons for whome the BREF is available.

Finally, regarding AD patients, a correlation appears with the BREF and RI-RL-16, especially with *PLI*. Globally, we notice a relationship between EEG markers and clinical markers in some aspects; however, it is not relevant. This allows to infer that EEG markers could be complementary to clinical markers that we assessed in this study.

8.4 Conclusion

The present study relates to an automatic method for EEG signal analysis based on features extracted at different frequency bands, electrode locations and density network scales; thus involving feature selection and data fusion.

We have proposed a multi-scale density analysis of brain networks, which allows fusing different brain functional organizations, by considering the combination of different threshold values to construct the brain networks. Indeed, in the literature, the common adopted methodology to distinguish between populations is to conduct the brain network analysis based on an optimal threshold for which a significant statistical difference between populations is observed in terms of topological parameters. Nevertheless, as we have shown in the present work, small variations of the threshold value leads to high variability of classification performance.

The conducted experiments revealed that fusing different network densities leads to an improvement of classification performance between the three groups, with a better balance between sensitivity and specificity. In addition, it offers a better stability of the results. These findings have been observed whatever the considered connectivity measure and graph parameter.

The originality of our proposal relies on the fact that: (*i*) it allows extracting a huge amount of information using a single EEG marker; (*ii*) it quantifies functional connectivity between all channels without specifying upstream brain regions, following a multi-scale methodology with different connectivity thresholds of EEG network. Indeed, by using a proportional thresholding, we provide a complete network analysis across different network densities; (*iii*) it allows selecting relevant combination of EEG markers, in terms of frequency band, proportional threshold and electrode location.

Our study presents some limitations. First, we used only one algorithm to identify relevant features; so, the obtained features may be dependent to the algorithm used. Besides, the proposed methodology is very fine since it allows selecting features mixing frequency band, electrode location and density scale. This has the drawback of making the interpretation more difficult to bring out a global trend. Also, it raises the question regarding the generalization of the results.

One of the objectives of forthcoming research will be to go further in our analysis by testing other feature selection methods, such as genetic algorithm and XGBoost. Besides, our findings need to be validated on other data in order to be confirmed.

8.5 Supplementary materials

8.5.1 Binary graph framework with LDA classifier

Table 8.26: LDA classification performance (in %) when discriminating SCI from AD with different graph parameters, using *EpEn*.

EpEn	**CC**	**K**	**L**	E_{loc}	**BW**
PT interval	10-70	10-90	10-50	10-70	10-80
Accuracy	94	80	92	92	86
Specificity	95.45	72.73	95.45	86.36	77.72
Sensitivity	92.86	85.71	89.29	96.43	92.86

Table 8.27: LDA classification performance (in %) when discriminating SCI from AD with different graph parameters, using *PLI*.

PLI	**CC**	**K**	**L**	E_{loc}	**BW**
PT interval	10-60	10-90	10-50	10-40	10-90
Accuracy	84	82	84	82	90
Specificity	81.82	77.27	81.82	86.36	81.82
Sensitivity	92.86	89.28	85.71	75.71	96.46

Table 8.28: LDA classification performance (in %) when discriminating SCI from AD with different graph parameters, using *MI*.

MI	**CC**	**K**	**L**	E_{loc}	**BW**
PT interval	10-60	10-90	10-50	10-40	10-90
Accuracy	94	82	86	88	88
Specificity	90.91	81.82	81.82	81.82	81.82
Sensitivity	96.43	82.14	89.29	92.86	92.86

Table 8.29: LDA classification performance (in %) when discriminating SCI from MCI with different binary graph parameters, using *EpEn*.

EpEn	**CC**	**K**	**L**	E_{loc}	**BW**
PT interval	10-50	10-50	10-50	10-70	10-80
Accuracy	88	90	90	90	86
Specificity	86.36	86.36	95.45	86.36	77.72
Sensitivity	89.28	92.86	92.86	92.86	92.86

Table 8.30: LDA classification performance (in %) when discriminating SCI from MCI with different binary graph parameters, using *PLI*.

PLI	**CC**	**K**	**L**	E_{loc}	**BW**
PT interval	10-80	10-70	10-50	10-80	10-80
Accuracy	92	90	70	92	88
Specificity	90.91	90.91	59.09	81.82	90.91
Sensitivity	92.86	89.29	78.57	100	88.71

Table 8.31: LDA classification performance (in %) when discriminating SCI from MCI with different binary graph parameters, using *MI*.

EpEn	**CC**	**K**	**L**	E_{loc}	**BW**
PT interval	10-90	10-50	10-50	10-90	10-90
Accuracy	86	88	84	82	88
Specificity	81.82	81.82	86.36	77.27	86.36
Sensitivity	89.29	92.86	82.14	85.71	100

Table 8.32: LDA classification performance (in %) when discriminating AD from MCI with different binary graph parameters, using *EpEn*.

EpEn	**CC**	**K**	**L**	E_{loc}	**BW**
PT interval	10-30	10-50	10-50	10-80	10-50
Accuracy	80.36	85.71	80.36	89.29	87.5
Specificity	78.57	85.17	75	89.29	89.29
Sensitivity	82.14	85.17	85.71	89.28	85.71

Table 8.33: LDA classification performance (in %) when discriminating AD from MCI with different binary graph parameters, using *PLI*.

PLI	**CC**	**K**	**L**	E_{loc}	**BW**
PT interval	10-80	10-80	10-50	10-70	10-90
Accuracy	92.86	85.71	78.57	89.29	91.07
Specificity	89.29	82.14	75	85.71	96.43
Sensitivity	96.43	89.29	82.14	92.86	82.14

Table 8.34: LDA classification performance (in %) when discriminating AD from MCI with different binary graph parameters, using *MI*.

MI	**CC**	**K**	**L**	E_{loc}	**BW**
PT interval	10-50	10-90	10-60	10-80	10-50
Accuracy	82.14	78.57	87.5	85.71	82.14
Specificity	78.57	78.57	89.29	82.14	75
Sensitivity	85.71	78.57	85.71	89.28	89.29

8.5.2 Weighted graph framework

Table 8.35: SVM Classification performance (in %) when discriminating SCI from AD with different weighted graph parameters, using *EpEn*.

EpEn	**CC**	**K**	**L**	E_{loc}	**BW**
PT interval	10-50	10-80	10-50	10-80	10-80
Accuracy	90	86	82	86	98
Specificity	86.36	81.82	77.27	90.91	95.45
Sensitivity	92.86	89.28	85.71	82.14	100

Table 8.36: SVM Classification performance (in %) when discriminating SCI from AD with different weighted graph parameters, using *PLI*.

PLI	**CC**	**K**	**L**	E_{loc}	**BW**
PT interval	10-50	10-90	10-50	10-50	10-90
Accuracy	84	86	72	78	98
Specificity	86.36	81.82	68.18	77.27	100
Sensitivity	82.14	89.28	75	78.57	96.46

Table 8.37: SVM Classification performance (in %) when discriminating SCI from AD with different weighted graph parameters, using *MI*.

MI	**CC**	**K**	**L**	E_{loc}	**BW**
PT interval	10-90	10-90	10-30	10-80	10-90
Accuracy	70	82	78	80	90
Specificity	72.73	81.82	68.18	86.36	81.82
Sensitivity	67.86	82.14	85.71	75	96.43

Table 8.38: SVM Classification performance (in %) when discriminating SCI from MCI with weighted different graph parameters, using *EpEn*.

EpEn	**CC**	**K**	**L**	E_{loc}	**BW**
PT interval	10-90	10-50	10-40	10-70	10-70
Accuracy	98	90	94	88	86
Specificity	95.45	90.91	90.91	77.27	77.27
Sensitivity	100	89.28	96.43	96.43	92.86

Table 8.39: SVM Classification performance (in %) when discriminating SCI from MCI with different weighted graph parameters, using *PLI*.

PLI	**CC**	**K**	**L**	E_{loc}	**BW**
PT interval	10-70	10-70	10-40	10-20	10-80
Accuracy	86	82	70	82	96
Specificity	72.73	86.36	59.1	63.64	95.45
Sensitivity	96.43	78.57	78.57	96.43	96.43

Table 8.40: SVM Classification performance (in %) when discriminating SCI from MCI with different weighted graph parameters, using *MI*.

MI	**CC**	**K**	**L**	E_{loc}	**BW**
PT interval	10-60	10-50	10-40	10-30	10-30
Accuracy	90	88	96	82	90
Specificity	86.36	86.36	95.45	90.91	86.36
Sensitivity	92.86	89.29	96.43	75	92.86

Table 8.41: SVM Classification performance (in %) when discriminating AD from MCI with different weighted graph parameters, using *EpEn*.

EpEn	**CC**	**K**	**L**	E_{loc}	**BW**
PT interval	10-40	10-70	10-30	10-40	10-70
Accuracy	82.14	87.5	89.29	82.14	96.4
Specificity	82.14	89.29	85.71	82.14	92.8
Sensitivity	82.14	85.17	92.86	82.14	100

Table 8.42: SVM Classification performance (in %) when discriminating AD from MCI with different weighted graph parameters, using *PLI*.

PLI	**CC**	**K**	**L**	E_{loc}	**BW**
PT interval	10-90	10-40	10-20	10-90	10-90
Accuracy	91.07	83.93	73.21	83.93	91.07
Specificity	89.29	92.85	85.71	82.14	89.29
Sensitivity	92.86	75	60.71	85.71	92.86

Table 8.43: SVM Classification performance (in %) when discriminating AD from MCI with different weighted graph parameters, using *MI*.

MI	**CC**	**K**	**L**	E_{loc}	**BW**
PT interval	10-50	10-90	10-40	10-40	10-80
Accuracy	87.5	80.36	91.07	87.5	91.07
Specificity	92.85	78.57	89.29	89.29	85.71
Sensitivity	82.14	82.14	92.86	85.71	96.43

Table 8.44: Confusion matrices for differential AD diagnosis with the three groups of patients, using weighted graph parameters combination with the three connectivity measures.

Weighted graph		**SCI**	**MCI**	**AD**	**Total accuracy**
EpEn	SCI (n = 22)	21	0	1	96.15%
	MCI (n = 28)	0	28	0	
	AD (n = 28)	1	1	26	
PLI	SCI (n = 22)	21	0	1	94.87%
	MCI (n = 28)	0	26	2	
	AD (n = 28)	1	0	27	
MI	SCI (n = 22)	20	1	1	93.59%
	MCI (n = 28)	0	28	0	
	AD (n = 28)	3	0	25	

Table 8.45: The selected features with *EpEn* when combining all graph parameters.

Groups	**Selected features**
SCI .vs AD	δ_50_$K(T6)$; α_10_$K(FC4)$; β_60_$L(FP1)$; β_20_$K(FC3)$; θ_80_E_{loc}(Cz)
SCI .vs MCI	β_20_$K(Oz)$; β_40_$CC(TP7)$; α_30_$CC(P3)$; α_50_$L(FC4)$ θ_40_$K(F8)$; δ_40_$K(Fz)$; β_70_$BW(F4)$; α_90_$CC(Pz)$; θ_30_$E_{loc}(TP7)$; α_40_$CC(Fz)$
AD .vs MCI	δ_30_$CC(FP1)$; β_20_$BW(C4)$; δ_40_$BW(P3)$; β_50_$K(P4)$; δ_60_$BW(O2)$; α_20_$BW(FT7)$; β_70_$BW(F8)$; α_40_$BW(F7)$; θ_30_$E_{loc}(FT8)$

Chapter 9

Conclusion and perspectives

This thesis addresses the early diagnosis of Alzheimer's disease (AD) at preclinical and prodromal stages using electroencephalography (EEG), and concentrates on the extraction, the selection and the analysis of pertinent EEG markers for early AD diagnosis.

A retrospective study was performed using a clinical database including EEG signals recorded in real-life conditions at Charles-Foix Hospital (Ivry-sur-Seine, France). This database contains resting-state EEG data from patients with Subjective Cognitive Impairment (SCI), Mild Cognitive Impairment (MCI) and Mild AD.

In this thesis, we investigated the progression towards AD by studying the behavior of the extracted EEG markers that quantify functional connectivity, in a transversal way from SCI, MCI to Mild AD. In addition, we addressed EEG brain network analysis across the three stages of cognitive decline (SCI, MCI and Mild AD) using the graph theory at the cortical level. This allowed conducting a topological analysis of the brain functional organization in a differential context. Actually, we analyzed in a refine way the extracted graph parameters in each group of patients, and we confronted them to the task of distinguishing AD patients from SCI and MCI subjects. Finally, we performed a preliminary analysis on the correlation between the extracted EEG markers and three clinical tests available in the database (MMSE, RL/RI-16, BREF), in order to realize the clinical relevance of EEG.

Hereafter, we summarize the content of this manuscript to give a global vision on the conducted research:

In Chapter 1, we presented the scientific context, and stated the objectives and the contributions of this research.

In Chapter 2, we presented Alzheimer's disease, its symptoms, the main factors of cognitive decline, and the associated five stages. Moreover, we presented the current diagnostic tools of AD. Finally, we briefly explain the underlying mechanisms to capture the brain dynamics with EEG, and we motivated the utility of EEG for early diagnosis of AD.

In Chapter 3, we reviewed the three main effects of AD on EEG signals, especially the perturbation in EEG functional connectivity, and summarized related works. We concluded that the majority of connectivity measures that have been largely exploited were applied on EEG signals without

considering the non-stationarity, nonlinearity and multivariate properties of EEG time series. This way, we proposed to exploit a specific spatiotemporal connectivity measure, termed "Epoch-based Entropy" (*EpEn*). This entropy measure is based on the statistical modeling of EEG signals with Hidden Markov Models (HMM) on piecewise stationary epochs.

In Chapter 4, we presented the graph brain network framework and summarized the conducted works that have exploited graph theory in the context of AD diagnosis.

Then, we presented in next chapters four major experimental studies, aiming at improving some of the literature lacks. The main outcomes of the thesis are summarized below:

- The statistical entropy measure (*EpEn*) is by far more reliable to discriminate between AD, SCI and MCI groups than commonly used measures in the literature. Indeed, the advantage of the statistical measure lies on the fact that it quantifies on piecewise stationary epochs, the information content conveyed by EEG signals locally over time and spatially by estimating inter-channels relationship. This allows a better estimation of the spatiotemporal characteristics of EEG signals merged into a single figure. Moreover, the structure of HMM seems to be adapted for modeling the neural dynamics underlying the observed EEG signals. In addition, HMM can manage multidimensional signals by applying multivariate probability density functions on the signals. Thus, *EpEn* is very effective when considering a set of EEG signals to obtain an entropy measure associated to a brain region.

- The analysis of functional connectivity in terms of its topological organization in the brain network, and not only in terms of its values, allows a good understanding on the evolution of functional connectivity networks throughout SCI, MCI and AD.

- Functional connectivity and graph analysis are frequency band-dependent and functional alterations starts at the MCI stage with a specific scheme. In delta, SCI group exhibits a reduction of brain activity quantified by EpEn, a decrease of clustering coefficient and an increase of the path length compared to MCI and AD. This indicates the ability of AD and MCI networks to form locally dense cliques. In high frequencies, especially in alpha, opposite behavior appears, suggesting a rapid and high efficiency in information transmission across the SCI network. We concluded that the brain network at SCI stage tends to have a small world topology compared to MCI and AD stages. Moreover, the modular structure of brain networks has revealed that in case of damage, the SCI network is more resilient to neuronal damage compared to that of MCI and even more compared to that of AD stage. Finally, our results added new pieces of evidence in the understanding of the early brain changes, confirming that MCI is a transitional stage between SCI and AD. In addition, all the results pointed out the predominance of high strength intrinsic connectivity that appears at the MCI stage, which may reflect the compensatory response to the neuronal damage occurring early in the disease process.

- Graph brain network analysis led to a better discrimination between SCI, MCI and AD stages in terms of graph parameters, when the graph networks have been constructed from *EpEn* adjacency matrices. We reached a total accuracy between 91% and 94.8% for the three-class classification depending on the considered graph parameter. Moreover, the misclassification errors obtained with EpEn have more sense compared to the other connectivity measures: most of the misclassified SCI and AD patients are classified as MCI patients, which is more coherent with the evolution stages of cognitive impairment. MCI being an intermediate stage in the evolution towards AD.

- The crucial aspect in functional networks studies is how to fix the threshold value to construct the graph. The common adopted strategy is to use different threshold values in an arbitrary interval, from which graph parameters are calculated. Then, the threshold leading to a significant difference between populations is kept. However, the effect of the threshold choice in not completely understood in the literature and it could lead to different study conclusions. We have demonstrated in our research that small variations of the threshold may lead to high variability of classification performance.

- The conducted experiments demonstrated that fusing the information extracted from different graph representations obtained at different density scales (different threshold values), leads on the one hand to an improvement of classification performance between the three populations, with a better balance between sensitivity and specificity. On the other hand, to a better stability of the performance across threshold intervals. These findings have been observed whatever the connectivity measure and the graph parameter used.

- Finally, we have proposed a new methodology to extract EEG markers and identify the relevant ones. Using a single connectivity measure, we computed the connectivity between all pairs of electrodes in all frequency bands, and following a multi-scale approach, which involves the construction of the adjacency matrices at different threshold values. Hence, a huge amount of information emerged from a single measure. By performing a feature selection procedure, the final extracted relevant feature vector combines different triplets fusing frequency band, density network scale and electrode location. Note that the proposed feature selection method is completely independent from the classifier algorithm. Also, classification was performed with linear SVM and LDA classifiers, which are very simple algorithms. Experiments have shown the effectiveness of our proposal to discriminate between SCI, MCI and AD in terms of accuracy, specificity and sensitivity. By also considering the graph parameter, additionally to frequency band, electrode location and density scale, the accuracy value increases.

In the light of such promising results, it would be of high interest to progress in our research work on graph network analysis, taking into account the limitations of our previous studies.

Actually, the obtained results should be considered limited to the context of cortical EEG analysis. It is largely acknowledged that sensor-level analysis is prone to the effects of volume conduction and poor SNR. Currently, there is no method that guarantees to discard volume conduction effects. One way to manage this issue consists in using connectivity measures that are relatively less sensitive to these effects, such as *PLI* and *EpEn*. However, further investigation could be performed using EEG source estimation approach, which is merging as a potential method that addresses the effects of volume conduction.

Besides, our findings are based on a specific feature selection method, namely Orthogonal Forward Regression. It could be of high interest to confront such feature selection method to other algorithms in order to investigate the stability of the obtained EEG features.

In addition, our proposal extracts the features locally at the level of the electrode location. For the purpose of interpreting the obtained features and confronting them to the clinical knowledge, it would be interesting to investigate the effect of considering a brain regions instead of electrodes' location.

Also, our conducted work raises the question regarding the generalization of the results. Hence, our findings need to be validated on other data in order to be confirmed. Our conducted work in this thesis is therefore a preliminary work that requires conducting an in-depth research, which should involve more patients. One of the objectives of this forthcoming research will also be to go further in our analysis by confronting our EEG-based results to the available neuropsychological and clinical markers.

Finally, our proposal relies on a refine methodology that extracted a high number of handcrafted features, and involved a sophisticated feature selection procedure. This could lead to problems of generalization of the results. Therefore, it could be interesting to go a step forward by exploiting Graph Neural Network (GNN) framework for EEG analysis. We will consider the connectivity graph network as input to the model, taking advantage of our previous findings to generate different representations of graph inputs. We will exploit GNN for the automatic extraction of high-level EEG markers. We will also target to conduct a reasoning process on the extracted features to identify brain region of interest and frequency ranges, which proved the most active during the progression to AD.

Bibliography

Joseph Gaugler, Bryan James, Tricia Johnson, Jessica Reimer, Michele Solis, Jennifer Weuve, Rachel F Buckley, and Timothy J Hohman. 2022 alzheimer's disease facts and figures. *Alzheimers & dementia*, 18(4):700–789, 2022.

Henry W Querfurth and Frank M LaFerla. Alzheimer's disease. *The new england journal of medicine*, 329:10, 2010.

Stefania Forner, David Baglietto-Vargas, Alessandra C Martini, Laura Trujillo-Estrada, and Frank M LaFerla. Synaptic impairment in alzheimer's disease: a dysregulated symphony. *Trends in neurosciences*, 40(6):347–357, 2017.

Martin James Prince, Anders Wimo, Maelenn Mari Guerchet, Gemma Claire Ali, Yu-Tzu Wu, and Matthew Prina. World alzheimer report 2015-the global impact of dementia: An analysis of prevalence, incidence, cost and trends. 2015.

Frank Jessen, Rebecca E Amariglio, Martin Van Boxtel, Monique Breteler, Mathieu Ceccaldi, Gaël Chételat, Bruno Dubois, Carole Dufouil, Kathryn A Ellis, Wiesje M Van Der Flier, et al. A conceptual framework for research on subjective cognitive decline in preclinical alzheimer's disease. *Alzheimer's & dementia*, 10(6):844–852, 2014.

Alex J Mitchell, Helen Beaumont, David Ferguson, Motahare Yadegarfar, and Brendon Stubbs. Risk of dementia and mild cognitive impairment in older people with subjective memory complaints: meta-analysis. *Acta Psychiatrica Scandinavica*, 130(6):439–451, 2014.

Bruno Dubois, Harald Hampel, Howard H Feldman, Philip Scheltens, Paul Aisen, Sandrine Andrieu, Hovagim Bakardjian, Habib Benali, Lars Bertram, Kaj Blennow, et al. Preclinical alzheimer's disease: definition, natural history, and diagnostic criteria. *Alzheimer's & Dementia*, 12(3): 292–323, 2016.

Guy M McKhann, David S Knopman, Howard Chertkow, Bradley T Hyman, Clifford R Jack Jr, Claudia H Kawas, William E Klunk, Walter J Koroshetz, Jennifer J Manly, Richard Mayeux, et al. The diagnosis of dementia due to alzheimer's disease: recommendations from the national institute on aging-alzheimer's association workgroups on diagnostic guidelines for alzheimer's disease. *Alzheimer's & dementia*, 7(3):263–269, 2011.

Bruno Dubois, Howard H Feldman, Claudia Jacova, Harald Hampel, José Luis Molinuevo, Kaj Blennow, Steven T DeKosky, Serge Gauthier, Dennis Selkoe, Randall Bateman, et al. Advancing research diagnostic criteria for alzheimer's disease: The iwg-2 criteria correction appears in lancet neurol. 2014 aug;13(8):757. lancet neurol. 2014;13(6):614-629. 2014.

Harald Hampel, Nicola Toschi, Claudio Babiloni, Filippo Baldacci, Keith L Black, Arun LW Bokde, René S Bun, Francesco Cacciola, Enrica Cavedo, Patrizia A Chiesa, et al. Revolution of alzheimer precision neurology. passageway of systems biology and neurophysiology. *Journal of Alzheimer's Disease*, 64(s1):S47–S105, 2018.

Claudio Babiloni, Katarzyna Blinowska, Laura Bonanni, Andrej Cichocki, Willem De Haan, Claudio Del Percio, Bruno Dubois, Javier Escudero, Alberto Fernández, Giovanni Frisoni, et al. What electrophysiology tells us about alzheimer's disease: a window into the synchronization and connectivity of brain neurons. *Neurobiology of aging*, 85:58–73, 2020.

Salvatore Giaquinto and Giuseppe Nolfe. The eeg in the normal elderly: a contribution to the interpretation of aging and dementia. *Electroencephalography and clinical neurophysiology*, 63 (6):540–546, 1986.

Ruth CG Briel, Ian Mckeith, William A Barker, Y Hewitt, Robert Perry, Paul Ince, and A.F. Fairbairn. Eeg findings in dementia with lewy bodies and alzheimer's disease. *Journal of neurology, neurosurgery, and psychiatry*, 66:401–3, 04 1999. doi: 10.1136/jnnp.66.3.401.

Nesma Houmani, Majd Abazid, Kylliann De Santiago, Jerome Boudy, Bernadette Dorizzi, Jean Mariani, and Kiyoka Kinugawa. Eeg signal analysis with a statistical entropy-based measure for alzheimer's disease detection, open access book. *Advances in Signal Processing: Reviews, Book Series*, 2, 2021.

Majd Abazid, Nesma Houmani, Bernadette Dorizzi, Jerome Boudy, Jean Mariani, and Kiyoka Kinugawa. Weighted brain network analysis on different stages of clinical cognitive decline. *Bioengineering*, 9(2):62, 2022.

Majd Abazid, Nesma Houmani, Jérôme Boudy, Bernadette Dorizzi, Jean Mariani, and Kiyoka Kinugawa. A comparative study of functional connectivity measures for brain network analysis in the context of ad detection with eeg. *Entropy*, 23(11):1553, 2021.

Christiane Reitz, Carol Brayne, and Richard Mayeux. Epidemiology of alzheimer disease. *Nature Reviews Neurology*, 7(3):137–152, 2011.

Cleusa P Ferri, Martin Prince, Carol Brayne, Henry Brodaty, Laura Fratiglioni, Mary Ganguli, Kathleen Hall, Kazuo Hasegawa, Hugh Hendrie, Yueqin Huang, et al. Global prevalence of dementia: a delphi consensus study. *The lancet*, 366(9503):2112–2117, 2005.

Chengxuan Qiu, Miia Kivipelto, and Eva von Strauss. Epidemiology of alzheimer's disease: occurrence, determinants, and strategies toward intervention. *Dialogues in clinical neuroscience*, 11 (2):111, 2009.

María M Corrada, Ron Brookmeyer, Annlia Paganini-Hill, Daniel Berlau, and Claudia H Kawas. Dementia incidence continues to increase with age in the oldest old: the 90+ study. *Annals of neurology*, 67(1):114–121, 2010.

Hanta Ramaroson, Catherine Helmer, Pascale Barberger-Gateau, Luc Letenneur, JF Dartigues, et al. Prevalence of dementia and alzheimer's disease among subjects aged 75 years or over: updated results of the paquid cohort. *Revue neurologique*, 159(4):405–411, 2003.

Li Li, David Ruau, Rong Chen, Susan Weber, and Atul J Butte. Systematic identification of risk factors for alzheimer's disease through shared genetic architecture and electronic medical records. In *Biocomputing 2013*, pages 224–235. World Scientific, 2013.

Konrad Maurer, Stephan Volk, and Hector Gerbaldo. Auguste d and alzheimer's disease. *The lancet*, 349(9064):1546–1549, 1997.

Mayur Bagad, Debjoyti Chowdhury, and Zaved Khan. Towards understanding alzheimer's disease: An overview. *Research Journal of Pharmaceutical, Biological and Chemical Sciences*, 4:286–298, 10 2013.

Saeed Sadigh-Eteghad, Babak Sabermarouf, Alireza Majdi, Mahnaz Talebi, Mehdi Farhoudi, and Javad Mahmoudi. Amyloid-beta: a crucial factor in alzheimer's disease. *Medical principles and practice*, 24(1):1–10, 2015.

Caine W Wong, Vito Quaranta, and George G Glenner. Neuritic plaques and cerebrovascular amyloid in alzheimer disease are antigenically related. *Proceedings of the National Academy of Sciences*, 82(24):8729–8732, 1985.

Mak Adam Daulatzai. Early stages of pathogenesis in memory impairment during normal senescence and alzheimer's disease. *Journal of Alzheimer's Disease*, 20(2):355–367, 2010.

Zhengxuan Shen. Brain cholinesterases: Iii. future perspectives of ad research and clinical practice. *Medical hypotheses*, 63(2):298–307, 2004.

Jean Pierre Brion. Neurofibrillary tangles and alzheimer's disease. *European neurology*, 40(3): 130–140, 1998.

Daniel Famer. *Implications of Cholesterol and CholesterolLowering Therapy in Alzheimer's Disease*. Karolinska Institutet (Sweden), 2007.

Agneta Nordberg. Amyloid plaque imaging in vivo: current achievement and future prospects. *European journal of nuclear medicine and molecular imaging*, 35(1):46–50, 2008.

Florence Rémy, Nathalie Vayssière, Laure Saint-Aubert, Emmanuel Barbeau, and Jérémie Pariente. White matter disruption at the prodromal stage of alzheimer's disease: relationships with hippocampal atrophy and episodic memory performance. *NeuroImage: Clinical*, 7:482–492, 2015.

Eva Braak, Katherine Griffing, Kimihito Arai, Jürgen Bohl, Hansjürgen Bratzke, and Heiko Braak. Neuropathology of alzheimer's disease: what is new since a. alzheimer? *European archives of psychiatry and clinical neuroscience*, 249(3):S14–S22, 1999.

Rudolph E Tanzi. The genetics of alzheimer disease. *Cold Spring Harbor perspectives in medicine*, 2(10):a006296, 2012.

Marcos Vinícius Ferreira Silva, Cristina de Mello Gomide Loures, Luan Carlos Vieira Alves, Leonardo Cruz de Souza, Karina Braga Gomes Borges, and Maria das Graças Carvalho. Alzheimer's disease: risk factors and potentially protective measures. *Journal of biomedical science*, 26(1):1–11, 2019.

Joseph L Price, Daniel W McKeel Jr, Virginia D Buckles, Catherine M Roe, Chengjie Xiong, Michael Grundman, Lawrence A Hansen, Ronald C Petersen, Joseph E Parisi, Dennis W Dickson, et al. Neuropathology of nondemented aging: presumptive evidence for preclinical alzheimer disease. *Neurobiology of aging*, 30(7):1026–1036, 2009.

Ronald C Petersen, Rosebud O Roberts, David S Knopman, Bradley F Boeve, Yonas E Geda, Robert J Ivnik, Glenn E Smith, and Clifford R Jack. Mild cognitive impairment: ten years later. *Archives of neurology*, 66(12):1447–1455, 2009.

Niklas Mattsson, Henrik Zetterberg, Oskar Hansson, Niels Andreasen, Lucilla Parnetti, Michael Jonsson, Sanna-Kaisa Herukka, Wiesje M van der Flier, Marinus A Blankenstein, Michael Ewers, et al. Csf biomarkers and incipient alzheimer disease in patients with mild cognitive impairment. *Jama*, 302(4):385–393, 2009.

Bruno Dubois, Howard H Feldman, Claudia Jacova, Steven T DeKosky, Pascale Barberger-Gateau, Jeffrey Cummings, André Delacourte, Douglas Galasko, Serge Gauthier, Gregory Jicha, et al. Research criteria for the diagnosis of alzheimer's disease: revising the nincds–adrda criteria. *The Lancet Neurology*, 6(8):734–746, 2007.

Marilyn S Albert, Steven T DeKosky, Dennis Dickson, Bruno Dubois, Howard H Feldman, Nick C Fox, Anthony Gamst, David M Holtzman, William J Jagust, Ronald C Petersen, et al. The diagnosis of mild cognitive impairment due to alzheimer's disease: recommendations from the national institute on aging-alzheimer's association workgroups on diagnostic guidelines for alzheimer's disease. *Alzheimer's & dementia*, 7(3):270–279, 2011.

Elizabeth P Helzner, Nikolaos Scarmeas, Stephanie Cosentino, MX Tang, Nicole Schupf, and Yaakov Stern. Survival in alzheimer disease: a multiethnic, population-based study of incident cases. *Neurology*, 71(19):1489–1495, 2008.

Justin Dauwels, Francois Vialatte, and Andrzej Cichocki. Diagnosis of alzheimer's disease from eeg signals: where are we standing? *Current Alzheimer Research*, 7(6):487–505, 2010a.

Reisa Sperling, Elizabeth Mormino, and Keith Johnson. The evolution of preclinical alzheimer's disease: implications for prevention trials. *Neuron*, 84(3):608–622, 2014.

Ane Alberdi, Asier Aztiria, and Adrian Basarab. On the early diagnosis of alzheimer's disease from multimodal signals: A survey. *Artificial intelligence in medicine*, 71:1–29, 2016.

Clifford R Jack Jr, Marilyn S Albert, David S Knopman, Guy M McKhann, Reisa A Sperling, Maria C Carrillo, Bill Thies, and Creighton H Phelps. Introduction to the recommendations from the national institute on aging-alzheimer's association workgroups on diagnostic guidelines for alzheimer's disease. *Alzheimer's & dementia*, 7(3):257–262, 2011.

Reisa A Sperling, Paul S Aisen, Laurel A Beckett, David A Bennett, Suzanne Craft, Anne M Fagan, Takeshi Iwatsubo, Clifford R Jack Jr, Jeffrey Kaye, Thomas J Montine, et al. Toward defining the preclinical stages of alzheimer's disease: Recommendations from the national institute on aging-alzheimer's association workgroups on diagnostic guidelines for alzheimer's disease. *Alzheimer's & dementia*, 7(3):280–292, 2011.

Guy MCKHANN. Report of the nincds-adrda work group under the auspices of department of health and human service task force on alzheimer's disease. *Neurology*, 34:939–944, 1984.

Marshal F Folstein, Susan E Folstein, and Paul R McHugh. Mini-mental state: a practical method for grading the cognitive state of patients for the clinician. *Journal of psychiatric research*, 12 (3):189–198, 1975.

Alex J Mitchell. A meta-analysis of the accuracy of the mini-mental state examination in the detection of dementia and mild cognitive impairment. *Journal of psychiatric research*, 43(4): 411–431, 2009.

Yvonne Freund-Levi, Maria Eriksdotter-Jönhagen, Tommy Cederholm, Hans Basun, Gerd Faxen-Irving, Anita Garlind, Inger Vedin, Bengt Vessby, Lars-Olof Wahlund, and Jan Palmblad. ω-3 fatty acid treatment in 174 patients with mild to moderate alzheimer disease: Omegad study: a randomized double-blind trial. *Archives of neurology*, 63(10):1402–1408, 2006.

Ziad S Nasreddine, Natalie A Phillips, Valérie Bédirian, Simon Charbonneau, Victor Whitehead, Isabelle Collin, Jeffrey L Cummings, and Howard Chertkow. The montreal cognitive assessment, moca: a brief screening tool for mild cognitive impairment. *Journal of the American Geriatrics Society*, 53(4):695–699, 2005.

Pavagada S Mathuranath, Peter J Nestor, GE Berrios, Wojtek Rakowicz, and JR Hodges. A brief cognitive test battery to differentiate alzheimer's disease and frontotemporal dementia. *Neurology*, 55(11):1613–1620, 2000.

Piero Amodio, Helmut Wenin, Franco Del Piccolo, Daniela Mapelli, Sara Montagnese, Andrea Pellegrini, Carmine Musto, Angelo Gatta, and Carlo Umiltà. Variability of trail making test, symbol digit test and line trait test in normal people. a normative study taking into account age-dependent decline and sociobiological variables. *Aging clinical and experimental research*, 14 (2):117–131, 2002.

Kenneth I Shulman. Clock-drawing: is it the ideal cognitive screening test? *International journal of geriatric psychiatry*, 15(6):548–561, 2000.

Noor Kamal Al-Qazzaz, Sawal Hamid Bin Ali, Siti Anom Ahmad, Kalaivani Chellappan, Md Islam, Javier Escudero, et al. Role of eeg as biomarker in the early detection and classification of dementia. *The Scientific World Journal*, 2014, 2014.

Tero Tapiola, Irina Alafuzoff, Sanna-Kaisa Herukka, Laura Parkkinen, Päivi Hartikainen, Hilkka Soininen, and Tuula Pirttilä. Cerebrospinal fluid β-amyloid 42 and tau proteins as biomarkers of alzheimer-type pathologic changes in the brain. *Archives of neurology*, 66(3):382–389, 2009.

Daniel Ferreira, Lilisbeth Perestelo-Pérez, Eric Westman, Lars-Olof Wahlund, Antonio Sarría, and Pedro Serrano-Aguilar. Meta-review of csf core biomarkers in alzheimer's disease: the state-of-the-art after the new revised diagnostic criteria. *Frontiers in aging neuroscience*, 6:47, 2014.

Bob Olsson, Ronald Lautner, Ulf Andreasson, Annika Öhrfelt, Erik Portelius, Maria Bjerke, Mikko Hölttä, Christoffer Rosén, Caroline Olsson, Gabrielle Strobel, et al. Csf and blood biomarkers for the diagnosis of alzheimer's disease: a systematic review and meta-analysis. *The Lancet Neurology*, 15(7):673–684, 2016.

Hanspeter Pfister, Verena Kaynig, Charl P Botha, Stefan Bruckner, Vincent J Dercksen, Hans-Christian Hege, and Jos BTM Roerdink. Visualization in connectomics. In *Scientific Visualization*, pages 221–245. Springer, 2014.

Paul L Nunez. A study of origins of the time dependencies of scalp eeg: I-theoretical basis. *IEEE Transactions on Biomedical Engineering*, BME-28(3):271–280, 1981.

Jaakko Malmivuo, Robert Plonsey, et al. *Bioelectromagnetism: principles and applications of bioelectric and biomagnetic fields*. Oxford University Press, USA, 1995.

Priyanka A. Abhang, Bharti W. Gawali, and Suresh C. Mehrotra. Chapter 2 - technological basics of eeg recording and operation of apparatus. In Priyanka A. Abhang, Bharti W. Gawali,

and Suresh C. Mehrotra, editors, *Introduction to EEG- and Speech-Based Emotion Recognition*, pages 19–50. Academic Press, 2016. ISBN 978-0-12-804490-2. doi: https://doi.org/10.1016/B978-0-12-804490-2.00002-6.

Frank H Duffy, Marilyn S Albert, and Gloria McAnulty. Brain electrical activity in patients with presenile and senile dementia of the alzheimer type. *Annals of Neurology: Official Journal of the American Neurological Association and the Child Neurology Society*, 16(4):439–448, 1984.

Claudio Babiloni, Roberta Lizio, Nicola Marzano, Paolo Capotosto, Andrea Soricelli, Antonio Ivano Triggiani, Susanna Cordone, Loreto Gesualdo, and Claudio Del Percio. Brain neural synchronization and functional coupling in alzheimer's disease as revealed by resting state eeg rhythms. *International Journal of Psychophysiology*, 103:88–102, 2016.

Vesna Jelic, Sven Erik Johansson, Ove Almkvist, Masahiro Shigeta, Per Julin, Agneta Nordberg, Bengt Winblad, and Lars Olof Wahlund. Quantitative electroencephalography in mild cognitive impairment: longitudinal changes and possible prediction of alzheimer's disease. *Neurobiology of aging*, 21(4):533–540, 2000.

Stefanie Brassen and Georg Adler. Short-term effects of acetylcholinesterase inhibitor treatment on eeg and memory performance in alzheimer patients: an open, controlled trial. *Pharmacopsychiatry*, 36(06):304–308, 2003.

Marco Onofrj, Astrid Thomas, Diego Iacono, Anna Lisa Luciano, and Angelo Di Iorio. The effects of a cholinesterase inhibitor are prominent in patients with fluctuating cognition: a part 3 study of the main mechanism of cholinesterase inhibitors in dementia. *Clinical neuropharmacology*, 26 (5):239–251, 2003.

Natalya V Ponomareva, Natalia V Selesneva, and Grigory A Jarikov. Eeg alterations in subjects at high familial risk for alzheimer's disease. *Neuropsychobiology*, 48(3):152–159, 2003.

Jaeseung Jeong. Eeg dynamics in patients with alzheimer's disease. *Clinical neurophysiology*, 115 (7):1490–1505, 2004.

Justin Dauwels, K Srinivasan, M Ramasubba Reddy, Toshimitsu Musha, François-Benoît Vialatte, Charles Latchoumane, Jaeseung Jeong, and Andrzej Cichocki. Slowing and loss of complexity in alzheimer's eeg: two sides of the same coin? *International journal of Alzheimer's disease*, 2011, 2011.

Ralf Ihl, Thomas Dierks, Eva-Maria Martin, Lutz Frölich, and Konrad Maurer. Topography of the maximum of the amplitude of eeg frequency bands in dementia of the alzheimer type. *Biological Psychiatry*, 39(5):319–325, 1996.

François-B Vialatte, Justin Dauwels, Monique Maurice, Toshimitsu Musha, and Andrzej Cichocki. Improving the specificity of eeg for diagnosing alzheimer's disease. *International Journal of Alzheimer's Disease*, 2011, 2011.

Claudio Babiloni, Raffaele Ferri, Davide V Moretti, Andrea Strambi, Giuliano Binetti, Gloria Dal Forno, Florinda Ferreri, Bartolo Lanuzza, Claudio Bonato, Flavio Nobili, et al. Abnormal fronto-parietal coupling of brain rhythms in mild alzheimer's disease: A multicentric eeg study. *European Journal of Neuroscience*, 19(9):2583–2590, 2004a.

Jules J Claus, Bram W Ongerboer de Visser, Gerard JM Walstra, Albert Hijdra, Bernard Verbeeten, and Willem A van Gool. Quantitative spectral electroencephalography in predicting survival in patients with early alzheimer disease. *Archives of neurology*, 55(8):1105–1111, 1998.

Jacek W Kowalski, Malgorzata Gawel, Anna Pfeffer, and Maria Barcikowska. The diagnostic value of eeg in alzheimer disease: correlation with the severity of mental impairment. *Journal of clinical neurophysiology*, 18(6):570–575, 2001.

Lawrence A Coben, Warren Danziger, and Martha Storandt. A longitudinal eeg study of mild senile dementia of alzheimer type: changes at 1 year and at 2.5 years. *Electroencephalography and clinical neurophysiology*, 61(2):101–112, 1985.

Claudio Babiloni, Giovanni B Frisoni, Fabrizio Vecchio, Roberta Lizio, Michela Pievani, Geroldi Cristina, Claudia Fracassi, Fabrizio Vernieri, Guido Rodriguez, Flavio Nobili, et al. Stability of clinical condition in mild cognitive impairment is related to cortical sources of alpha rhythms: an electroencephalographic study. *Human brain mapping*, 32(11):1916–1931, 2011.

Luke Tait, Francesco Tamagnini, George Stothart, Edoardo Barvas, Chiara Monaldini, Roberto Frusciante, Mirco Volpini, Susanna Guttmann, Elizabeth Coulthard, Jon T Brown, et al. Eeg microstate complexity for aiding early diagnosis of alzheimer's disease. *Scientific reports*, 10(1): 1–10, 2020.

Hojjat Adeli, Samanwoy Ghosh-Dastidar, and Nahid Dadmehr. A spatio-temporal wavelet-chaos methodology for eeg-based diagnosis of alzheimer's disease. *Neuroscience letters*, 444(2):190–194, 2008.

Mehran Ahmadlou, Hojjat Adeli, and Anahita Adeli. Fractality and a wavelet-chaos-methodology for eeg-based diagnosis of alzheimer disease. *Alzheimer Disease & Associated Disorders*, 25(1): 85–92, 2011.

Peter Grassberger. Generalized dimensions of strange attractors. *Physics Letters A*, 97(6):227–230, 1983.

Peter Grassberger and Itamar Procaccia. Measuring the strangeness of strange attractors. In *The theory of chaotic attractors*, pages 170–189. Springer, 2004.

Hojjat Adeli, Samanwoy Ghosh-Dastidar, and Nahid Dadmehr. Alzheimer's disease: models of computation and analysis of eegs. *Clinical EEG and Neuroscience*, 36(3):131–140, 2005.

Brechtje Jelles, JH Van Birgelen, Joris P.J Slaets, Ruben E.M Hekster, Erik J Jonkman, and Cornelis Jan Stam. Decrease of non-linear structure in the eeg of alzheimer patients compared to healthy controls. *Clinical Neurophysiology*, 110(7):1159–1167, 1999.

Jaeseung Jeong, Soo Yong Kim, and Seol-Heui Han. Non-linear dynamical analysis of the eeg in alzheimer's disease with optimal embedding dimension. *Electroencephalography and clinical Neurophysiology*, 106(3):220–228, 1998.

Jaeseung Jeong, Jeong-Ho Chae, Soo Yong Kim, and Seol-Heui Han. Nonlinear dynamic analysis of the eeg in patients with alzheimer's disease and vascular dementia. *Journal of Clinical Neurophysiology*, 18(1):58–67, 2001a.

Tetsuya Takahashi. Complexity of spontaneous brain activity in mental disorders. *Progress in Neuro-Psychopharmacology and Biological Psychiatry*, 45:258–266, 2013.

Takami Yagyu, Jiri Wackermann, Masahiro Shigeta, Vesna Jelic, Toshihiko Kinoshita, Kieko Kochi, Per Julin, Ove Almkvist, Lars-Olof Wahlund, Istvan Kondakor, et al. Global dimensional complexity of multichannel eeg in mild alzheimer's disease and age-matched cohorts. *Dementia and geriatric cognitive disorders*, 8(6):343–347, 1997.

Cover Thomas and Thomas Joy. *Elements of information theory*. WileyInterscience, 2006.

Daniel Abásolo, Roberto Hornero, Pedro Espino, Daniel Alvarez, and Jesus Poza. Entropy analysis of the eeg background activity in alzheimer's disease patients. *Physiological measurement*, 27(3): 241, 2006a.

Thibaut J De Bock, Satyajit Das, Maruf Mohsin, Nancy B Munro, Lee M Hively, Yang Jiang, Charles D Smith, David R Wekstein, Gregory A Jicha, Adam Lawson, et al. Early detection of alzheimer's disease using nonlinear analysis of eeg via tsallis entropy. In *2010 Biomedical Sciences and Engineering Conference*, pages 1–4. IEEE, 2010.

Daniel Abásolo, Roberto Hornero, Pedro Espino, Jesús Poza, Clara I Sánchez, and Ramón de la Rosa. Analysis of regularity in the eeg background activity of alzheimer's disease patients with approximate entropy. *Clinical neurophysiology*, 116(8):1826–1834, 2005.

Steven M Pincus. Approximate entropy as a measure of irregularity for psychiatric serial metrics. *Bipolar disorders*, 8(5p1):430–440, 2006.

J Escudero, Daniel Abásolo, Roberto Hornero, Pedro Espino, and Miguel López. Analysis of electroencephalograms in alzheimer's disease patients with multiscale entropy. *Physiological measurement*, 27(11):1091, 2006.

Daniel Abásolo, Roberto Hornero, Carlos Gómez, María García, and Miguel López. Analysis of eeg background activity in alzheimer's disease patients with lempel–ziv complexity and central tendency measure. *Medical engineering & physics*, 28(4):315–322, 2006b.

Dhiya Al-Jumeily, Shamaila Iram, Francois-Benois Vialatte, Paul Fergus, and Abir Hussain. A novel method of early diagnosis of alzheimer's disease based on eeg signals. *The Scientific World Journal*, 2015, 2015.

Xavier Delbeuck, Martial Van der Linden, and Fabienne Collette. Alzheimer's disease as a disconnection syndrome? *Neuropsychology review*, 13(2):79–92, 2003.

Justin Dauwels, François Vialatte, Toshimitsu Musha, and Andrzej Cichocki. A comparative study of synchrony measures for the early diagnosis of alzheimer's disease based on eeg. *NeuroImage*, 49(1):668–693, 2010b.

Javier Escudero, Saeid Sanei, Delaram Jarchi, Daniel Abásolo, and Roberto Hornero. Regional coherence evaluation in mild cognitive impairment and alzheimer's disease based on adaptively extracted magnetoencephalogram rhythms. *Physiological measurement*, 32(8):1163, 2011.

Ziad Sankari, Hojjat Adeli, and Anahita Adeli. Wavelet coherence model for diagnosis of alzheimer disease. *Clinical EEG and neuroscience*, 43(4):268–278, 2012.

Arkady Pikovsky, Michael Rosenblum, and Juergen Kurths. Synchronization in a population of globally coupled chaotic oscillators. *EPL (Europhysics Letters)*, 34(3):165, 1996.

Justin Dauwels, François Vialatte, and Andrzej Cichocki. A comparative study of synchrony measures for the early detection of alzheimer's disease based on eeg. In *International Conference on Neural Information Processing*, pages 112–125. Springer, 2007a.

Balázs Czigler, Dóra Csikós, Zoltán Hidasi, Zsófia Anna Gaál, Éva Csibri, Éva Kiss, Pál Salacz, and Márk Molnár. Quantitative eeg in early alzheimer's disease patients—power spectrum and complexity features. *International Journal of Psychophysiology*, 68(1):75–80, 2008.

Young-Min Park, Hee-Jae Che, Chang-Hwan Im, Hyung-Tae Jung, Sung-Man Bae, and Seung-Hwan Lee. Decreased eeg synchronization and its correlation with symptom severity in alzheimer's disease. *Neuroscience research*, 62(2):112–117, 2008.

Shinya Kasakawa, Teruya Yamanishi, Tetsuya Takahashi, Kanji Ueno, Mitsuru Kikuchi, and Haruhiko Nishimura. Approaches of phase lag index to eeg signals in alzheimer's disease from complex network analysis. In *Innovation in Medicine and Healthcare 2015*, pages 459–468. Springer, 2016.

Cornelis Jan Stam, Guido Nolte, and Andreas Daffertshofer. Phase lag index: assessment of functional connectivity from multi channel eeg and meg with diminished bias from common sources. *Human brain mapping*, 28(11):1178–1193, 2007a.

Martin Vinck, Robert Oostenveld, Marijn Van Wingerden, Franscesco Battaglia, and Cyriel MA Pennartz. An improved index of phase-synchronization for electrophysiological data in the presence of volume-conduction, noise and sample-size bias. *Neuroimage*, 55(4):1548–1565, 2011.

Tiziana Locatelli, Marco Cursi, Diego Liberati, Massimo Franceschi, and Giancarlo Comi. Eeg coherence in alzheimer's disease. *Electroencephalography and clinical neurophysiology*, 106(3): 229–237, 1998.

Claudio Babiloni, Michela Pievani, Fabrizio Vecchio, Cristina Geroldi, Fabrizio Eusebi, Claudia Fracassi, Evan Fletcher, Charles De Carli, Marina Boccardi, Paolo Maria Rossini, et al. White-matter lesions along the cholinergic tracts are related to cortical sources of eeg rhythms in amnesic mild cognitive impairment. *Human Brain Mapping*, 30(5):1431–1443, 2009a.

Georg Adler, Stefanie Brassen, and Ana Jajcevic. Eeg coherence in alzheimer's dementia. *Journal of neural transmission*, 110(9):1051–1058, 2003.

Christoph Besthorn, Hans Förstl, Claudia Geiger-Kabisch, Heribert Sattel, Theo Gasser, and Ursula Schreiter-Gasser. Eeg coherence in alzheimer disease. *Electroencephalography and clinical neurophysiology*, 90(3):242–245, 1994.

Yolande AL Pijnenburg, Yolande Vd Made, AM Van Cappellen Van Walsum, DL Knol, Philip Scheltens, and Cornelis Jan Stam. Eeg synchronization likelihood in mild cognitive impairment and alzheimer's disease during a working memory task. *Clinical neurophysiology*, 115(6):1332–1339, 2004.

Mark A Kramer, Fen-Lei Chang, Maurice E Cohen, Donna Hudson, and Andrew J Szeri. Synchronization measures of the scalp electroencephalogram can discriminate healthy from alzheimer's subjects. *International journal of neural systems*, 17(02):61–69, 2007.

Jaeseung Jeong, John C Gore, and Bradley S Peterson. Mutual information analysis of the eeg in patients with alzheimer's disease. *Clinical neurophysiology*, 112(5):827–835, 2001b.

Brigitta Tóth, Bálint File, Roland Boha, Zsófia Kardos, Zoltán Hidasi, Zsófia Anna Gaál, Éva Csibri, Pál Salacz, Cornelis Jan Stam, and Márk Molnár. Eeg network connectivity changes in mild cognitive impairment—preliminary results. *International Journal of Psychophysiology*, 92 (1):1–7, 2014.

Andreas Stevens, Tilo Kircher, Matthias Nickola, Mathias Bartels, Natascha Rosellen, and Henning Wormstall. Dynamic regulation of eeg power and coherence is lost early and globally in probable dat. *European archives of psychiatry and clinical neuroscience*, 251(5):199–204, 2001.

Stefanie Brassen, Dieter F Braus, Wolfgang Weber-Fahr, Heike Tost, Steffen Moritz, and Georg Adler. Late-onset depression with mild cognitive deficits: electrophysiological evidences for a preclinical dementia syndrome. *Dementia and Geriatric Cognitive Disorders*, 18(3-4):271–277, 2004.

Yuji Wada, Yuko Nanbu, Yoshifumi Koshino, Nariyoshi Yamaguchi, and Takuma Hashimoto. Reduced interhemispheric eeg coherence in alzheimer disease: analysis during rest and photic stimulation. *Alzheimer disease and associated disorders*, 1998.

Michael J Hogan, Gregory RJ Swanwick, Jochen Kaiser, Michael Rowan, and Brian Lawlor. Memory-related eeg power and coherence reductions in mild alzheimer's disease. *International journal of psychophysiology*, 49(2):147–163, 2003.

Renato Anghinah, PAULO Afonso Medeiros Kanda, MÁRIO SILVA Jorge, EEP Lima, LUIZ Pascuzzi, and ACP Melo. Alpha band coherence analysis of eeg in healthy adult and alzheimer's type dementia subjects. *Arquivos de neuropsiquiatria*, 58(2):272–275, 2000.

Zoltán Hidasi, Balázs Czigler, Pál Salacz, Éva Csibri, and Márk Molnár. Changes of eeg spectra and coherence following performance in a cognitive task in alzheimer's disease. *International journal of psychophysiology*, 65(3):252–260, 2007.

Brechtje Jelles, Ph Scheltens, WM Van der Flier, EJ Jonkman, FH Lopes da Silva, and Cornelis Jan Stam. Global dynamical analysis of the eeg in alzheimer's disease: frequency-specific changes of functional interactions. *Clinical neurophysiology*, 119(4):837–841, 2008.

Erol Başar, Bahar Güntekin, Elif Tülay, and Görsev G Yener. Evoked and event related coherence of alzheimer patients manifest differentiation of sensory–cognitive networks. *Brain Research*, 1357:79–90, 2010.

Cornelis Jan Stam and Bob Wilhelm Van Dijk. Synchronization likelihood: an unbiased measure of generalized synchronization in multivariate data sets. *Physica D: Nonlinear Phenomena*, 163 (3-4):236–251, 2002.

Cornelis Jan Stam, Y Van Der Made, Yolande AL Pijnenburg, and PH Scheltens. Eeg synchronization in mild cognitive impairment and alzheimer's disease. *Acta neurologica scandinavica*, 108 (2):90–96, 2003.

Vesna Jelic, Per Julin, Masahiro Shigeta, Agneta Nordberg, Lars Lannfelt, Bengt Winblad, and Lars-Olof Wahlund. Apolipoprotein e $\varepsilon 4$ allele decreases functional connectivity in alzheimer's disease as measured by eeg coherence. *Journal of Neurology, Neurosurgery & Psychiatry*, 63(1): 59–65, 1997.

Andrew Leuchter, Jennifer Dunkin, Robert B Lufkin, Yuichiro Anzai, Ian A Cook, and Thomas F Newton. Effect of white matter disease on functional connections in the aging brain. *Journal of Neurology, Neurosurgery & Psychiatry*, 57(11):1347–1354, 1994.

Lineu C Fonseca, Gloria MAS Tedrus, Priscila N Carvas, and Elaine CFA Machado. Comparison of quantitative eeg between patients with alzheimer's disease and those with parkinson's disease dementia. *Clinical Neurophysiology*, 124(10):1970–1974, 2013.

Verner Knott, Erich Mohr, Colleen Mahoney, and Vadim Ilivitsky. Electroencephalographic coherence in alzheimer's disease: comparisons with a control group and population norms. *Journal of geriatric psychiatry and neurology*, 13(1):1–8, 2000.

Claudio Babiloni, Giovanni B Frisoni, Fabrizio Vecchio, Michela Pievani, Cristina Geroldi, Charles De Carli, Raffaele Ferri, Fabrizio Vernieri, Roberta Lizio, and Paolo M Rossini. Global functional coupling of resting eeg rhythms is related to white-matter lesions along the cholinergic tracts in subjects with amnesic mild cognitive impairment. *Journal of Alzheimer's Disease*, 19(3):859–871, 2010.

Fabrizio Vecchio, Claudio Babiloni, Roberta Lizio, Fabrizio De Vico Fallani, Katarzyna Blinowska, Giulio Verrienti, Giovanni Frisoni, and Paolo M Rossini. Resting state cortical eeg rhythms in alzheimer's disease: toward eeg markers for clinical applications: a review. *Supplements to Clinical neurophysiology*, 62:223–236, 2013.

Thomas König, Leslie Prichep, Thomas Dierks, Daniela Hubl, Lars O Wahlund, Erwin R John, and Vesna Jelic. Decreased eeg synchronization in alzheimer's disease and mild cognitive impairment. *Neurobiology of aging*, 26(2):165–171, 2005.

Justin Dauwels, François Vialatte, Charles Latchoumane, Jaeseung Jeong, and Andrzej Cichocki. Loss of eeg synchrony in early-stage ad patients: a study with multiple synchrony measures and multiple eeg data sets. In *31st Annual International Conference of the IEEE engineering in Medicine and Biology Society,(EMBC'09)*. IEEE, 2009a.

Claudio Babiloni, Giuliano Binetti, Emanuele Cassetta, Daniele Cerboneschi, Gloria Dal Forno, Claudio Del Percio, Florinda Ferreri, Raffaele Ferri, Bartolo Lanuzza, Carlo Miniussi, et al. Mapping distributed sources of cortical rhythms in mild alzheimer's disease. a multicentric eeg study. *Neuroimage*, 22(1):57–67, 2004b.

Claudio Babiloni, Raffaele Ferri, Giuliano Binetti, Andrea Cassarino, Gloria Dal Forno, Matilde Ercolani, Florinda Ferreri, Giovanni B Frisoni, Bartolo Lanuzza, Carlo Miniussi, et al. Fronto-parietal coupling of brain rhythms in mild cognitive impairment: a multicentric eeg study. *Brain research bulletin*, 69(1):63–73, 2006.

Cornelis Jan Stam, Teresa Montez, BF Jones, SARB Rombouts, Yolande Van Der Made, Yolande AL Pijnenburg, and Philip Scheltens. Disturbed fluctuations of resting state eeg synchronization in alzheimer's disease. *Clinical neurophysiology*, 116(3):708–715, 2005.

Yolande AL Pijnenburg, Rob LM Strijers, Yolande vd Made, Wiesje M van der Flier, Philip Scheltens, and Cornelis Jan Stam. Investigation of resting-state eeg functional connectivity in frontotemporal lobar degeneration. *Clinical neurophysiology*, 119(8):1732–1738, 2008.

Justin Dauwels, François Vialatte, Charles Latchoumane, Jaeseung Jeong, and Andrzej Cichocki. Eeg synchrony analysis for early diagnosis of alzheimer's disease: a study with several synchrony

measures and eeg data sets. In *2009 Annual International Conference of the IEEE Engineering in Medicine and Biology Society*, pages 2224–2227. IEEE, 2009b.

Claudio Babiloni, Raffaele Ferri, Giuliano Binetti, Fabrizio Vecchio, Giovanni B Frisoni, Bartolo Lanuzza, Carlo Miniussi, Flavio Nobili, Guido Rodriguez, Francesco Rundo, et al. Directionality of eeg synchronization in alzheimer's disease subjects. *Neurobiology of aging*, 30(1):93–102, 2009b.

Esteve Gallego-Jutglà, Mohamed Elgendi, Francois Vialatte, Jordi Solé-Casals, Andrzej Cichocki, Charles Latchoumane, Jaesung Jeong, and Justin Dauwels. Diagnosis of alzheimer's disease from eeg by means of synchrony measures in optimized frequency bands. In *2012 Annual International Conference of the IEEE Engineering in Medicine and Biology Society*, pages 4266–4270. IEEE, 2012.

Justin Dauwels, François Vialatte, Tomasz Rutkowski, and Andrzej Cichocki. Measuring neural synchrony by message passing. *Advances in neural information processing systems*, 20, 2007b.

Men-Tzung Lo, Ping-Huang Tsai, Pei-Feng Lin, Chen Lin, and Yue Loong Hsin. The nonlinear and nonstationary properties in eeg signals: probing the complex fluctuations by hilbert–huang transform. *Advances in Adaptive Data Analysis*, 1(03):461–482, 2009.

Wlodzimierz Klonowski. Everything you wanted to ask about eeg but were afraid to get the right answer. *Nonlinear biomedical physics*, 3(1):1–5, 2009.

Alexander Ya Kaplan, Andrew A Fingelkurts, Alexander A Fingelkurts, Sergei V Borisov, and Boris S Darkhovsky. Nonstationary nature of the brain activity as revealed by eeg/meg: methodological, practical and conceptual challenges. *Signal processing*, 85(11):2190–2212, 2005.

Vasily A Vakorin, Anthony R McIntosh, Bratislav Mišić, Olga Krakovska, Catherine Poulsen, Kristina Martinu, and Tomáš Paus. Exploring age-related changes in dynamical non-stationarity in electroencephalographic signals during early adolescence. *PloS one*, 8(3):e57217, 2013.

Gunter Bodenstein and H Michael Praetorius. Feature extraction from the electroencephalogram by adaptive segmentation. *Proceedings of the IEEE*, 65(5):642–652, 1977.

Daniel Brandeis, Dietrich Lehmann, Christoph M Michel, and Walter Mingrone. Mapping event-related brain potential microstates to sentence endings. *Brain topography*, 8(2):145–159, 1995.

Dietrich Lehmann and Wolfgang Skrandies. Reference-free identification of components of checkerboard-evoked multichannel potential fields. *Electroencephalography and clinical neurophysiology*, 48(6):609–621, 1980.

Arthur Flexer and Herbert Bauer. Discovery of common subsequences in cognitive evoked potentials. In *European Symposium on Principles of Data Mining and Knowledge Discovery*, pages 309–317. Springer, 1998.

Walter J Freeman. A cinematographic hypothesis of cortical dynamics in perception. *International journal of psychophysiology*, 60(2):149–161, 2006.

Nesma Houmani, François B Vialatte, Charles Latchoumane, Jaeseung Jeong, and Gérard Dreyfus. Stationary epoch-based entropy estimation for early diagnosis of alzheimer's disease. In *2013 IEEE Faible Tension Faible Consommation*, pages 1–4. IEEE, 2013.

Nesma Houmani, Gérard Dreyfus, and François B Vialatte. Epoch-based entropy for early screening of alzheimer's disease. *International journal of neural systems*, 25(08):1550032, 2015.

Nesma Houmani, François B Vialatte, Esteve Gallego-Jutglà, Gérard Dreyfus, Vi-Huong Nguyen-Michel, Jean Mariani, and Kiyoka Kinugawa. Diagnosis of alzheimer's disease with electroencephalography in a differential framework. *PloS one*, 13(3):e0193607, 2018.

Lawrence Rabiner and Biinghwang Juang. An introduction to hidden markov models. *ieee assp magazine*, 3(1):4–16, 1986.

Amira Aljane and Nesma Houmani. Alzheimer's disease diagnosis using synchrony and disorder measures. In *JDSE 2017: 2nd Junior Conference on Data Science and Engineering*, volume 1, pages 117–119. JDSE, 2017.

Lawrence Rabiner and Biing-Hwang Juang. *Fundamentals of speech recognition*. Prentice-Hall, Inc., 1993.

Ed Bullmore and Olaf Sporns. Complex brain networks: graph theoretical analysis of structural and functional systems. *Nature reviews neuroscience*, 10(3):186–198, 2009.

Cornelis Jan Stam. Modern network science of neurological disorders. *Nature Reviews Neuroscience*, 15(10):683–695, 2014.

Qingbao Yu, Yuhui Du, Jiayu Chen, Jing Sui, Tülay Adalē, Godfrey D Pearlson, and Vince D Calhoun. Application of graph theory to assess static and dynamic brain connectivity: Approaches for building brain graphs. *Proceedings of the IEEE*, 106(5):886–906, 2018.

Betty M Tijms, Alle Meije Wink, Willem de Haan, Wiesje M van der Flier, Cornelis Jan Stam, Philip Scheltens, and Frederik Barkhof. Alzheimer's disease: connecting findings from graph theoretical studies of brain networks. *Neurobiology of aging*, 34(8):2023–2036, 2013.

Mikail Rubinov and Olaf Sporns. Complex network measures of brain connectivity: uses and interpretations. *Neuroimage*, 52(3):1059–1069, 2010.

Cornelis Jan van Stam and ECW Van Straaten. The organization of physiological brain networks. *Clinical neurophysiology*, 123(6):1067–1087, 2012.

Olaf Sporns. Graph theory methods: applications in brain networks. *Dialogues in clinical neuroscience*, 2022.

Duncan J Watts and Steven H Strogatz. Collective dynamics of 'small-world'networks. *nature*, 393 (6684):440–442, 1998.

Mark EJ Newman and Michelle Girvan. Finding and evaluating community structure in networks. *Physical review E*, 69(2):026113, 2004.

Willem De Haan, Yolande AL Pijnenburg, Rob LM Strijers, Yolande van der Made, Wiesje M van der Flier, Philip Scheltens, and Cornelis J Stam. Functional neural network analysis in frontotemporal dementia and alzheimer's disease using eeg and graph theory. *BMC neuroscience*, 10(1):1–12, 2009.

Yong He, Zhang Chen, and Alan Evans. Structural insights into aberrant topological patterns of large-scale cortical networks in alzheimer's disease. *Journal of Neuroscience*, 28(18):4756–4766, 2008.

Zhijun Yao, Yuanchao Zhang, Lei Lin, Yuan Zhou, Cunlu Xu, Tianzi Jiang, and Alzheimer's Disease Neuroimaging Initiative. Abnormal cortical networks in mild cognitive impairment and alzheimer's disease. *PLoS computational biology*, 6(11):e1001006, 2010.

Cornelis Jan Stam, BF Jones, Guido Nolte, Michael Breakspear, and Philip Scheltens. Small-world networks and functional connectivity in alzheimer's disease. *Cerebral cortex*, 17(1):92–99, 2007b.

Jesús Poza, María García, Carlos Gómez, Alejandro Bachiller, Alicia Carreres, and Roberto Hornero. Characterization of the spontaneous electroencephalographic activity in alzheimer's disease using disequilibria and graph theory. In *2013 35th Annual International Conference of the IEEE Engineering in Medicine and Biology Society (EMBC)*, pages 5990–5993. IEEE, 2013.

Ruofan Wang, Jiang Wang, Haitao Yu, Xile Wei, Chen Yang, and Bin Deng. Decreased coherence and functional connectivity of electroencephalograph in alzheimer's disease. *Chaos: An Interdisciplinary Journal of Nonlinear Science*, 24(3):033136, 2014.

Fabrizio Vecchio, Francesca Miraglia, Camillo Marra, Davide Quaranta, Maria Gabriella Vita, Placido Bramanti, and Paolo Maria Rossini. Human brain networks in cognitive decline: a graph theoretical analysis of cortical connectivity from eeg data. *Journal of Alzheimer's Disease*, 41 (1):113–127, 2014.

Saeedeh Afshari and Mahdi Jalili. Directed functional networks in alzheimer's disease: disruption of global and local connectivity measures. *IEEE journal of biomedical and health informatics*, 21 (4):949–955, 2016.

Fabrizio Vecchio, Francesca Miraglia, Francesco Iberite, Giordano Lacidogna, Valeria Guglielmi, Camillo Marra, Patrizio Pasqualetti, Francesco Danilo Tiziano, and Paolo Maria Rossini. Sustainable method for alzheimer dementia prediction in mild cognitive impairment: Electroencephalographic connectivity and graph theory combined with apolipoprotein e. *Annals of neurology*, 84 (2):302–314, 2018.

Francesca Miraglia, Fabrizio Vecchio, Camillo Marra, Davide Quaranta, Francesca Alù, Benedetta Peroni, Giuseppe Granata, Elda Judica, Maria Cotelli, and Paolo Maria Rossini. Small world index in default mode network predicts progression from mild cognitive impairment to dementia. *International Journal of Neural Systems*, 30(02):2050004, 2020.

Raffaella Franciotti, Nicola Walter Falasca, Dario Arnaldi, Francesco Famà, Claudio Babiloni, Marco Onofrj, Flavio Mariano Nobili, and Laura Bonanni. Cortical network topology in prodromal and mild dementia due to alzheimer's disease: graph theory applied to resting state eeg. *Brain Topography*, 32(1):127–141, 2019.

Jiangkuan Chen, Cong Liu, Chung-Kang Peng, Jong-Ling Fuh, Fengzhen Hou, and Albert C Yang. Topological reorganization of eeg functional network is associated with the severity and cognitive impairment in alzheimer's disease. *Physica A: Statistical Mechanics and its Applications*, 513: 588–597, 2019.

Fabrizio Vecchio, Francesca Miraglia, Francesca Alù, Matteo Menna, Elda Judica, Maria Cotelli, and Paolo Maria Rossini. Classification of alzheimer's disease with respect to physiological aging with innovative eeg biomarkers in a machine learning implementation. *Journal of Alzheimer's Disease*, 75(4):1253–1261, 2020.

Ramtin Mehraram, Marcus Kaiser, Ruth Cromarty, Sara Graziadio, John T O'Brien, Alison Killen, John-Paul Taylor, and Luis R Peraza. Weighted network measures reveal differences between dementia types: An eeg study. *Human brain mapping*, 41(6):1573–1590, 2020.

Mahdi Jalili. Graph theoretical analysis of alzheimer's disease: Discrimination of ad patients from healthy subjects. *Information Sciences*, 384:145–156, 2017.

Fabrizio Vecchio, Francesca Miraglia, Francesca Alú, Alessandro Orticoni, Elda Judica, Maria Cotelli, and Paolo Maria Rossini. Contribution of graph theory applied to eeg data analysis for alzheimer's disease versus vascular dementia diagnosis. *Journal of Alzheimer's Disease*, 82(2): 871–879, 2021.

David López-Sanz, Pilar Garcés, Blanca Álvarez, María Luisa Delgado-Losada, Ramón López-Higes, and Fernando Maestú. Network disruption in the preclinical stages of alzheimer's disease: from subjective cognitive decline to mild cognitive impairment. *International journal of neural systems*, 27(08):1750041, 2017.

Raffaella Franciotti, Davide V Moretti, Alberto Benussi, Laura Ferri, Mirella Russo, Claudia Carrarini, Filomena Barbone, Dario Arnaldi, Nicola W Falasca, Giacomo Koch, et al. Cortical network modularity changes along the course of frontotemporal and alzheimer's dementing diseases. *Neurobiology of aging*, 110:37–46, 2022.

Ece Kocagoncu, Andrew Quinn, Azadeh Firouzian, Elisa Cooper, Andrea Greve, Roger Gunn, Gary Green, Mark W Woolrich, Richard N Henson, Simon Lovestone, et al. Tau pathology in early alzheimer's disease is linked to selective disruptions in neurophysiological network dynamics. *Neurobiology of aging*, 92:141–152, 2020.

Luke Tait, George Stothart, Elizabeth Coulthard, Jon T Brown, Nina Kazanina, and Marc Goodfellow. Network substrates of cognitive impairment in alzheimer's disease. *Clinical Neurophysiology*, 130(9):1581–1595, 2019.

Rihui Li, Thinh Nguyen, Thomas Potter, and Yingchun Zhang. Dynamic cortical connectivity alterations associated with alzheimer's disease: An eeg and fnirs integration study. *NeuroImage: Clinical*, 21:101622, 2019.

Giordano Cecchetti, Federica Agosta, Silvia Basaia, Camilla Cividini, Marco Cursi, Roberto Santangelo, Francesca Caso, Fabio Minicucci, Giuseppe Magnani, and Massimo Filippi. Resting-state electroencephalographic biomarkers of alzheimer's disease. *NeuroImage: Clinical*, 31:102711, 2021.

Ian G McKeith, Dennis W Dickson, J Lowe, M Emre, JT O'brien, H Feldman, J Cummings, JE Duda, C Lippa, EK Perry, et al. Diagnosis and management of dementia with lewy bodies: third report of the dlb consortium. *Neurology*, 65(12):1863–1872, 2005.

Heiko Braak and Eva Braak. Neuropathological stageing of alzheimer-related changes. *Acta neuropathologica*, 82(4):239–259, 1991.

Johannes Pantel, Peter Schönknecht, Marco Essig, and Johannes Schröder. Distribution of cerebral atrophy assessed by magnetic resonance imaging reflects patterns of neuropsychological deficits in alzheimer's dementia. *Neuroscience letters*, 361(1-3):17–20, 2004.

Arne Brun and Elisabet Englund. Regional pattern of degeneration in alzheimer's disease: neuronal loss and histopathological grading. *Histopathology*, 5(5):549–564, 1981.

Surya Das and Subha D Puthankattil. Complex network analysis of mci-ad eeg signals under cognitive and resting state. *Brain research*, 1735:146743, 2020.

Sinead Gaubert, Federico Raimondo, Marion Houot, Marie-Constance Corsi, Lionel Naccache, Jacobo Diego Sitt, Bertrand Hermann, Delphine Oudiette, Geoffroy Gagliardi, Marie-Odile Habert, et al. Eeg evidence of compensatory mechanisms in preclinical alzheimer's disease. *Brain*, 142 (7):2096–2112, 2019.

Serena Dattola, Nadia Mammone, Francesco Carlo Morabito, Domenico Rosaci, Giuseppe Maria Luigi Sarné, and Fabio La Foresta. Testing graph robustness indexes for eeg analysis in alzheimer's disease diagnosis. *Electronics*, 10(12):1440, 2021.

Karim Bennys, Gérard Rondouin, Christine Vergnes, and Jacques Touchon. Diagnostic value of quantitative eeg in alzheimer's disease. *Neurophysiologie Clinique/Clinical Neurophysiology*, 31 (3):153–160, 2001.

Mikail Rubinov and Olaf Sporns. Weight-conserving characterization of complex functional brain networks. *Neuroimage*, 56(4):2068–2079, 2011.

Cornelis Jan Stam, Willem De Haan, Andreas Daffertshofer, BF Jones, I Manshanden, Anne-Marie van Cappellen van Walsum, Teresa Montez, Jeroen Verbunt, Jan C De Munck, Bob Wilhelm Van Dijk, et al. Graph theoretical analysis of magnetoencephalographic functional connectivity in alzheimer's disease. *Brain*, 132(1):213–224, 2009.

Cornelis Jan Stam and Jaap C Reijneveld. Graph theoretical analysis of complex networks in the brain. *Nonlinear biomedical physics*, 1(1):1–19, 2007.

Margherita Lai, Matteo Demuru, Arjan Hillebrand, and Matteo Fraschini. A comparison between scalp-and source-reconstructed eeg networks. *Scientific reports*, 8(1):1–8, 2018.

André M Bastos and Jan-Mathijs Schoffelen. A tutorial review of functional connectivity analysis methods and their interpretational pitfalls. *Frontiers in systems neuroscience*, 9:175, 2016.

Mahmoud Hassan and Fabrice Wendling. Electroencephalography source connectivity: toward high time/space resolution brain networks. *arXiv preprint arXiv:1801.02549*, 2018.

Kathleen A Garrison, Dustin Scheinost, Emily S Finn, Xilin Shen, and R Todd Constable. The (in) stability of functional brain network measures across thresholds. *Neuroimage*, 118:651–661, 2015.

Sheng Chen, Stephen A Billings, and Wan Luo. Orthogonal least squares methods and their application to non-linear system identification. *International Journal of control*, 50(5):1873–1896, 1989.

Gérard Dreyfus. *Neural networks: methodology and applications*. Springer Science & Business Media, 2005.

Colin Campbell and Yiming Ying. Learning with support vector machines. *Synthesis lectures on artificial intelligence and machine learning*, 5(1):1–95, 2011.

Bernhard E Boser, Isabelle M Guyon, and Vladimir N Vapnik. A training algorithm for optimal margin classifiers. In *Proceedings of the fifth annual workshop on Computational learning theory*, pages 144–152, 1992.

Danielle S Bassett and Edward T Bullmore. Human brain networks in health and disease. *Current opinion in neurology*, 22(4):340, 2009.

Hervé Stoppiglia, Gérard Dreyfus, Rémi Dubois, and Yacine Oussar. Ranking a random feature for variable and feature selection. *The Journal of Machine Learning Research*, 3:1399–1414, 2003.

Stefan Knerr, Léon Personnaz, and Gérard Dreyfus. Single-layer learning revisited: a stepwise procedure for building and training a neural network. In *Neurocomputing*, pages 41–50. Springer, 1990.

Martijn P Van Den Heuvel and Alex Fornito. Brain networks in schizophrenia. *Neuropsychology review*, 24(1):32–48, 2014.

Bernadette CM Van Wijk, Cornelis J Stam, and Andreas Daffertshofer. Comparing brain networks of different size and connectivity density using graph theory. *PloS one*, 5(10):e13701, 2010.

Sophie Achard and Edward Bullmore. Efficiency and cost of economical brain functional networks. *PLoS computational biology*, 3(2):e17, 2007.

Sebastianus Petrus van den Broek, F Reinders, M Donderwinkel, and MJ Peters. Volume conduction effects in eeg and meg. *Electroencephalography and clinical neurophysiology*, 106(6):522–534, 1998.

Jens Braun. Fermion interactions and universal behavior in strongly interacting theories. *Journal of Physics G: Nuclear and Particle Physics*, 39(3):033001, 2012.

Cedric E Ginestet, Thomas E Nichols, Ed T Bullmore, and Andrew Simmons. Brain network analysis: separating cost from topology using cost-integration. *PloS one*, 6(7):e21570, 2011.

DOCTORAL SCHOOL

Titre : Etude topologique de l'organisation fonctionnelle cérébrale aux stades précoces de la MA par EEG

Mots clés : Signaux EEG cliniques ; Maladie d'Alzheimer ; Connectivité fonctionnelle ; Théorie de graphe

Résumé : L'électroencéphalographie (EEG) est une technologie de neuroimagerie non-invasive et peu coûteuse, qui présente un grand intérêt pour les applications cliniques. Elle a été largement exploitée dans la littérature pour analyser les altérations dans la dynamique cérébrale liées à la Maladie d'Alzheimer (MA). En l'absence de traitement curatif, nous observons un intérêt croissant à la caractérisation de l'activité cérébrale aux stades précoces de la maladie. Cette thèse s'intéresse au diagnostic précoce de la MA aux stades préclinique et prodromal en utilisant l'EEG au repos, et aborde l'analyse des réseaux cérébraux en étudiant la connectivité fonctionnelle à différents stades cliniques du déclin cognitif (SCI, MCI et MA au stade léger). Pour cela, nous avons mené une étude rétrospective en exploitant une base de données clinique qui contient des signaux EEG enregistrés en conditions réelles.

En premier lieu, nous avons proposé d'exploiter une mesure d'entropie, appelée "Epoch-based Entropy" (*EpEn*), pour quantifier la connectivité fonctionnelle. Cette mesure repose sur une modélisation statistique fine des signaux EEG avec des modèles de Markov cachés, qui permet de caractériser les changements spatio-temporels des signaux EEG.

Par la suite, nous avons effectué une analyse du réseau cérébral cortical de manière différentielle sur les trois stades du déclin cognitif en exploitant la théorie des graphes. Il s'agit du premier travail qui : (*i*) aborde l'analyse du réseau cérébral chez les trois groupes (SCI, MCI et MA) simultanément, et (*ii*) combine la mesure d'entropie à la théorie des graphes puisque nous avons démontré son efficacité à quantifier les changements spatio-temporels liés à la MA.

Nous avons aussi abordé le problème de la grande quantité d'information extraite des signaux EEG, analysés sur plusieurs bandes de fréquences, plusieurs électrodes, et plusieurs échelles de densité de réseau. Par conséquent, une autre contribution à ce travail concerne l'extraction de marqueurs EEG les plus pertinents pour discriminer automatiquement les trois groupes de patients. Ainsi, nous avons proposé une méthode hiérarchique pour l'analyse des signaux EEG, permettant d'identifier les descripteurs les plus pertinents à partir d'une grande quantité d'information issue d'une seule mesure de connectivité fonctionnelle. Enfin, nous avons évalué la corrélation entre les marqueurs numériques extraits des signaux EEG et des marqueurs cliniques.

Title : Topological study of the brain functional organization at the early stages of AD using EEG

Keywords : Clinical EEG data ; Alzheimer's disease ; Functional connectivity ; Graph theory ; Brain network

Abstract : Electroencephalography (EEG) is a non-invasive and cost-effective neuroimaging technology of high interest in clinical applications. It has been largely studied in the literature to analyze brain activity alterations due to Alzheimer's disease (AD). There is a growing interest in the earlier stages of AD since curative treatments are still lacking. This thesis investigates the early diagnosis of AD at preclinical and prodromal stages using resting-state EEG, and addresses brain network analysis by studying the functional connectivity over several clinical stages of cognitive decline (SCI, MCI and Mild AD). To this end, we conduct a retrospective study using a clinical database that contains EEG signals recorded in real-life conditions.

We first propose to exploit an entropy measure, termed "epoch-based entropy" (*EpEn*), as a measure of functional connectivity, that relies on a refined statistical modeling of EEG signals based on Hidden Markov Models, which permits to characterize the spatiotemporal changes in EEG signals.

Furthermore, we conduct a differential brain network analysis over the three stages of cognitive decline by employing the Graph Theory. Actually, this is the first work that : (*i*) addresses EEG brain network analysis over SCI, MCI and Mild AD stages simultaneously, and (*ii*) combines *EpEn* to Graph Theory since we have shown its effectiveness in quantifying the complete spatiotemporal alteration due to AD.

In this thesis, we decided to invest the largest amount of EEG information for brain network analysis, by exploiting several frequency ranges, several electrodes locations, and several network density scales. Therefore, another issue tackled in this thesis concerns the identification of relevant EEG markers to discriminate automatically between SCI, MCI and AD patients in the context of graph analysis framework. To this end, we propose an automatic hierarchical method for EEG analysis, which allows the extraction of relevant markers from large amount of information based on a single EEG connectivity measure. Finally, we assess the correlation between the relevant EEG markers and clinical markers.

Institut Polytechnique de Paris
91120 Palaiseau, France